UNIVERSITEIT VAN PRETORIA
UNIVERSITY OF PRETORIA
YUNIBESITHI YA PRETORIA

AN OFFSET MODULATION METHOD USED TO CONTROL THE PAPR OF AN OFDM TRANSMISSION

by

Kahesh Dhuness

Submitted in partial fulfilment of the requirements for the degree

Philosophiae Doctor (Engineering)

in the

Department of Electrical, Electronic and Computer Engineering
Faculty of Engineering, Built Environment and Information Technology
UNIVERSITY OF PRETORIA

April 2012

UNIVERSITEIT VAN PRETORIA
UNIVERSITY OF PRETORIA
YUNIBESITHI YA PRETORIA

SUMMARY

AN OFFSET MODULATION METHOD USED TO CONTROL THE PAPR OF AN OFDM TRANSMISSION

by

Kahesh Dhuness

Promoter(s):	Professor Dr B.T. Maharaj
Department:	Electrical, Electronic and Computer Engineering
University:	University of Pretoria
Degree:	Philosophiae Doctor (Engineering)
Keywords:	ACE, Clipping, Cognitive Radio, DVB-T2, OFDM, OM-ACE, OM- OFDM, PAPR, ROC, TR

Orthogonal frequency division multiplexing (OFDM) has become a very popular method for high-data-rate communication. However, it is well known that OFDM is plagued by a large peak-to-average power ratio (PAPR) problem. This high PAPR results in overdesigned power amplifiers, which amongst other things leads to inefficient amplifier usage, which is undesirable. Various methods have been recommended to reduce the PAPR of an OFDM transmission; however, all these methods result in a number of drawbacks.

In this thesis, a novel method called offset modulation (OM-OFDM) is proposed to control the PAPR of an OFDM signal. The proposed OM-OFDM method does not result in a number of the drawbacks being experienced by current methods in the field. The theoretical bandwidth occupancy and theoretical bit error rate (BER) expression for an OM-OFDM transmission is derived. A newly applied power performance decision metric is also introduced, which can be utilised throughout the PAPR field, in order to compare various methods.

The proposed OM-OFDM method appears to be similar to a well-known constant envelope OFDM (CE-OFDM) transmission. The modulation, structural and performance differences between an OM-OFDM and a CE-OFDM method are discussed. By applying the power performance decision metric, the OM-OFDM method is shown to offer significant performance gains when compared to CE-OFDM and traditional OFDM transmissions.

In addition, the OM-OFDM method is able to accurately control the PAPR of a transmission for a targeted BER. By applying the power performance decision metric and complementary cumulative distribution function (CCDF), the proposed OM-OFDM method is shown to offer further performance gains when compared to existing PAPR methods, under frequency selective fading conditions.

In this thesis, the OM-OFDM method has been combined with an existing active constellation extended (ACE) PAPR reduction method. To introduce a novel method called offset modulation with active constellation extension (OM-ACE), to control the PAPR of an OFDM signal. The theoretical BER expression for an OM-ACE transmission is presented and validated. Thereafter, by applying the decision metric and CCDF, the OM-ACE method is shown to offer performance improvements when compared to various PAPR methods.

The use of OM-OFDM for cognitive radio applications is also investigated. Cognitive radio applications require transmissions that are easily detectable. The detection characteristics of an OM-OFDM and OFDM transmission are studied by using receiver operating characteristic curves. A derivation of a simplified theoretical closed-form expression, which relates the probability of a missed detection to the probability of a false alarm, for an unknown deterministic signal, at various signal-to-noise ratio (SNR) values is derived and validated. Previous expressions have been derived, which relate the probability of a missed detection to the probability of a false alarm. However, they have not been presented in such a generic closed-form expression that can be used for any unknown deterministic signal (for instance OFDM and OM-OFDM). Thereafter, an examination of the spectrum characteristics of an OM-OFDM transmission indicates its attractive detection characteristics. The proposed OM-OFDM method is further shown to

operate at a significantly lower SNR value than an OFDM transmission, while still offering better detection characteristics than that of an OFDM transmission under Rician, Rayleigh and frequency selective fading channel conditions.

In addition to its attractive PAPR properties, OM-OFDM also offers good detection characteristics for cognitive radio applications. These aspects make OM-OFDM a promising candidate for future deployment.

OPSOMMING

'N AFSETMODULASIE METODE OM DIE PGDV VAN 'N OFVM-SEIN TE BEHEER

deur

Kahesh Dhuness

Promotor(s):	Professor Dr B.T. Maharaj
Departement:	Elektriese, Elektroniese en Rekenaar-Ingenieurswese
Universiteit:	Universiteit van Pretoria
Graad:	Philosophiae Doctor (Ingenieurswese)
Sleutelwoorde:	AKV, Knip, Kognitiewe Radio, DVB-T2, OFVM, OM-AKV, OM- OFVM, PGDV, ROC, TR

Ortogonale-frekwensie-verdeling-multipleksering (OFVM) is 'n baie gewilde metode vir hoëdata-tempokommunikasie. Dit is egter bekend dat OFVM deur 'n groot piek-tot-gemiddelde drywingverhouding (PGDV) probleem geteister word. Hierdie hoë PGDV, verminder die batteryleeftyd van die mobiele toestel, wat ongewens is. Daar is verskeie metodes om die PGDV van 'n OFVM-sein te verminder, maar al hierdie metodes het nadele. Hierdie proefskrif beskryf dus 'n nuwe metode, genaamd afsetmodulasie (OM-OFVM), om die PGDV-effek van 'n OFVM-sein te beheer. Die voorgestelde OM-OFVM-metode vermy van die nadele van die ander methodes. Die teoretiese bandwydte wat benodig word, sowel as die teoretiese bisfoutwaarskynlikheid (BFW), vir 'n afsetgemoduleerde oordrag, word afgelei en bevestig. 'n Nuwe toegepaste drywings-prestasie-besluitnemings-maatstaf word voorgestel, wat gebruik kan word in die PGDV-veld, om die verskillende metodes met mekaar te vergelyk.

Die voorgestelde OM-OFVM-metode lyk soos die welbekende konstante omhalling-OFVM-methode (KO-OFVM). Die voorgestelde modulasie, strukturele en prestasie-verskille tussen

die OM-OFVM-en KO-OFVM-metodes word bespreek. Deur gebruik te maak van die nuwe toegepaste drywing-prestasie-besluitnemingsmaatstaf, toon die OM-OFVM-metode beduidende prestasie-winste wanneer dit vergelyk word met ’n KO-OFVM-en tradisionele OFVM-metode.

Verder kan die OM-OFVM-metode die PGDV van ’n sein vir ’n geteikende BFW akkuraat beheer. Deur gebruik te maak van ’n nuwe toegepaste drywing-prestasie-besluitnemingsmaatstaf en die kumulatiewe verdelingsfunksie (KV), toon die voorgestelde OM-OFVM-metode dat dit verdere prestasiewinste kan aan bied wanneer dit vergelyk word met bestaande PGDV metodes, onder frekwensie-selektiewe deiningtoestande.

In hierdie proefskrif word dit voorgestel om die OM-OFVM-metode te kombineer met ’n bestaande aktiewe konstellasie-uitbreiding (AKU) PGDV-verminderingmetode om die PGDV van ’n OFVM-sein te beheer. Die voorgestelde metode word afsetmodulasie met aktiewe konstellasie-uitbreiding (OM-AKU) genoem. Die teoretiese BFW-uitdrukking vir ’n OM-AKV-oordrag word aangebied en geverifieer. Daarna, deur gebruik te maak van die voorgestelde drywings-prestasie-besluitnemings-maatstaf en KV, word daar getoon dat die OM-AKU metode prestasie-verbeterings teweegbring wanneer dit vergelyk word met bestaande PGDV-metodes.

Die gebruik van OM-OFVM vir kognitiewe radio word ook ondersoek. Die opspo-ring-seienskappe van ’n OM-OFVM-en OFVM-sein word bestudeer deur gebruik te maak van die ontvanger-bedryfstelsel se kenmerkende kurwes. ’n Afleiding van die vereenvoud-igde teoretiese geslote vormuitdrukking, wat die verband tussen die waarskynlikheid van ’n gemisde opsporing tot die waarskynlikheid van ’n vals alarm op verskillende sein-tot-geraas-verhouding (SGV) waardes vir ’n onbekende deterministiese sein beskryf, is afgelei en geverifieer. Daarna het ’n ondersoek van die spektrum-eienskappe van ’n OM-OFVM-oordrag daarop gedui dat aantreklike opsporingseienskappe gevind is. Die voorgestelde OM-OFVM-metode blyk verder teen ’n aansienlik laer SGV-waarde te funksioneer as ’n OFVM-sein, terwyl dit steeds beter sein-opsporingseienskappe bied as ’n OFVM oordrag onder Rician, Rayleigh en frekwensie-selektiewe deiningkanaal-toestande. Benewens sy

aantreklike PGDV-eienskappe, bied OM-OFVM ook goeie sein-opsporing-eienskappe vir kognitiewe radio. Hierdie aspekte maak OM-OFVM ’n belowende kandidaat vir toekomstige gebruik.

I dedicate this work to

My Creator for giving me the ability and opportunity to undertake it

All those from whom I have come to understand what Ubuntu means

ACKNOWLEDGEMENT

I would like to thank

- My parents, Jyothi and Rajindranath, and sister Laticia for their enduring love, support and encouragement.

- My study leader Professor, B. T. Maharaj, for his sage advice and support throughout the course of my studies.

- All my colleagues and a special thanks to Dare Sokoya, Philip Botha, Pieter Jansen van Vuuren, Robin Thomas, Simon Barnes and Thinus Prinsloo at the Sentech Chair in Broadband Wireless Multimedia Communication at the University of Pretoria.

- The University of Pretoria, the Sentech Chair in Broadband Wireless Multimedia Communication and the National Research Foundation for the financial sponsorship of my PhD degree.

- My entire family and my friends for their continuous encouragement during this study.

LIST OF ABBREVIATIONS

ACE	Active Constellation Extension
ADC	Analog-to-digital Converter
AWGN	Additive White Gaussian Noise
BER	Bit Error Rate
BPSK	Binary Phase Shift Keying
CCDF	Complementary Cumulative Distribution Function
CE-OFDM	Constant Envelope OFDM phase modulation
CP	Cyclic Prefix
CR	Cognitive Radio
CSI	Channel State Information
DAC	Digital-to-analog Converter
DAR	Decision-aided Reconstruction
DRM	Digital Radio Mondiale
DVB	Digital Video Broadcasting
FCC	Federal Communications Commission
FDE	Frequency-domain Equaliser
FDM	Frequency-division Multiplexing
FFT	Fast Fourier Transform
GI	Guard Intervals
HPA	High-power Amplifier
IFFT	Inverse Fast Fourier Transform
IFT	Inverse Fourier Transform
ISI	Inter-symbol Interference

LNA	Low-noise Amplifier
LPF	Low Pass Filter
LTE	Long-term Evolution
OFDM	Orthogonal Frequency Division Multiplexing
OM-ACE	Offset Modulation with Active Constellation Extension
OM-OFDM	Offset Modulation
OTS	Off-the-Shelf
PAE	Power Added Efficiency
PAM	Pulse-amplitude Modulation
PAPR	Peak-to-average Power Ratio
PDF	Probability Density Function
PDP	Power Delay Profile
PEP	Peak Envelop Power
POCS	Projection Onto Convex Sets
PSK	Phase-shift Keying
PTS	Partial Transmitted Sequence
QAM	Quadrature Amplitude Modulation
QPSK	Quadrature Phase-shift Keying
RF	Radio Frequency
RMS	Root Mean Square
ROC	Receiver Operating Characteristic
SER	Symbol Error Rate
SLM	Selective Mapping
SNR	Signal-to-noise Ratio
TR	Tone Reservation
Wi-Fi	Wireless Fidelity
WiMAX	Worldwide inter-operability for Microwave Access

LIST OF NOTATION

$\chi(.,.)$	Lower incomplete gamma function
$\Gamma(.,.)$	Upper incomplete gamma function
$\Im$	The imaginary number field
$\log(.)$	The natural logarithm
$\log_2(.)$	The binary logarithm
erfc	Error function
$\max(.)$	The maximum
$\min(.)$	The minimum
$\Re$	The real number field
$\star$	Convolution
E [ ]	Expected value
$G(f)$	Fourier transform
$J_l(\beta)$	Bessel functions of the first kind of order l with argument β
$Q_u(.,.)$	Marcum Q-function

LIST OF SYMBOLS

α	Phase deviations of the OFDM signal
α_1	Real phase deviations of the OFDM signal
α_2	Imaginary phase deviations of the OFDM signal
β	Adapted phase deviation of an OM-OFDM signal
β_1	Adapted real phase deviation of an OM-OFDM signal
β_2	Adapted imaginary phase deviation of an OM-OFDM signal
λ	Decision threshold
$\overline{\Upsilon}$	Average signal-to-noise ratio
$\Phi(t)$	Phase of the offset modulated signal
$\Phi_1(t)$	Real OFDM phase mapping
$\Phi_2(t)$	Imaginary OFDM phase mapping
$\Phi_n(t)$	Phase of the band-pass noise
Φ_{1n}	Discrete real OFDM phase mapping
Φ_{2n}	Discrete imaginary OFDM phase mapping
σ	Variance
Υ	Signal-to-noise ratio
ς	Constant division term
ξ_{av}	Average energy per symbol
ξ_s	Energy per symbol
Ψ_{os}	Constant offset term
a	Non-centrality parameter
A_c	Signal amplitude
D	Decision metric
d	Euclidean distance
E_b	Energy per bit
E_s	Energy per symbol
E_t	Total energy per bit

E_w	Wasted energy per bit
f_c	Carrier frequency
f_d	Integer multiple of the modulation frequency
h	Modulation index
Hz	Hertz
K	Rician distribution factor
L	Maximum constellation extension limit
n	Additive white Gaussian noise
N	N-Point FFT/IFFT
n_c	Co-sinusoidal noise
N_o	Noise power spectrum
n_s	Sinusoidal noise
$N_s(t)$	Quadrature components of noise
$N_c(t)$	In-phase components of noise
P_{fa}	Probability of a false alarm
P_{md}	Probability of a missed detection
P_d	Probability of a detection
R_b	Data rate
T_s	The signal duration
T_G	Guard interval
$V_n(t)$	Envelope of the band-pass noise
W	Bandwidth occupancy
M	Constellation size

TABLE OF CONTENTS

CHAPTER 1

INTRODUCTION

1.1 BACKGROUND AND MOTIVATION

Orthogonal frequency division multiplexing (OFDM) has become a very popular method for high-data-rate communication, primarily because of its tight spectral efficiency and its robustness to multi-path fading. This has led to it being deployed in various standards, such as digital subscriber lines, digital video broadcasting (DVB), digital radio mondiale (DRM), worldwide inter-operability for microwave access (WiMAX) IEEE 802.16d standard, wireless fidelity (Wi-Fi) IEEE 802.11n standard and recently in long-term evolution (LTE). However, it is a well-known that OFDM is plagued by a large peak-to-average power ratio (PAPR) problem. This high PAPR occurs when the sinusoidal signals of the sub-carriers are added constructively. This results in a signal which consists of a number of infrequent peaks. This signal with infrequent peaks needs to be amplified before transmission through a channel. The irregularity of these peaks leads to inefficient use of the power amplifiers, amongst other things, which ultimately reduces the battery life of the mobile device, which is undesirable.

This has resulted in various methods being developed to reduce the PAPR of an OFDM transmission. These are clipping, decision-aided reconstruction clipping, coding, partial transmission sequence, selective mapping, companding transforms, active constellation extension (ACE), tone reservation and constant envelope OFDM phase modulation, amongst

others. However, these methods require high implementation complexity, additional bandwidth expansion or the transmission of side information to reconstruct the original message signal. Some of these methods also result in an average power increase, or lead to a severe bit error rate (BER) degradation as the number of carriers increases. Ideally a PAPR method which does not result in a number of the drawbacks that are being experienced by current methods in the field is required. In this thesis, such a method, called offset modulation, is proposed.

1.2 AUTHOR'S CONTRIBUTION AND OUTPUTS

1.2.1 Research contributions

The author's main research contribution can be summarised as follows

- A novel method called offset modulation (OM-OFDM) has been proposed to control the PAPR of an OFDM transmission for a targeted BER. The theoretical bandwidth occupancy of the proposed offset modulation signal was derived. Using these bandwidth occupancy results, a closed-form theoretical BER expression for an offset modulation transmission was derived and validated.

- A newly applied decision metric (D) has been introduced, which can be utilised throughout the PAPR field to compare various methods.

- An offset modulation with active constellation extension (OM-ACE) method has been proposed to control the PAPR of an OFDM transmission for a targeted BER. A closed-form BER expression for this OM-ACE transmission is presented and validated.

- A theoretical generic closed-form relationship between the probability of a missed detection (P_{md}) and the probability of a false alarm (P_{fa}) for any unknown deterministic signal (for instance OFDM and OM-OFDM) has been derived and validated.

- The receiver operating characteristic curves, which relate P_{md} to the P_{fa} for both a typical DVB-T2 OFDM and OM-OFDM transmission is presented.

1.2.2 Patents

The current patents that have been filed as outputs of this research are

- K. Dhuness and B. T. Maharaj, “An offset modulation scheme to control the PAPR of a signal", SA Patent, No. 2010/03368, provisional, May 2010.
- K. Dhuness and B. T. Maharaj, “Modulation of Signals", provisional - PCT/IB2011/052066, USPTO, May 2011.

1.2.3 Publications

The research as reflected in this thesis was partially based on the following conference and journal articles, published by the author

- K. Dhuness and B. T. Maharaj, “Comparative performance of OM-OFDM in broadband systems," Electronics Letters, vol 48, issue 2, pp. 127-129, January 2012.
- K. Dhuness and B. T. Maharaj, “A cognitive radio application of OM-OFDM," in Proceedings of the IEEE Africon, Livingston, Zambia, 13-15 September 2011, pp. 1-5. **Outstanding paper award**
- K. Dhuness and B. T. Maharaj, “An Offset Modulation scheme to control the PAPR of an OFDM transmission," in Proceedings of the IEEE 72nd Vehicular Technology Conference, Ottawa, Canada, 6-9 September 2010, pp. 1-5. **Invited paper**
- K. Dhuness, P. Botha and B. T. Maharaj, “A decision metric approach to PAPR performance analysis of an OM-OFDM transmission," in Proceedings of the Southern Africa Telecommunication Network and Application Conference, Stellenbosch, South Africa, 5-8 September 2010, pp. 1-6.

Two ISI accredited journal articles based on this work are currently under review.

1.3 OUTLINE OF THESIS

In Chapter 2, the OFDM concept is introduced and the origin of the PAPR problem associated with an OFDM transmission is presented. Various PAPR reduction methods in the field are discussed, and the drawbacks of these methods are presented.

An offset modulation method is developed in Chapter 3, which does not result in a number of the drawbacks experienced by current methods in the field. A closed-form bandwidth occupancy expression and BER expression for an OM-OFDM transmission is derived. Thereafter a newly applied power performance decision metric is introduced. This metric can be utilised throughout the PAPR field to compare various PAPR methods.

The proposed OM-OFDM method may appear to be similar if not identical to a well-known constant envelope OFDM phase modulation (CE-OFDM) method. In Chapter 4, the significant modulation and structural differences between an OM-OFDM and a CE-OFDM method are discussed. The OM-OFDM, OFDM and CE-OFDM methods are compared by using a BER analysis and the newly applied decision metric.

In Chapter 5, the proposed OM-OFDM method is compared to OFDM, as well as various other PAPR reduction methods, by utilising a power performance decision metric and a complementary cumulative distribution function, after which conclusions are drawn.

The author demonstrates, in Chapter 6, the ease with which an ACE method, which is a well-established PAPR reduction method, may be incorporated into an OM-OFDM transmission, resulting in an OM-ACE method. The proposed OM-ACE method is developed; thereafter the bandwidth occupancy of an OM-ACE transmission is introduced. The reasoning for the inclusion of the ACE method into an OM-OFDM transmission is discussed and a closed-form BER expression for an OM-ACE transmission is also presented. Thereafter the OFDM, clipped OFDM, OM-ACE and ACE methods are compared by using a BER performance analysis, power performance decision metric and complementary cumulative distribution function and conclusions are drawn.

In Chapter 7, the cognitive radio applications of OM-OFDM are investigated by studying the ability of a secondary user to detect OM-OFDM and OFDM transmissions. The receiver operating characteristic (ROC) expression for any unknown signal is derived and validated. The ROCs of OM-OFDM and OFDM transmissions are investigated, and conclusions are drawn.

Based on all these results, Chapter 8 summarises the conclusions of the various chapters and suggests opportunities for further research.

CHAPTER 2

ORTHOGONAL FREQUENCY DIVISION MULTIPLEXING

2.1 INTRODUCTION TO OFDM

In order to understand OFDM, it is useful to discuss frequency division multiplexing (FDM). In a FDM system [1], depicted in Fig. 2.1, multiple signals are transmitted simultaneously (in the same time slot) over different frequencies. Each sub-carrier contains different data streams and guard bands are used between sub-carriers to avoid inter-signal over-

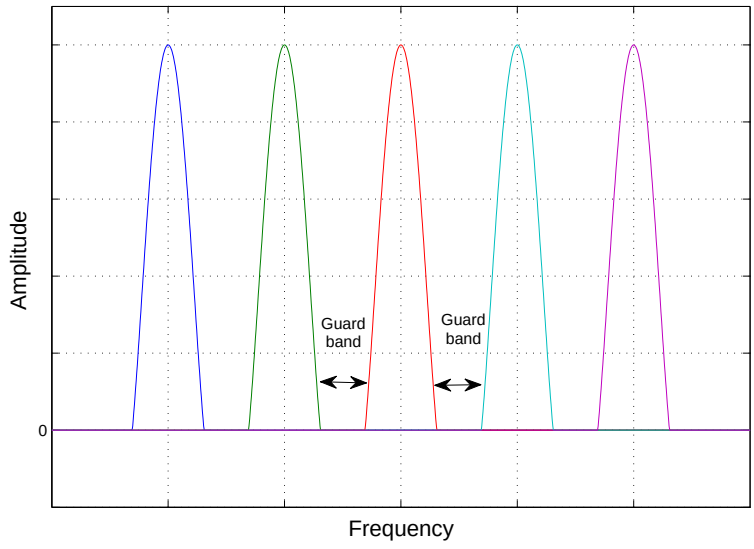

Figure 2.1: Frequency division multiplexing

lap/interference. Pulse-shaping filters are used to eliminate the inter-sub-carrier harmonics and thus eliminate inter-signal interference. Like FDM, OFDM [1] also uses multiple sub-carriers, but these sub-carriers are closely spaced to each other, depicted in Fig. 2.2, without causing inter-signal interference. This is possible because, as depicted in Fig. 2.2, the sub-carriers are orthogonal to each other, i.e. the peak of each sub-carrier coincides with the null of an adjacent sub-carrier. This type of orthogonal spacing removes the guard bands between adjacent sub-carriers and the subsequent inter-signal interference. A comparison between

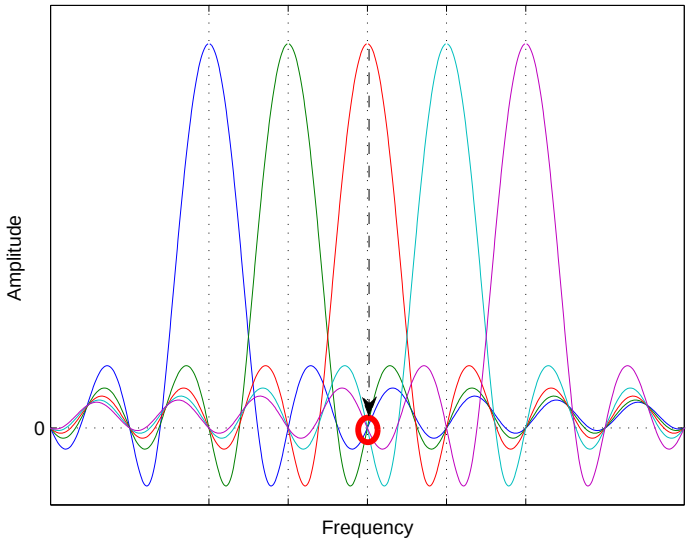

Figure 2.2: Orthogonal frequency division multiplexing

Fig. 2.1 and Fig. 2.2 indicates that OFDM requires less bandwidth than FDM, while transmitting the same amount of information. This translates to better spectral efficiency.

2.2 OFDM TRANSMITTER

In Fig. 2.3 an OFDM transmitter structure is presented. During an OFDM transmission [2], depicted in Fig. 2.3, binary input data are mapped (e.g. by using 4-QAM constellation) to complex symbols. These symbols undergo a serial-to-parallel conversion; thereafter pilot symbols are inserted. These pilot symbols will later be used by the equaliser to mitigate the effects of the channel. The subsequent symbols are passed through an inverse fast Fourier transform (IFFT), which places the complex input symbols orthogonal to each other. Part

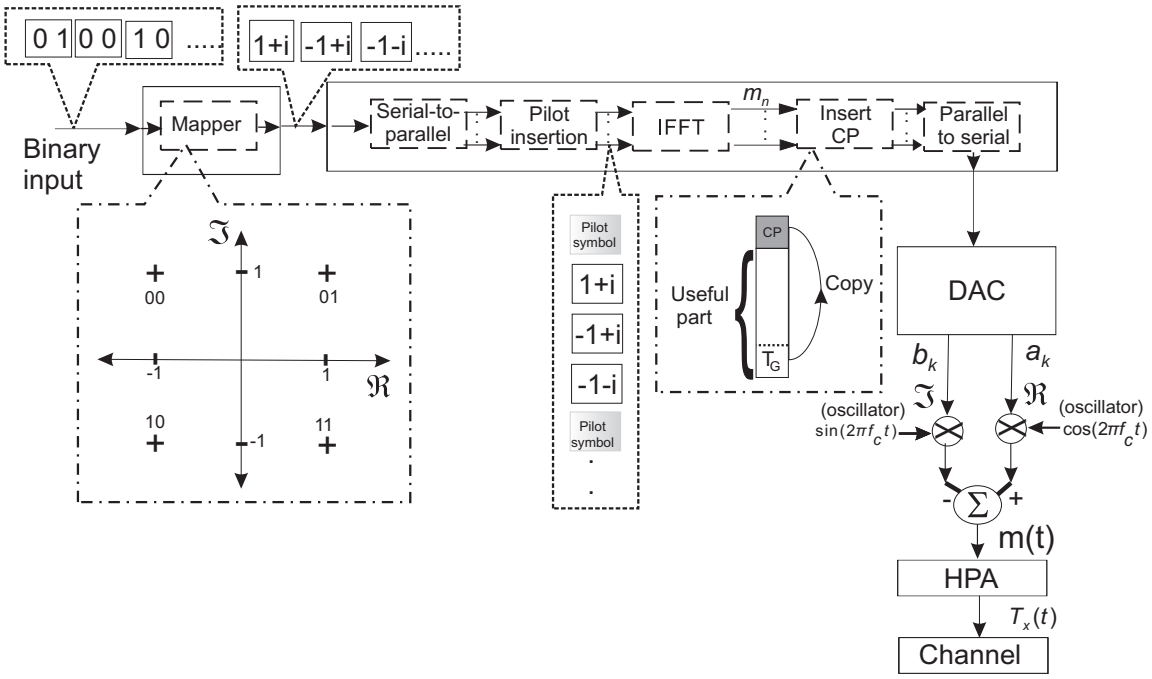

Figure 2.3: Orthogonal frequency division multiplexing transmitter structure

of the end of the resultant IFFT output (T_G guard interval) is copied and amended to the beginning of the signal. This process is referred to as adding a cyclic pre-fix (CP) or guard interval. This guard interval is used to mitigate some of the effects caused by multiple reflected, and delayed versions of the originally transmitted signal arriving at the receiver. The CP-amended IFFT output undergoes a parallel-to-serial conversion and is thereafter passed through a digital-to-analog converter (DAC). The subsequent real and imaginary components of the signals are modulated by using a sinusoid and co-sinusoid oscillator. The resultant real and imaginary modulated signals are combined and passed through a high-power amplifier (HPA).

This process can be mathematically explained, by considering that the IFFT is a transformation which maps the complex input data symbols (e.g. 4-QAM constellation symbols) $[x_0, x_1, ..., x_{N-1}]$ to OFDM symbols $[X_0, X_1, ..., X_{N-1}]$ such that the complex baseband

OFDM signal is given by [3]

$$m_n = \frac{1}{\sqrt{N}} \sum_{k=0}^{N-1} X_k e^{j\frac{2\pi nk}{N}}, \qquad n = 0,1,.....,N-1 \tag{2.1}$$

where N refers to the N-point IFFT and X_k represents the complex signal output $(a_k + jb_k)$ of the IFFT. The $e^{j\frac{2\pi nk}{N}}$ expression in Eq (2.1) uniformly spaces the OFDM $[X_0, X_1, ..., X_{N-1}]$ symbols. Thereafter, as depicted in Fig. 2.3, a CP or guard interval is amended to the resultant complex base band OFDM signal $\{X_v, n = 0,1....,N-1\}$, where the first X_v samples constitute the CP prefix. The CP is amended to the baseband OFDM signal between $n = -v,...,0$. As depicted in Fig. 2.3, this results in the signal in the $n = N-v, N-v+1,.....,N-1$ interval being placed in the $n = -v,-v+1,...,0$ interval [3]. The output of this CP block undergoes a parallel-to-serial conversion and is fed into a DAC. Thereafter the real and imaginary components are modulated by using an oscillator. The subsequent carrier frequency signal is then written as

$$\begin{aligned} m(t) &= \frac{1}{\sqrt{N}} \Re\left\{ \sum_{k=0}^{N-1} X_k e^{j2\pi t(f_c + \frac{k}{T_s})} \right\}, \qquad 0 \le t < T_s \\ &= \frac{1}{\sqrt{N}} \Re\left\{ \sum_{k=0}^{N-1} X_k e^{j(2\pi f_c t + \omega_k t)} \right\}. \end{aligned} \tag{2.2}$$

Here, $\Re\{.\}$ refers to the real components, T_s is the signal duration, f_c is the carrier frequency and $\omega_k = \frac{2\pi k}{T_s}$ are the subcarrier frequencies. After applying an Euler transform to Eq (2.2), the transmitted carrier frequency signal may be written as

$$\begin{aligned} m(t) &= \frac{1}{\sqrt{N}} \Re\left\{ \sum_{k=0}^{N-1} (a_k + jb_k)(\cos(2\pi f_c t + \omega_k t) + j\sin(2\pi f_c t + \omega_k t)) \right\} \\ &= \frac{1}{\sqrt{N}} \sum_{k=0}^{N-1} a_k \cos(2\pi f_c t + \omega_k t) - b_k \sin(2\pi f_c t + \omega_k t). \end{aligned} \tag{2.3}$$

The resultant signal $m(t)$ is amplified, by passing it through a HPA. In the case of a linear amplification process, the output can be written as

$$T_x(t) = A \cdot m(t). \tag{2.4}$$

In Eq (2.4), *A* refers to the amplification factor. The subsequent amplified OFDM signal is then transmitted through a channel.

2.3 OFDM TRANSMISSION

There are many kinds of channel interferences in wireless communication. A typical transmission might experience multi-path fading, depicted in Fig. 2.4(a), consisting of a direct path and two reflections. This type of channel interference is typically represented, as shown in Fig. 2.4(b), by a power delay profile (PDP). The PDP [4], in Fig. 2.4(b), represents each path (including amplitude degradation) of a transmission and the subsequent path delays (τ_0, τ_1 and τ_2), introduced by the channel. The purpose of the CP inclusion in Fig. 2.3

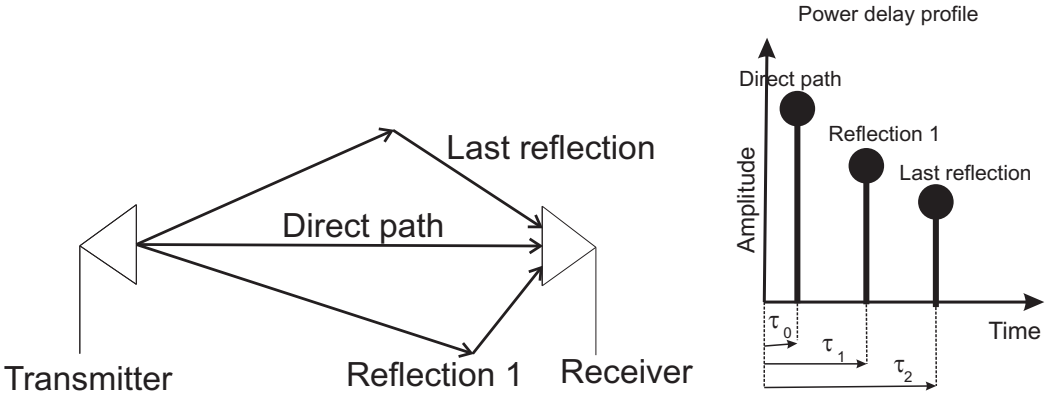

(a) 3-ray channel effects (b) 3-Tap power delay profile

Figure 2.4: Typical channel

is to mitigate some of the channel effects. The multi-path channel, depicted in Fig. 2.4(a), causes direct and multiple reflected versions of the signal of distinct signal strengths, phases and delays being received. This delay between the different received signals causes inter-symbol interference (ISI). In an OFDM system the CP [5] is used to mitigate these ISI effects.

This can be thought of as trying to communicate with a person at the end of a long cave. If one continuously yells without pausing, the person at the end of the cave will be unable to reconstruct the message because of the echoes (reflections). However, if each word (transmission) is separated by a pause of a few seconds, the echoes die away before the next word is spoken and the listener can hear each word. A CP insertion is seen to represent this

pause between transmissions or in this analogy, to let the echoes die away. A CP is amended to the beginning of the useful information of the signal. If zeros were sent in the CP, this would cause the radio frequency (RF) power amplifier to switch on and off and this might cause unwanted spectral output [5]. This interval can still be used to represent pauses in the transmission at the receiver if known signals are sent in this interval. As shown in Fig. 2.5,

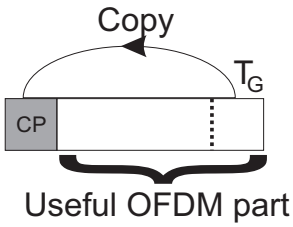

Figure 2.5: Cyclic prefix insertion

a CP is generated by amending a portion of the end of a signal to the front of the signal. Depending on the channel, an OFDM signal $T_x(t)$ linearly convolves with the channel $H(t)$ (e.g. the PDP in Fig. 2.4(b)) during its transmission. However an equaliser requires circular convolution [6] $T_x(t) \star H(t)$ in the time-domain, which is equivalent to multiplication in the frequency domain $t_x(f) \cdot h(f)$. Here $t_x(f)$ is a frequency-domain representation of the signal and $h(f)$ is the channel transfer function. A linearly convolved signal is different from a circularly convolved signal [6]. An equaliser will later use this circularly convolved relationship ($t_x(f) \cdot h(f)$) to mitigate the effects of the channel.

In order to achieve circular convolution a CP is inserted, i.e. a portion of the end of a signal is amended to the front of the signal. After adding a CP to $T_x(t)$ and transmitting the signal through the channel ($H(t)$), the desired circular convolution $T_x(t) \star H(t)$ may be achieved, provided the CP is of sufficient length, and the received signal removes the CP. The transmitted signal encounters both channel effects H(t) and additive white Gaussian noise (AWGN) denoted by $n(t)$. The subsequent received signal can be written as

$$R_x(t) = T_x(t) \cdot H(t) + n(t). \tag{2.5}$$

2.4 OFDM RECEIVER

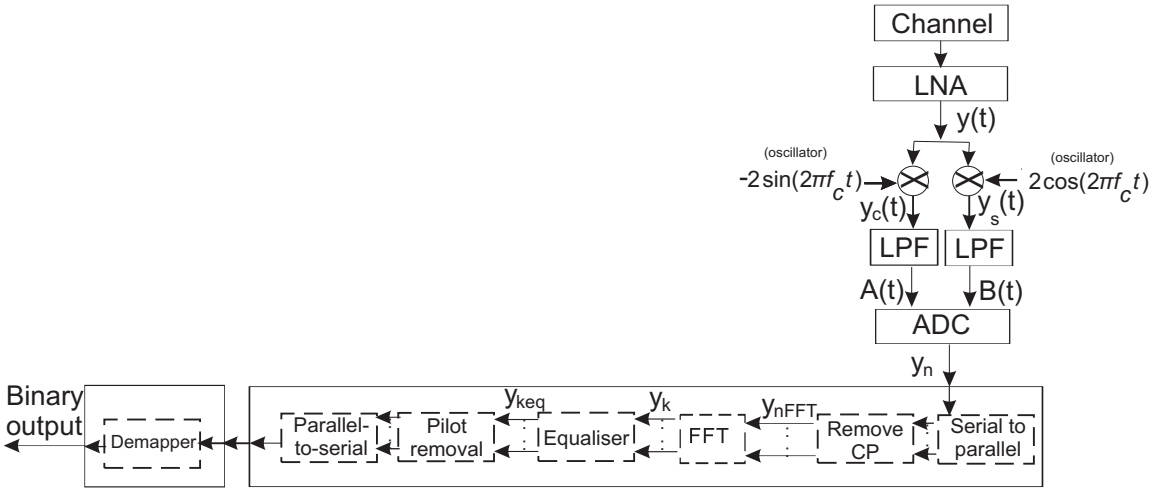

Figure 2.6: Orthogonal frequency division multiplexing receiver structure

At the receiver [2], as depicted in Fig. 2.6, the incoming signal is passed through a low-noise amplifier (LNA). In the case of a linear amplification process with an amplification factor of a, the output can be written as

$$\begin{aligned} y(t) &= (T_x(t)\cdot H(t)+n(t))\cdot a \\ &= m(t)\cdot \check{H}(t)+\check{n}(t). \end{aligned} \tag{2.6}$$

In Eq (2.6), $\check{H}(t) = A\cdot H(t)\cdot a$ and $\check{n}(t) = n(t)\cdot a$. Thereafter the signal is multiplied by a co-sinusoid and a sinusoid; this results in

$$\begin{aligned} y_c(t) &= 2\left(\frac{1}{\sqrt{N}}\sum_{k=0}^{N-1}\check{H}(t)\cdot(a_k\cos(2\pi f_c t+\omega_k t)-b_k\sin(2\pi f_c t+\omega_k t))+\check{n}(t)\right)\cdot\cos(2\pi f_c t) \\ &= \frac{1}{\sqrt{N}}\sum_{k=0}^{N-1}\Big(\check{H}(t)\cdot a_k\cos(\omega_k t)+\check{H}(t)\cdot a_k\cos(4\pi f_c t+\omega_k t)-\check{H}(t)\cdot b_k\sin(4\pi f_c t+\omega_k t) \\ &\quad -\check{H}(t)\cdot b_k\sin(\omega_k t)\Big)+\cos(2\pi f_c t)\cdot\check{n}(t) \end{aligned} \tag{2.7}$$

and

$$y_s(t) = -2\left(\frac{1}{\sqrt{N}}\sum_{k=0}^{N-1}\check{H}(t)\cdot(a_k\cos(2\pi f_c t+\omega_k t)-b_k\sin(2\pi f_c t+\omega_k t))+\check{n}(t)\right)\cdot\sin(2\pi f_c t)$$

$$= \frac{1}{\sqrt{N}}\sum_{k=0}^{N-1}\Big(-\check{H}(t)\cdot a_k\sin(4\pi f_c t+\omega_k t)+\check{H}(t)\cdot a_k\sin(\omega_k t)+\check{H}(t)\cdot b_k\cos(\omega_k t)$$
$$-\check{H}(t)\cdot b_k\cos(4\pi f_c t+\omega_k t)\Big)-\sin(2\pi f_c t)\cdot\check{n}(t). \tag{2.8}$$

The low pass filter (LPF) removes the high-frequency components ($4\pi f_c t$). This results in

$$\begin{aligned} A(t) &= \frac{1}{\sqrt{N}}\sum_{k=0}^{N-1}\Big(\check{H}(t)\cdot a_k\cos(\omega_k t)-\check{H}(t)\cdot b_k\sin(\omega_k t)\Big)+\cos(2\pi f_c t)\cdot\check{n}(t) \\ &= \frac{1}{\sqrt{N}}\sum_{k=0}^{N-1}\Big(\check{H}(t)\cdot a_k\cos(\omega_k t)-\check{H}(t)\cdot b_k\sin(\omega_k t)\Big)+\check{n}_c(t) \end{aligned} \tag{2.9}$$

and

$$\begin{aligned} B(t) &= \frac{1}{\sqrt{N}}\sum_{k=0}^{N-1}\Big(\check{H}(t)\cdot a_k\sin(\omega_k t)+\check{H}(t)\cdot b_k\cos(\omega_k t)\Big)-\sin(2\pi f_c t)\cdot\check{n}(t) \\ &= \frac{1}{\sqrt{N}}\sum_{k=0}^{N-1}\Big(\check{H}(t)\cdot a_k\sin(\omega_k t)+\check{H}(t)\cdot b_k\cos(\omega_k t)\Big)-\check{n}_s(t) \end{aligned} \tag{2.10}$$

where $\check{n}_c(t)$ and $\check{n}_s(t)$, refer to the noise components. The resultant signal is passed through an analog-to-digital converter (ADC), thus $t=\frac{nT_s}{N}$ and $\omega_k=\frac{2\pi k}{T_s}$. Thereafter the real components (Eq (2.9)) and the imaginary components (Eq (2.10)) are placed in a complex form given by

$$\begin{aligned} y_n &= (A_n+j\cdot B_n)+n_c s \\ &= \frac{1}{\sqrt{N}}\sum_{k=0}^{N-1}\check{H}_n\cdot\left(a_k\cos\left(\frac{2\pi nk}{N}\right)-b_k\sin\left(\frac{2\pi nk}{N}\right)\right) \\ &\quad +j\cdot\left(a_k\sin\left(\frac{2\pi nk}{N}\right)+b_k\cos\left(\frac{2\pi nk}{N}\right)\right)+n_c s \\ &= \frac{1}{\sqrt{N}}\sum_{k=0}^{N-1}\check{H}_n\cdot\left((a_k+jb_k)\cdot\left(\cos\left(\frac{2\pi nk}{N}\right)+j\cdot\sin\left(\frac{2\pi nk}{N}\right)\right)\right)+n_c s \\ &= \frac{1}{\sqrt{N}}\sum_{k=0}^{N-1}\check{H}_n\cdot X_k e^{j\frac{2\pi nk}{N}}+n_{cs}. \end{aligned} \tag{2.11}$$

In Eq (2.11), n_{cs} represents complex noise, $\check{H}_n$ is a discrete representation of the channel, A_n

and B_n are discrete ($t = \frac{nT_s}{N}$) representations of Eq (2.9) and Eq (2.10), respectively. This signal is similar to the initially transmitted signal Eq (2.1). The subsequent discrete signal undergoes a serial-to-parallel conversion and is passed into the CP removal unit. Provided the CP is of a sufficient length and the CP is removed, the input into the fast Fourier transform (FFT) can be written as

$$y_{nFFT} = \frac{1}{\sqrt{N}} \sum_{k=0}^{N-1} \check{H}_n \star X_k e^{j\frac{2\pi nk}{N}} + n_{cs}. \tag{2.12}$$

The FFT maps the OFDM symbols $[X_0, X_1, ...X_{N-1}]$ to constellation symbols $[x_0, x_1, ...x_{N-1}]$. The output of the FFT can be written as

$$y_k = h_k \cdot x_k + \eta_k \qquad k = 0, ..., N-1 \tag{2.13}$$

where h_k, is the channel impulse response and η_k is additive noise. At the output of the FFT, an equaliser estimates the channel effects ($\hat{h_k}$). This estimate is based on comparing the transmitted pilot symbols x_{ks} (which are known at the receiver) with the received pilot symbols y_{ks} ($\hat{h_k} = \frac{y_{ks}}{x_{ks}}$) and thereafter interpolating such that a channel estimate $\hat{h_k}$ can be obtained. Thereafter the channel effects can be mitigated by an equaliser as indicated below

$$\begin{aligned} y_{keq} &= \frac{h_k \cdot x_k + \eta_k}{\hat{h_k}}, \qquad k = 0, 1, ...N-1 \\ &\approx x_k + n_k \end{aligned} \tag{2.14}$$

where n_k refers to noise. The pilot symbols are removed and a parallel-to-serial conversion is performed. The symbols are de-mapped, resulting in the received binary data.

2.5 BRIEF HISTORY OF OFDM

The first OFDM-like radio found in the literature was the Kineplex system [7], developed in 1958. This radio used 20 tones, each differentially phase modulated and separated by 110 Hz with a total approximate bandwidth of 3400 Hz. Thereafter, a military radio called KATHRYN was developed in 1967 [8]. KATHRYN used 34 parallel phase modulated channels with a 82 Hz spacing. In 1968, ANDEFT [9] was created, this modem used 66 frequency

differentially phase modulated tones, each separated by 40 Hz. Theoretical contributions to the development of OFDM were made by B. R. Saltzberg [10] in 1967 and R. W. Chang [11] in 1968. Thereafter, Chang in 1970 obtained a US patent [12] for OFDM. Saltzberg in the same year obtained a patent [12] for an orthogonal transmission system. In 1971 Weinstein and Ebert [13] suggested using a discrete Fourier transform (DFT) for orthogonal sub-carrier placement. In 1985 Cimini [14], suggested using OFDM for wireless communication.

In the 1990's the work of J. M. Cioffi et al. [15–18], led to the acceptance of OFDM in the digital subscriber lines standards. It was the computational complexity required to implement the DFT, that had halted the implementation until the 1990's. Ever since then, OFDM has been used in various standards such as DVB, DRM, WiMAX, Wi-Fi and recently in LTE. However, no technology is perfect and OFDM is no different. A major problem associated with an OFDM transmission is its large PAPR. This high PAPR reduces the efficiency of the amplifiers, which is not desirable.

2.6 PEAK-TO-AVERAGE POWER RATIO

As previously mentioned, the sinusoidal signals of the sub-carriers of an OFDM transmission are given by

$$m(t) = \frac{1}{\sqrt{N}} \sum_{k=0}^{N-1} \left(a_k \cos(2\pi f_c t + \omega_k t) - b_k \sin(2\pi f_c t + \omega_k t) \right). \tag{2.15}$$

These series of sinusoidal signals add constructively, resulting as depicted in Fig. 2.7, in an OFDM transmission which consists of a number of infrequent peaks. This OFDM signal with infrequent peaks needs to be amplified before transmission through a channel.

This amplification process can be represented by Fig. 2.8(a). In this figure the blue curve is called the ideal gain characteristic of the amplifier, and the slope/gradient of this curve typically dictates the amount by which the incoming signal will be amplified. In practice, however, a typical gain curve indicated in green will be encountered. Ideally the amplifier should operate in the linear region of the gain curve, such that an exact amplified

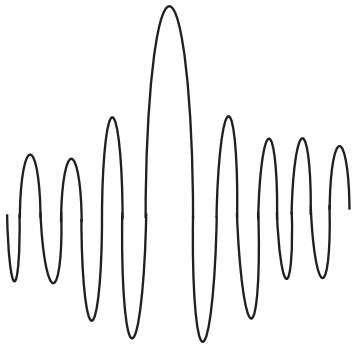

Figure 2.7: OFDM time-domain signal representation

output of the input signal is produced.

In Fig. 2.8(a), the bottom (black) input is an OFDM signal, which needs to be amplified and the output is represented by the (red) amplified OFDM signal, which is transmitted across the channel. For this type of OFDM signal, depicted in Fig. 2.8(a), the power amplifier would on average operate (at the red point) far below the optimum operating point (purple point). The power amplifier is powered up to just above the optimum operating point. However, on average, the amplifier is operated far below (at the red point) the optimum operating point. The region between these two points (optimum operational and average operational point) is reserved for amplification of the irregular peak values of an OFDM transmission.

On the contrary, for a sinusoid signal, depicted in Fig. 2.8(b), the power amplifier would on average operate just below (red point) the optimum operating point. This is closer to the optimum operating point than its OFDM counterpart. As previously mentioned, an OFDM signal backs off from its optimum operating point in order to accommodate the peaks of the signal. If a sufficient back-off were not present, as shown Fig. 2.8(c), the incoming signal would operate outside of the linear region of the amplifier. This would result in clipping and a subsequent BER degradation. For illustration purposes the optimum operating points and average operating points, from Fig. 2.8(a) and Fig. 2.8(b), are placed in Fig. 2.9. This represents the power efficiency characteristic curve of a standard off-the shelf (OTS) class AB amplifier. In Fig. 2.9 the y-axis indicates the power amplifier efficiency and

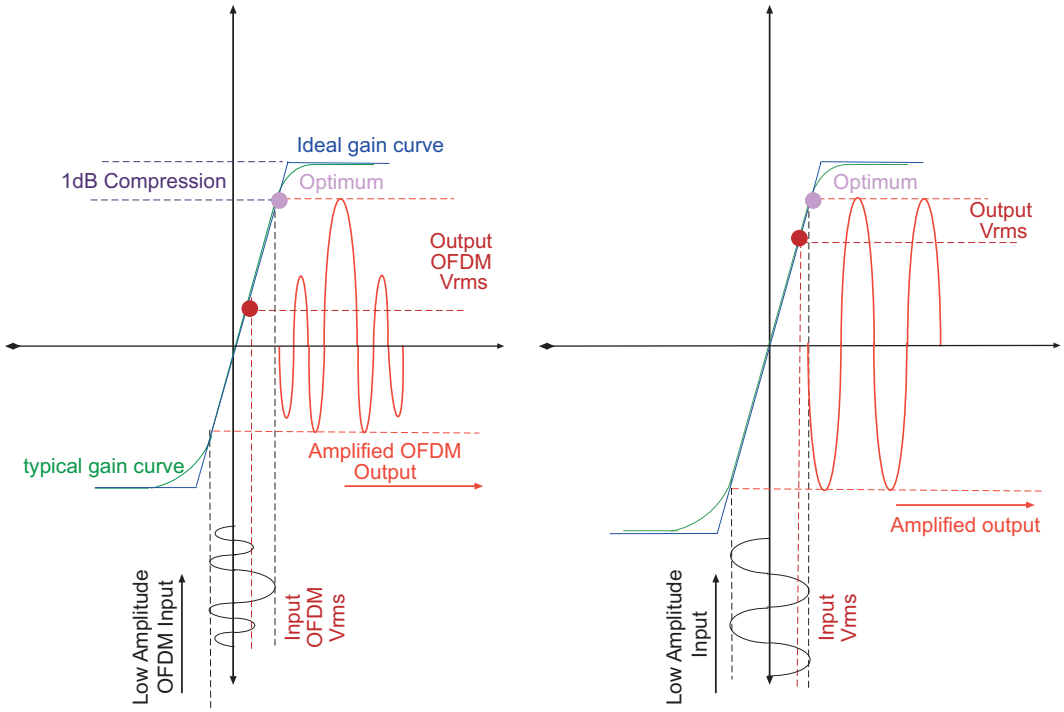

(a) OFDM amplification

(b) Sinusoid amplification

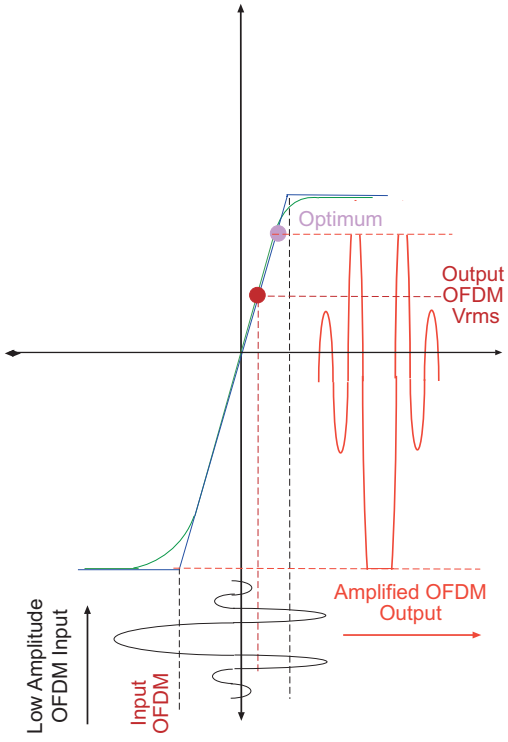

(c) Clipped OFDM amplification

Figure 2.8: An amplification process depiction

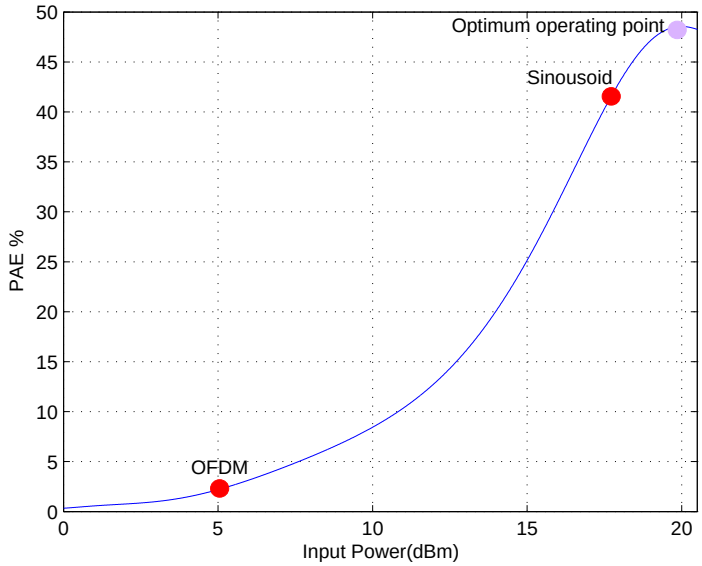

Figure 2.9: Typical power efficiency characteristics of a standard off-the shelf amplifier

the x-axis represents the average input power. From this illustration, when operating the amplifier in the upper regions, it is evident that the amplifier's efficiency is roughly 48%.

In the lower regions, this efficiency exponentially decays to only a few percent. In Fig. 2.9 it is seen that the sinusoid transmission is a more power-efficient transmission than its OFDM counterpart, which has an efficiency of a few percent. It is this inefficient use of the amplifier, due to the nature of the OFDM signal, which ultimately reduces the battery of a mobile device. An indication of the efficiency at which an amplifier is being operated can be obtained by using the PAPR term. The PAPR of a particular base band transmission is commonly defined as [19]

$$\text{PAPR}\{m_n\} = \max_{0\leq n<NL-1} \frac{|m_n|^2}{\text{E}\{|m_n^2|\}}. \tag{2.16}$$

In Eq (2.16), m_n refers to the signal of interest, N refers to the number of sub-carriers, L is the oversampling factor and $E\{\cdot\}$ is the expected value. For a sinusoidal transmission, depicted in Fig. 2.8(b), the PAPR is 3 dB [20], this indicates that the power amplifier is being used reasonably efficiently. Similarly, for an OFDM transmission, depicted in Fig. 2.8(a), the PAPR could be approximately 12 dB [21]. As the PAPR value of the transmission increases

as suggested in Fig. 2.9, the power amplifier efficiency exponentially decreases.

2.7 PEAK ENVELOPE POWER

Another term, called peak envelop power (PEP) is used to describe the characteristics of a particular transmission. The PEP of a complex pass band signal $m(t)$ is defined as [22]

$$\text{PEP}\{m(t)\} = \max|m(t)|^2. \tag{2.17}$$

PEP represents the maximum power of a complex baseband signal $m(t)$.

2.8 A LITERATURE REVIEW OF VARIOUS PAPR METHODS

Various methods [19, 22, 23] have been suggested to reduce the PAPR. These include clipping [19, 22–32], decision-aided reconstruction clipping [28], coding [23, 33–42], partial transmission sequence [22, 43–51], selective mapping [22, 52–58], companding transforms [59–67], active constellation extension [68–74], tone reservation [23, 75–81] and CE-OFDM [82–90], amongst others.

2.8.1 Clipping

Clipping [19, 22–32] is the simplest method of reducing the PAPR, as demonstrated in Fig. 2.8(c), by limiting the peak amplitude level of the input signal to a predetermined level. This clipping process is commonly denoted by [22]

$$m(t)^c = \begin{cases} -\text{A} & m(t) \leq -\text{A} \\ m(t) & |m(t)| < \text{A} \\ \text{A} & m(t) \geq \text{A}. \end{cases} \tag{2.18}$$

In Eq (2.18), $m(t)^c$ is the clipped OFDM transmission, $m(t)$ represents the OFDM transmission and A is the predetermined amplitude level. When classically clipping a signal (Fig. 2.10), at various clipping ratios, both in-band and out-of-band distortions are intro-

duced. Where the clipping ratio (CR) is defined as [22]

$$\text{CR} = \frac{A}{V_{rms}} \tag{2.19}$$

here, V_{rms} is the root mean square (RMS) value of the OFDM transmission. In order to minimise the in-band distortion, the classically clipped OFDM signal needs to be oversampled. To limit the out-of-band distortion, the clipped OFDM signal, depicted in Fig. 2.11, is filtered before transmission. The resultant filtered transmission is depicted in Fig. 2.12.

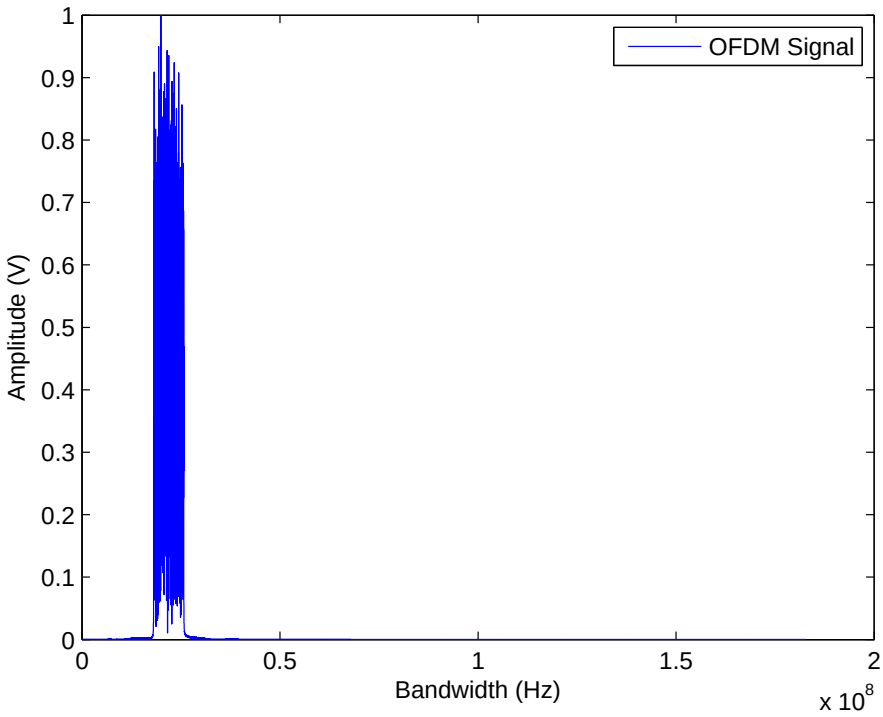

Figure 2.10: Normalised OFDM transmission

At the receiver, the clipped samples can be reconstructed by using a number of methods [19, 23, 27, 28].

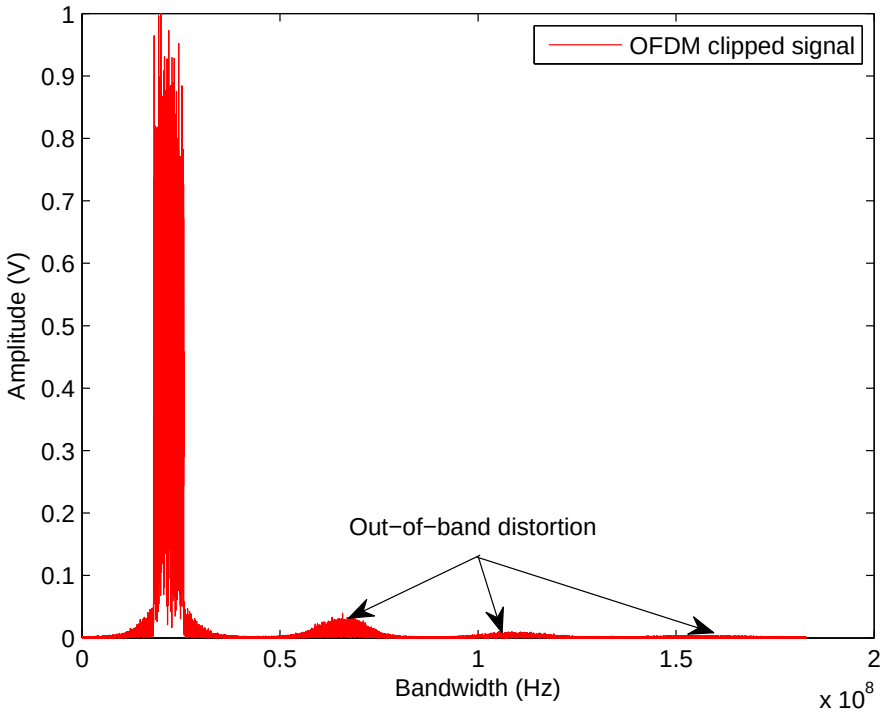

Figure 2.11: Normalised clipped OFDM transmission

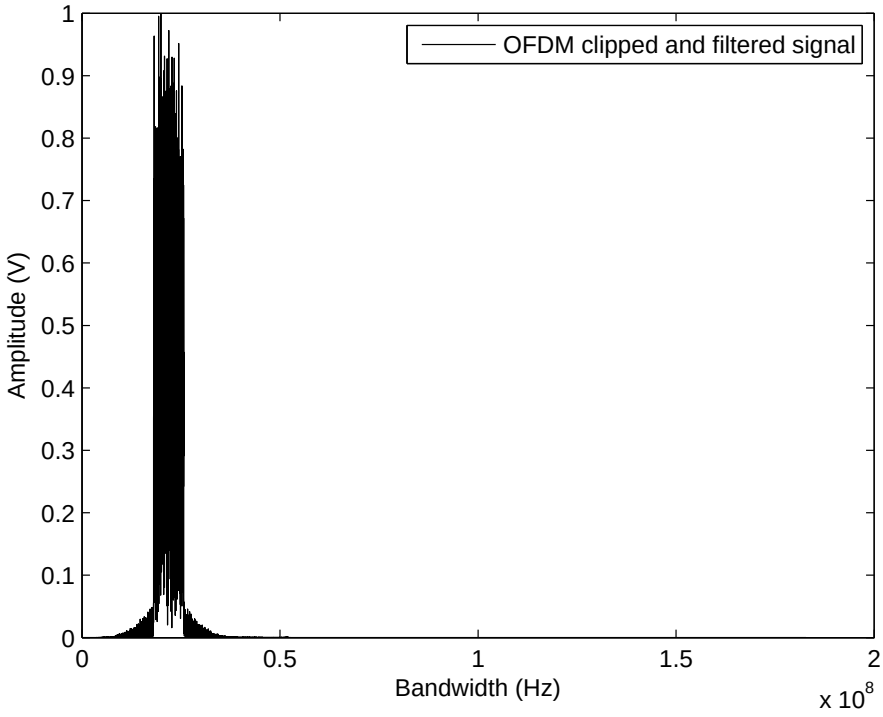

Figure 2.12: Normalised clipped and filtered OFDM transmission

Kim [28] has recommended using an iterative process called decision-aided reconstruction (DAR) clipping to reconstruct the clipped signal. During the DAR process, as depicted in

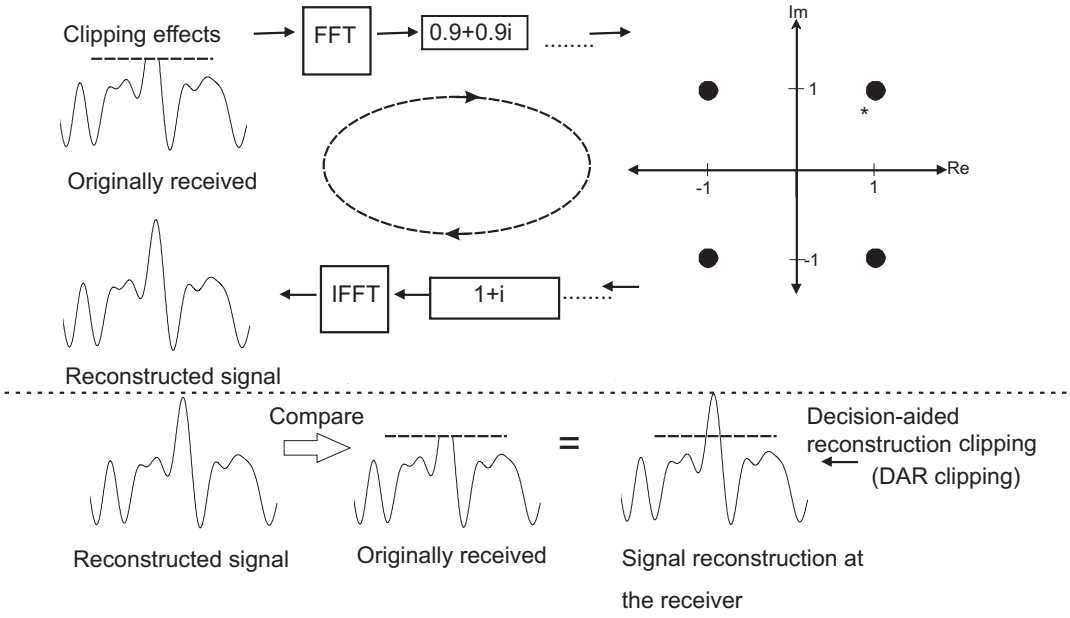

Figure 2.13: Decision-aided reconstruction process

Fig. 2.13, the received clipped OFDM signal is passed through a traditional OFDM receiver process. The received noisy clipped symbols (e.g. $0.9+0.9\text{i}, \ldots$) are compared to a set of known transmitted symbols (e.g. $1+\text{i}$, $1-\text{i}$, $-1-\text{i}$ and $-1+\text{i}$); where the most likely symbols (e.g. $1+\text{i}$, ...) are selected as the possible original symbols. These newly selected symbols (e.g. $1+\text{i}$, ...) are passed through the OFDM transmission process to produce a reconstructed OFDM signal. The originally received signal and reconstructed signals are compared. The receiver is assumed to have knowledge of the clipping threshold. By using this knowledge in regions above the clipping threshold, a DAR clipped signal is produced by amending the reconstructed signal to the originally received signal.

This DAR clipped signal is passed through an OFDM receiver process and thereafter through the OFDM transmission process. The subsequently reconstructed signal is compared to the originally received OFDM signal. With knowledge of this clipping threshold, further amendments are made to the originally received OFDM signal. This process is iteratively continued until convergence is reached. A limiting factor of clipping, as well as DAR clipping, is that as the number of peak amplitudes increases, this leads to a severe

degradation. Furthermore, the iterative nature of the DAR technique requires increased computational complexity. In addition, the DAR method is not suitable for real world frequency selective fading conditions.

2.8.2 Coding

In contrast to clipping, coding [23, 33–42] can also be used to reduce the PAPR, by selecting a codeword which minimises the PAPR. Various coding schemes have been recommended by Jiang [23] and Jones [34]. Jones [34], as shown in Fig. 2.14, has recommended using a block encoding scheme to reduce the PAPR of a transmission. During this process, depicted

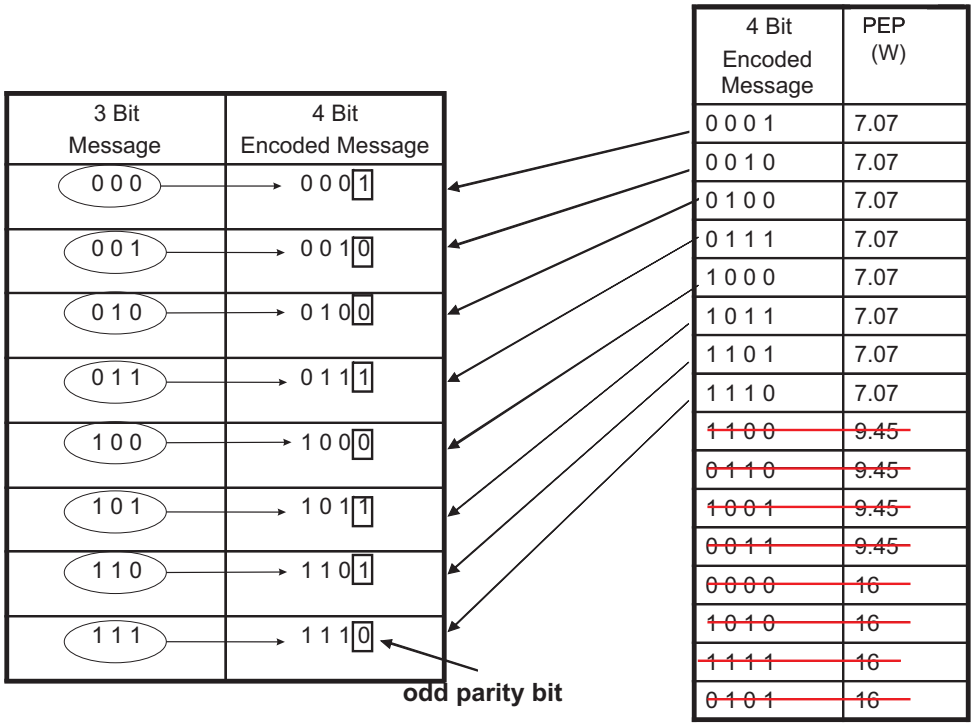

Figure 2.14: Coding

in Fig. 2.14, each 3-bit message will be encoded onto a 4-bit encoded message. All possible 4-bit encoded messages, as well as their subsequent PEP, are determined. All 4-bit encoded messages with large PEPs are eliminated. The 3-bit message is mapped onto the remaining low PEP 4-bit encoded message. In this particular case, for the 4-bit encoded message, the first 3-bits of the codeword and message are the same; the fourth bit is used as an odd parity check bit to determine the presence of an error in the transmission. An error in transmission

is observed if the received encoded message does not contain either three 1's or three 0's. Davis [33] has further shown that it is possible to combine block coding (with its encoding, decoding and error-correcting capability) and Golay complementary sequences (with their attractive PAPR properties), to reduce the PAPR. Coding can reduce the PAPR; however, it is not always possible to achieve a specific PAPR value. In certain cases coding gain is sacrificed for this PAPR decrease. In addition, an exhaustive search for good codewords for an OFDM system with a large number of carriers is difficult.

2.8.3 Partial transmitted sequence

An alternative method, employed in PAPR reduction, is the partial transmitted sequence (PTS) [22, 43–51] technique. In this PTS technique, depicted in Fig. 2.15, the input data block of N symbols is partitioned into V disjointed equally sized sub-blocks, which can be written as [22]

$$x = [x_1, x_2, x_3 \ldots\ldots, x_V]^T. \tag{2.20}$$

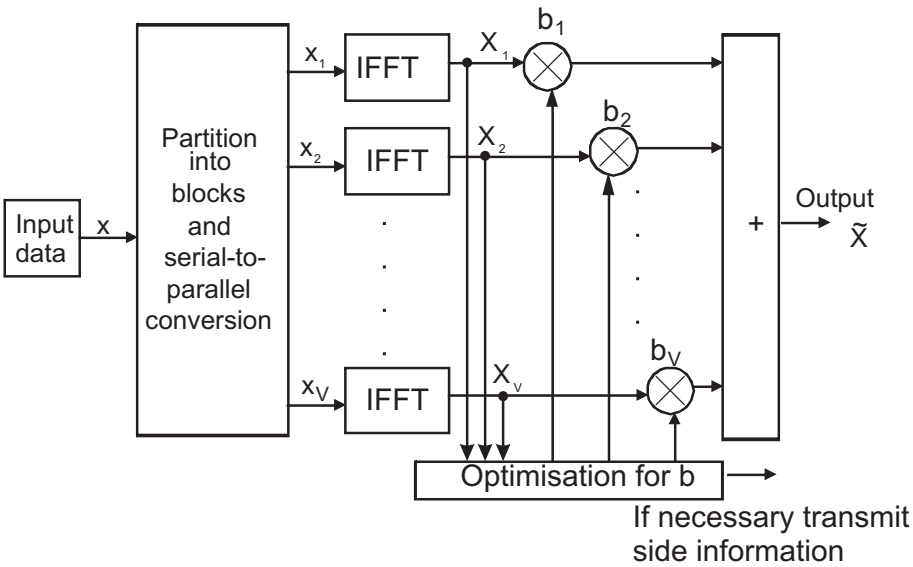

Figure 2.15: Partial transmitted sequence [22]

These sub-blocks are inverse fast Fourier transformed. Thereafter, each partitioned sub-block

is multiplied by a corresponding complex phase rotation factor $b_v = e^{j\phi v}$, $v = 1,2,....V$ to yield

$$\tilde{X} = \sum_{v=1}^{V} b_v \cdot IFFT\{x_v\} = \sum_{v=1}^{V} b_v \cdot X_v. \tag{2.21}$$

The objective of this phase rotation is to combine these sub-blocks optimally to achieve a minimum PAPR. The phase rotation factor is chosen such that [43]

$$[b_1, b_2...., b_V] = \arg\min_{[b_1,b_2....,b_V]} \left(\max_{n=0,1....N-1} \left| \sum_{v=1}^{V} b_v \cdot X_v \right| \right). \tag{2.22}$$

A limiting factor of PTS is that it requires high computational overhead to find an optimum phase-rotated sub-block combination and requires additional side information to be transmitted to allow the receiver to reconstruct the original signal.

2.8.4 Selective mapping

In selective mapping (SLM) [22,52–58], depicted in Fig. 2.16, the input data block is mapped onto different candidate data blocks, all representing the same information as the original data block. These subsequent mapped data blocks are inverse fast Fourier transformed and the data transmission with the lowest PAPR is selected for transmission.

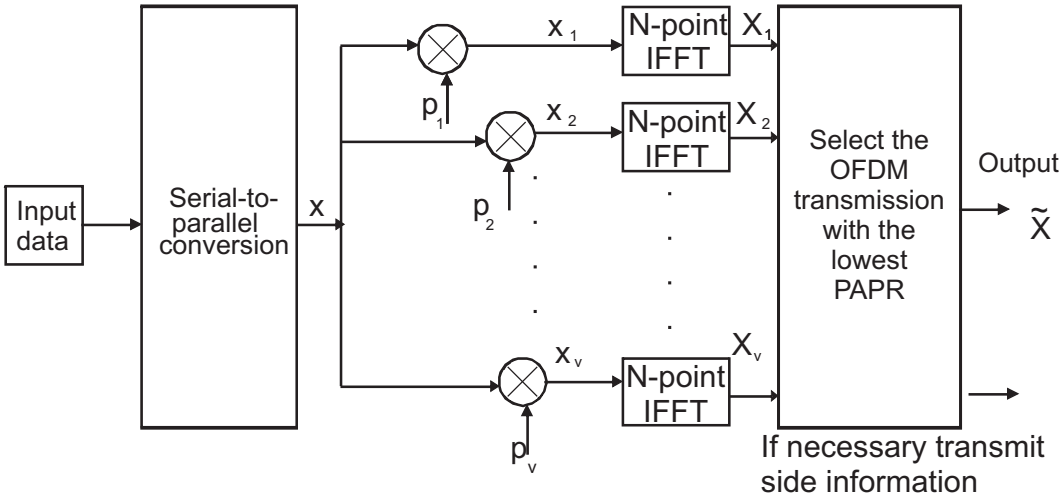

Figure 2.16: Selective mapping [22]

For a SLM transmission the input data block, given by [52]

$$x = [x_1, x_2, x_3 \ldots\ldots\ldots, x_N] \tag{2.23}$$

is multiplied by v different phase sequences each of length N. These phase sequences can be written as

$$\begin{aligned} p_V &= [p_{\{V,1\}}, p_{\{V,2\}}, p_{\{V,3\}} \ldots\ldots\ldots, p_{\{V,N\}}]^T && (2.24) \\ &= [e^{j\phi_{\{V,1\}}}, e^{j\phi_{\{V,2\}}}, e^{j\phi_{\{V,3\}}} \ldots\ldots\ldots, e^{j\phi_{\{V,N\}}}]^T. && (2.25) \end{aligned}$$

In Eq (2.24), $V = 1, 2, 3 \ldots\ldots v$, $\phi_{\{V,1\}}, \phi_{\{V,2\}} \ldots\ldots\ldots \phi_{\{V,N\}} \in [0, 2\pi)$. This multiplication of Eq (2.23) with Eq (2.24) produces modified data blocks, all representing the same information as the original data block given by

$$x_V = [x_{\{V,1\}}, x_{\{V,2\}}, x_{\{V,3\}} \ldots\ldots\ldots, x_{\{V,N\}}]^T, \tag{2.26}$$

where as previously mentioned $V = 1, 2, 3 \ldots\ldots v$. The subsequent signals in Eq (2.26) are passed through an IFFT and thereafter, the transmission with the lowest PAPR is selected for transmission.

Just as in the case of PTS, this method requires high computational overhead, as well as the transmission of side information. Various authors [54, 55, 57] have proposed methods of reducing the computational complexity, while Breiling [53] has suggested a method which does not require the transmission of side information. In addition, various methods [44–46, 48–50] have been recommended to reduce the complexity of the PTS method. Despite all of these methods, both PTS and SLM still require relatively high computational overhead and in some cases the transmission of side information.

2.8.5 Companding

Another method employed in PAPR reduction involves using a companding transform [59–67]. Wang [59] has proposed using a non-linear transform, illustrated in Fig. 2.17, which

enlarges the small signals while compressing the large signals. The idea behind non-linear companding transforms originates from speech processing. Similar to speech signals, OFDM signals contain peaks which occur irregularly, thus similar companding techniques to those used in speech processing may be applied to improve the PAPR of an OFDM transmission.

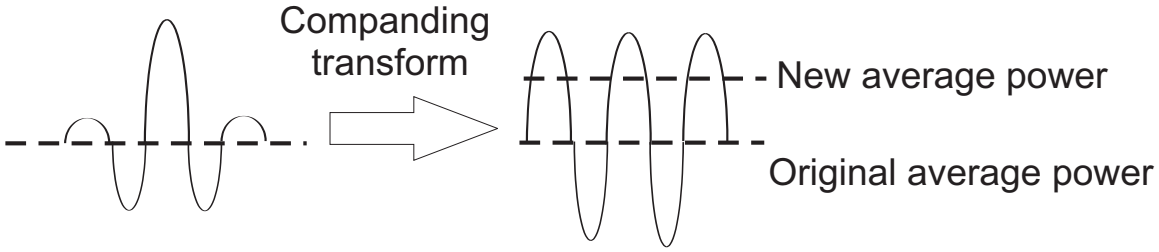

Figure 2.17: Depiction of a companding transform

The design criteria for a non-linear companding transform that can be used on an OFDM signal have been discussed in [66]. With knowledge of both the distribution of an OFDM signal (for instance a Rayleigh distribution) and a desired distribution of a companded OFDM signal, a non-linear companding transform function can be obtained through theoretical analysis. For example, suppose an original OFDM signal is required to have a desirable probability density function of $f(s) = ks + b \quad (k < 0, b > 0)$. The non-linear companding function which can be used for this type of distribution is given by [66]

$$C(x) = \sqrt{6}\sigma\left[1 - e^{-\frac{x^2}{2\sigma^2}}\right]. \tag{2.27}$$

In Eq (2.27), x refers to the input OFDM signal and σ is the variance of the OFDM signal. Huang [62] has also proposed a companding method based on μ law companding, which combined clipping and Wang companding, to reduce the PAPR of OFDM signals. In addition, Jiang [61] has proposed an alternative companding technique, which uses the statistical distribution of an OFDM transmitted signal to reduce the PAPR. These companding methods increase the average power, as indicated in Fig. 2.17, of the signal and require larger linear amplifiers. Furthermore, by physically changing the appearance of an OFDM signal, some of the attractive OFDM signal properties are removed. This in turn results in a BER degradation.

2.8.6 Active constellation extension

A further PAPR reduction method is active constellation extension [68–74]. The ACE method, as depicted in Fig. 2.18, makes use of an iterative filtering and clipping process. As previously mentioned when classically clipping a signal at various clipping ratios, both in-band and out-of-band distortions are introduced.

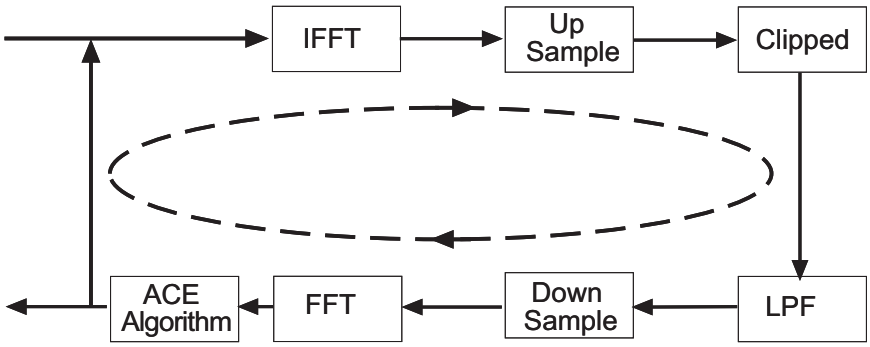

Figure 2.18: Active constellation extension method

For the ACE method, as depicted in Fig. 2.18, an up-sampled OFDM signal (after the IFFT) is clipped and filtered. The resultant signal is thereafter down-sampled and passed through a FFT. For a 16-QAM constellation after the FFT, depicted in Fig. 2.19(a), the resultant noise introduced by the clipping process is presented.

The outer constellation points of this clipped and filtered signal, which lies within a certain region that does not affect the BER, are left unaltered, hence the constellation is said to be extended [68]. As depicted in Fig. 2.19(b), the remaining constellation points are returned to their original position, before the clipping and filtering process. This process is iteratively continued.

Extending the outer constellation points leads to an average power increase. Generally the outer constellation points have a maximum tolerable constellation extension limit. Various projection methods [69, 71, 73] (e.g. projection onto convex sets approach) have been recommended to assist with this constellation shaping. Extending the outer

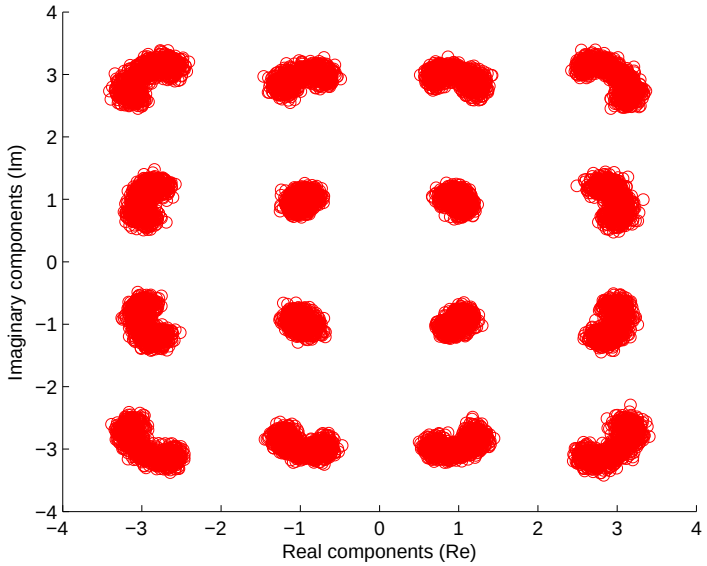

(a) Clipped and filtered OFDM constellation

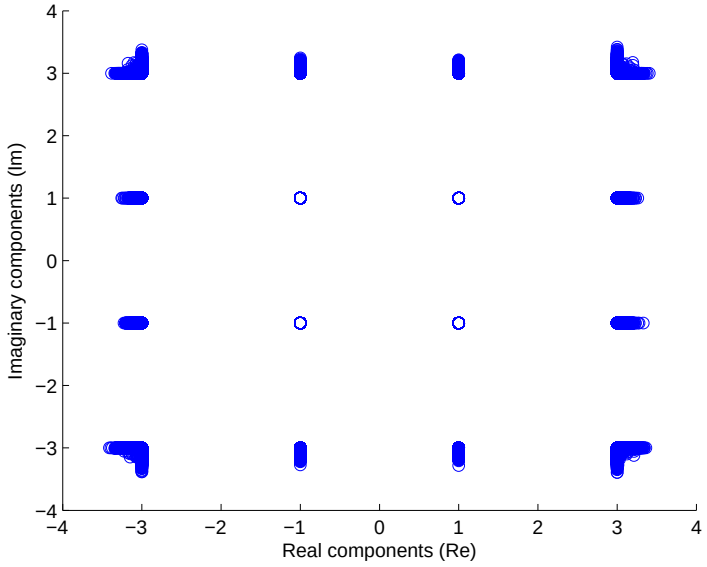

(b) Active constellation extension constellation

Figure 2.19: Constellation extension

constellation points leads to an average power increase and an average energy per bit increase. Furthermore, extending the constellation intelligently requires the use of an iterative clipping process. The iterative nature of this process increases the computational complexity. In addition, the optimum choice of clipping parameters may prove difficult and it is not always possible to achieve a specific PAPR value.

2.8.7 Tone reservation

An alternate method employed during PAPR reduction is tone reservation (TR) [23, 75–81]. With TR, the transmitter does not send data on a specified set of sub-carriers. The objective of TR is to find a time-domain signal c which can be added to the original OFDM time-domain signal x, such that the PAPR is reduced. This can be accomplished by adding a frequency-domain vector [75]

$$C = [C_0, C_1 ..... C_{N-1}]^T \tag{2.28}$$

to a frequency domain OFDM vector X; the new time domain signal can be written as

$$x + c = IFFT\{X + C\}. \tag{2.29}$$

The peak reduction vector C lies in a disjointed subspace i.e.

$$X_n = 0, n \in \{i_1, i_2, i_3, ...i_l\} \text{ and } C_n = 0, \notin \{i_1, i_2, i_3, ...i_l\}. \tag{2.30}$$

The l non-zero positions in vector C are called peak reduction carriers. These C subcarriers are orthogonal to X and cause no distortion on the data-bearing subcarriers. The C subcarriers may be obtained as suggested by [75], as depicted in Fig. 2.20, by clipping and filtering an up-sampled OFDM signal (after the IFFT containing TR symbols). The resultant signal is thereafter down-sampled and passed through an FFT. The resultant noise introduced by the clipping and filtering process (after the FFT) is mapped onto the TR symbols and the remaining symbols are left unaltered.

Similar to the ACE method, the iterative nature of the TR process increases the computational complexity and finding the optimum choice of the clipping parameter may prove difficult. Furthermore, the reservation of sub-carriers compromises throughput and it is not always possible to achieve a specific PAPR value.

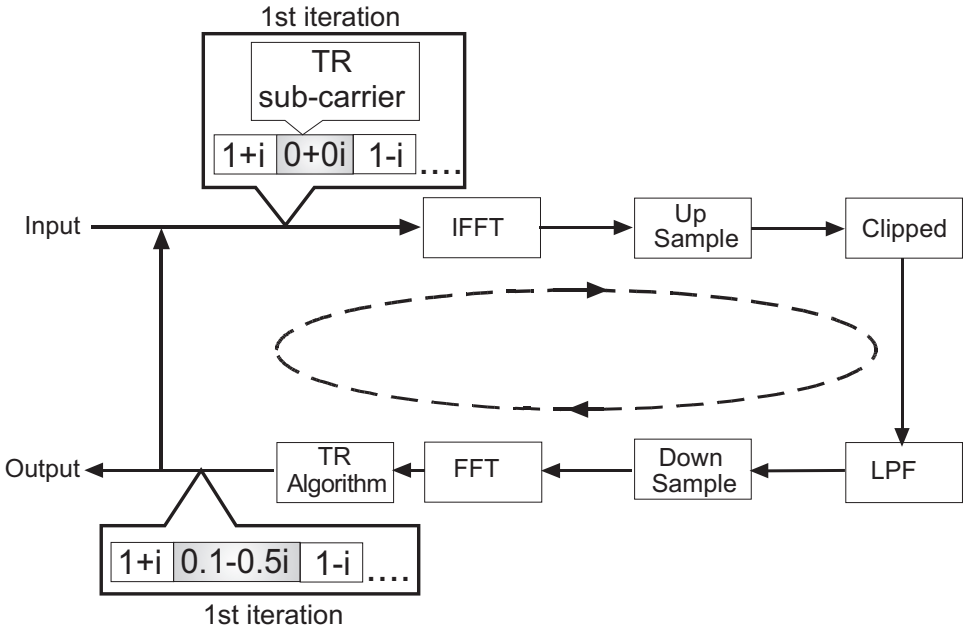

Figure 2.20: Tone reservation scheme

2.8.8 Constant envelope OFDM phase modulation

In contrast to tone reservation, constant envelope OFDM phase modulation [82–90] combines OFDM and phase modulation. A CE-OFDM transmission is ideally suited for constellations without imaginary components (e.g. BPSK). In cases where imaginary components exist (e.g. such as in 16-QAM), this constellation is uniquely mapped onto a constellation without imaginary components (e.g. 16-QAM to 16-PAM mapping). After the mapping process, an IFFT is performed on the mapped signal. The resultant OFDM signal is phase modulated. A drawback of CE-OFDM is its bandwidth expansion. Narrow band constraining of the transmission affects the BER of the system (the classical feature of a phase modulated signal). In addition, the mapping process affects the BER. In Chapter 4, an in-depth discussion of this method is provided.

2.9 CONCLUDING REMARKS

Ideally, a PAPR method that does not result in a number of the draw backs being experienced by current methods in the field is required. In Table 2.1, the disadvantages associated with the various methods are summarised. In this thesis, a method called offset modulation (OM-

Table 2.1: Disadvantages associated with the various PAPR reduction methods.

Methods	**Disadvantages**
Partial transmitted sequence Selective mapping DAR clipping Active constellation extension Tone reservation	High implementation complexity
Companding Active constellation extension Tone reservation	Leads to an increase in average power
Coding	Affects the coding gain
CE-OFDM Partial transmitted sequence Selective mapping Tone reservation	Requires further bandwidth expansion or the transmission of side information
Clipping DAR clipping CE-OFDM	Leads to a severe BER degradation as the number of carriers increases

OFDM) is proposed, which does not result in a number of the disadvantages summarised in Table 2.1.

CHAPTER 3

OFFSET MODULATION

3.1 INTRODUCTION

In Chapter 2 the draw backs associated with the various methods in the PAPR field were discussed. Ideally a method which requires low implementation complexity and does not lead to a severe BER degradation, as the number of carriers increases, is desired. It should also not require any additional bandwidth expansion or the transmission of any side information to reconstruct the original message signal. This chapter begins by introducing a novel method called offset modulation, which meets a number of these requirements.

3.2 OFFSET MODULATION

Consider the discrete complex output of an N-point inverse fast Fourier transformed OFDM signal, given by

$$m_n = \frac{1}{\sqrt{N}} \sum_{k=0}^{N-1} X_k e^{j\frac{2\pi nk}{N}}, \qquad n = 0, 1, ..., N-1 \tag{3.1}$$

$$= \frac{1}{\sqrt{N}} \sum_{k=0}^{N-1} (a_k + jb_k) \cdot \left(\cos\left(\frac{2\pi nk}{N}\right) + j \sin\left(\frac{2\pi nk}{N}\right) \right). \tag{3.2}$$

In Eq (3.1), X_k represents the complex signal output $(a_k + jb_k)$ of the IFFT. This signal may be modulated using the method which follows.

$$\Phi_{1n} = \frac{\Re(m_n)}{\varsigma} = \frac{1}{\varsigma\sqrt{N}} \sum_{k=0}^{N-1} \left(a_k \cos\left(\frac{2\pi nk}{N}\right) - b_k \sin\left(\frac{2\pi nk}{N}\right) \right) \quad \text{and} \tag{3.3}$$

$$\Phi_{2n} = \frac{\Im(m_n)}{\varsigma} = \frac{1}{\varsigma\sqrt{N}} \sum_{k=0}^{N-1} \left(b_k \cos\left(\frac{2\pi nk}{N}\right) + a_k \sin\left(\frac{2\pi nk}{N}\right) \right). \tag{3.4}$$

Here $\Re$ and $\Im$ refer to the real and imaginary parts of the OFDM message signal, ς refers to a constant division term, whereas Φ_{1n} and Φ_{2n} represent the equivalent real and imaginary OFDM phase mapping. These discrete Φ_{1n} and Φ_{2n} terms are passed through a DAC and are now combined into a unique co-sinusoid

$$\cos(2\pi f_c t + \Phi_1(t) + \Psi_{os}) - \cos(2\pi f_c t + \Phi_2(t)). \tag{3.5}$$

After utilising the following identity [91]

$$\cos(z_1) - \cos(z_2) = 2\sin\left(\frac{z_2 - z_1}{2}\right) \cdot \sin\left(\frac{z_1 + z_2}{2}\right) \tag{3.6}$$

thereafter, Eq (3.5) can be written as

$$2\sin\left(\frac{\Phi_2(t) - \Phi_1(t) - \Psi_{os}}{2}\right) \cdot \sin\left(2\pi f_c t + \frac{\Phi_1(t) + \Psi_{os} + \Phi_2(t)}{2}\right) \tag{3.7}$$

where, Ψ_{os} refers to an offset term, $\Phi_1(t)$ and $\Phi_2(t)$ represent the equivalent real and imaginary OFDM phase mapping. In this type of modulation the parameters (Ψ_{os}, ς) are chosen such that $\Psi_{os} >> \Phi_2(t) - \Phi_1(t)$. This implies that the Ψ_{os} term will dominate the expression, hence the name offset modulation (OM-OFDM) [92, 93] is proposed to describe this operation. A block diagram, depicted in Fig. 3.1, shows the processes involved during an OM-OFDM transmission. In Appendix A a more detailed description of the OM modulator and OM demodulator structure is presented. The proposed OM-OFDM process, depicted in Fig. 3.1, still maintains the fundamental OFDM building blocks. During an OM-OFDM transmission, depicted in Fig. 3.1, binary input data are mapped to complex symbols. Pilot symbols are thereafter inserted between these complex symbols.

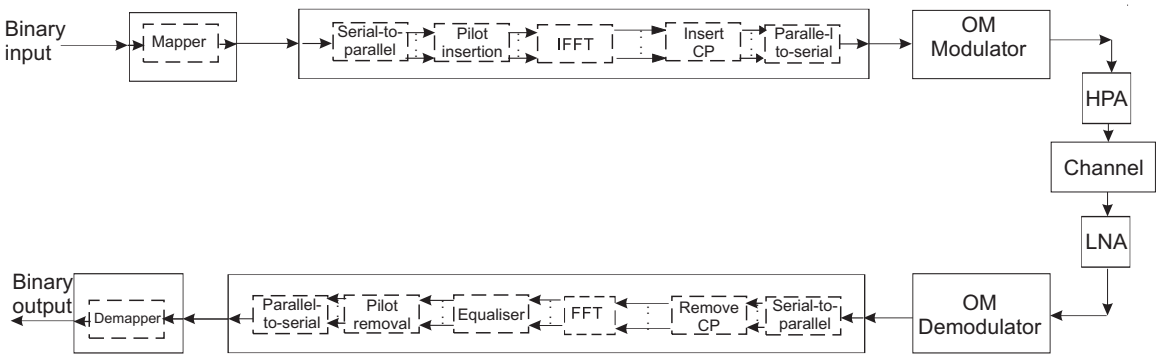

Figure 3.1: Transmitter receiver structure

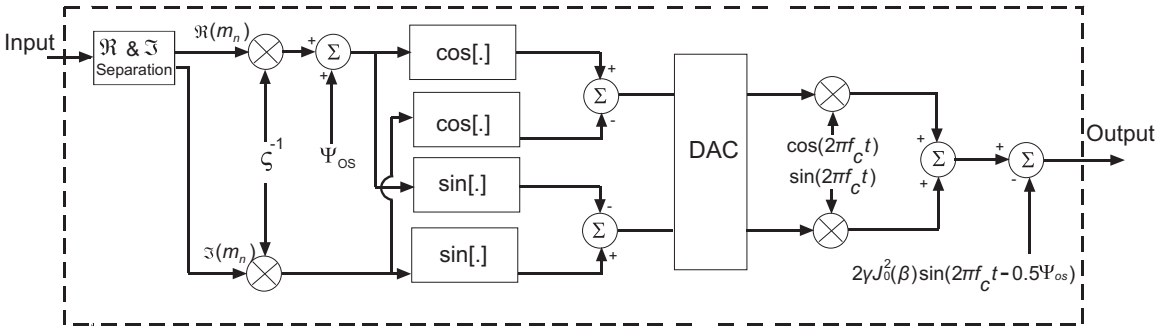

Figure 3.2: OM modulator structure

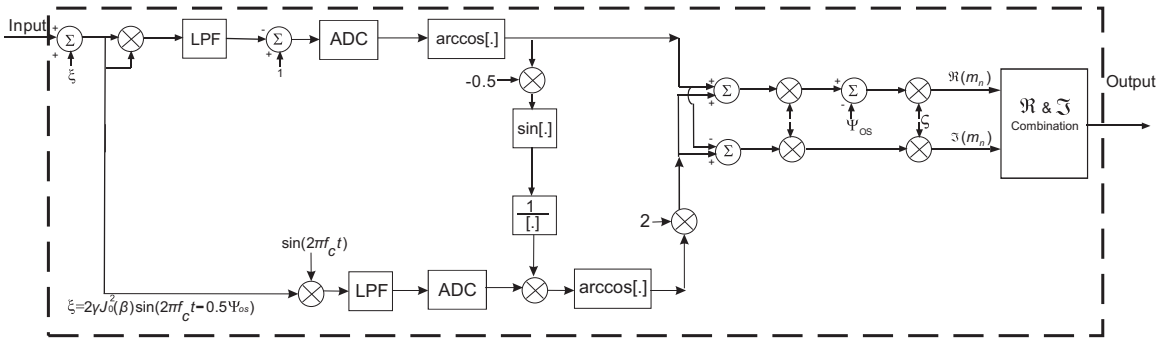

Figure 3.3: OM demodulator structure

The subsequent signal is passed through an IFFT; thereafter a cyclic pre-fix is appended to the signal. This process is identical to that previously seen in an OFDM transmission. The difference between an OFDM and OM-OFDM transmission lies in the modulation process. The OM modulator structure in an OM-OFDM transmission is used to reduce the PAPR of the OFDM transmission. The OM modulator structure receives a complex OFDM input and after various steps, depicted in Fig 3.2 and discussed in Appendix A, outputs

an OM-OFDM signal. This subsequent signal is passed through a HPA and transmitted across a channel. This process produces a spectrally efficient signal illustrated in Fig. 3.4, when compared to a classical OFDM transmission. The OM-OFDM transmission contains

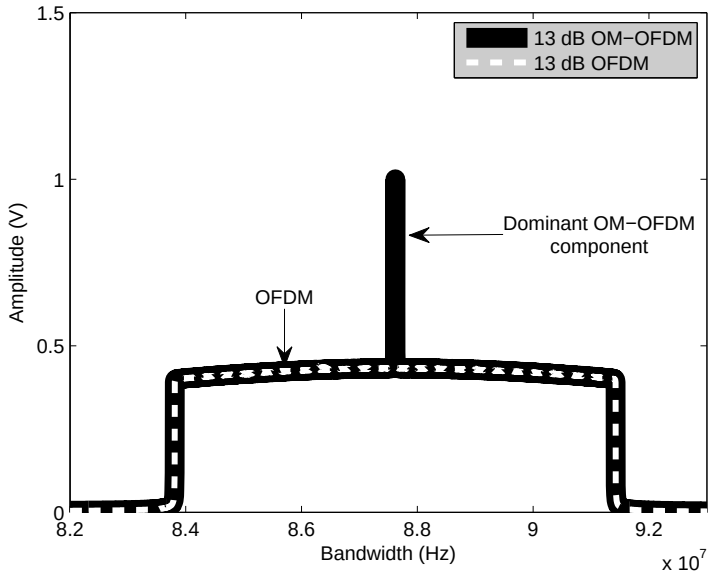

Figure 3.4: An averaged normalised bandwidth occupancy comparison between OM-OFDM and OFDM with identical throughput when, using a 64-QAM 8 k mode of the DVB - T2 standard.

a dominant component; as the dominant component becomes prominent, the PAPR of the signal decreases. However, in reality some energy restrictions are imposed on a transmitter, thus the other components can contain less energy, leading to a BER trade-off.

The received signal, depicted in Fig. 3.1, is passed through a LNA. This is followed by an OM demodulator, depicted in Fig 3.3, which receives the modulated signal and outputs a complex OFDM signal. The cyclic prefix is thereafter removed. The purpose of this CP, as previously discussed, is to mitigate some of the effects of the channel. Thereafter, an FFT is performed on the signal, in order to recover the original message signal.

The transmission may appear to be a phase modulated signal, therefore losing its attractive OFDM properties. However, the OM-OFDM system's transmitter receiver structure (Fig. 3.1.) maintains the fundamental OFDM building blocks. Thus, the OM-OFDM

equalisation process is identical to that employed in OFDM. Channel state information (CSI) is extracted from the pilot symbols and used during the equalisation process to mitigate the effects of fading. Thus, OM-OFDM maintains the ease of OFDM equalisation. The pilot symbols are thereafter removed and the complex symbols are de-mapped to binary output data.

3.3 BANDWIDTH OCCUPANCY OF OFFSET MODULATION

In this section the bandwidth occupancy of an OM-OFDM transmission may be investigated by considering a discrete complex OFDM signal

$$m_n = \frac{1}{\sqrt{N}} \sum_{k=0}^{N-1} X_k e^{j\frac{2\pi nk}{N}} = \frac{1}{\sqrt{N}} \sum_{k=0}^{N-1} X_k e^{jw_n k} \tag{3.8}$$

where w_n is an arbitrary chosen variable used to simplify the analysis, Eq (3.8) may also be written as

$$m_n = \frac{1}{\sqrt{N}} \sum_{k=0}^{N-1} (a_k + jb_k)(\cos(w_n k) + j\sin(w_n k)) \tag{3.9}$$

and it can then be shown that

$$\Phi_{1n} = \frac{\Re[m_n]}{\varsigma} \approx \sum_{k=0}^{N-1} \beta_1 \cos(w_n k) - \beta_2 \sin(w_n k) \tag{3.10}$$

$$\Phi_{2n} = \frac{\Im[m_n]}{\varsigma} \approx \sum_{k=0}^{N-1} \beta_2 \cos(w_n k) + \beta_1 \sin(w_n k). \tag{3.11}$$

where Φ_{1n} and Φ_{2n} are the equivalent real and imaginary discrete OFDM phase mapping, β_1 and β_2 are mean values defined as the adapted real and imaginary phase deviation of an OM-OFDM signal respectively. The approximation sign introduced in Eq (3.10) and Eq (3.11) is due to the fact that the β_1 and β_2 terms are message-dependent. An attempt is made to characterise the deviation of a message by the introduction of mean value terms, hence the introduction of the approximation. After incorporating this into the unique co-

sinusoidal (Eq (3.5)), the following expression is obtained

$$u_n \approx \Re\left[e^{j(2\pi f_c n+\Psi_{os}+\sum_{k=0}^{N-1}\beta_1\cos(w_n k)-\beta_2\sin(w_n k))}\right]-\Re\left[e^{j(2\pi f_c n+\sum_{k=0}^{N-1}\beta_2\cos(w_n k)+\beta_1\sin(w_n k))}\right], \tag{3.12}$$

in Eq (3.12), u_n is the discrete signal which is to be transmitted. With the aid of Bessel functions [94], the Fourier series can be written as

$$e^{j(\beta\sin(w_n k))}=\sum_{l=-\infty}^{\infty}J_l(\beta)e^{j(lw_n k)} \quad \text{and} \quad e^{j(\beta\cos(w_n k))}=\sum_{m=-\infty}^{\infty}J_m(\beta)e^{j(mw_n k+\frac{m\pi}{2})}. \tag{3.13}$$

In Eq (3.13), $J_l(\beta)$ and $J_m(\beta)$ are Bessel functions of the first kind of order l and m respectively with argument β. After substituting Eq (3.13) into Eq (3.12), it can then be shown that

$$\begin{aligned} u_n \approx \prod_{k=0}^{N-1}\Bigg(\Bigg[\sum_{l=-\infty}^{\infty}\sum_{m=-\infty}^{\infty}J_m(\beta_1)J_l(\beta_2)\cos\left(\frac{2\pi nk}{N}(f_c+l+m)+\Psi_{os}+\frac{m\pi}{2}\right)\Bigg] \\ -\Bigg[\sum_{l=-\infty}^{\infty}\sum_{m=-\infty}^{\infty}J_m(\beta_2)J_l(\beta_1)\cdot\cos\left(\frac{2\pi nk}{N}(f_c+l+m)+\frac{m\pi}{2}\right)\Bigg]\Bigg). \end{aligned} \tag{3.14}$$

Here, f_c is the carrier frequency. Consider the case when $l=m=\pm1$, $N=1$ and after using the $J_{-n}(\beta)=(-1)^n J_n(\beta)$ relationship, the various amplitude and phase components obtained from Eq (3.14) are summarised in Table 3.1. Upon studying the positive $(l+m\geq 0)$ and

Table 3.1: Components of Eq (3.14) when $l=m=\pm1$ and $N=1$

l	m	l+m	$J_m(\beta_1)\cdot J_l(\beta_2)$	$J_l(\beta_1)\cdot J_m(\beta_2)$
-1	-1	-2	$-J_1(\beta_1)\cdot -J_1(\beta_2)$	$-J_1(\beta_1)\cdot -J_1(\beta_2)$
0	-1	-1	$-J_1(\beta_1)\cdot J_0(\beta_2)$	$J_0(\beta_1)\cdot -J_1(\beta_2)$
-1	0	-1	$J_0(\beta_1)\cdot -J_1(\beta_2)$	$-J_1(\beta_1)\cdot J_0(\beta_2)$
1	-1	0	$-J_1(\beta_1)\cdot J_1(\beta_2)$	$J_1(\beta_1)\cdot -J_1(\beta_2)$
0	0	0	$J_0(\beta_1)\cdot J_0(\beta_2)$	$J_0(\beta_1)\cdot J_0(\beta_2)$
-1	1	0	$J_1(\beta_1)\cdot -J_1(\beta_2)$	$-J_1(\beta_1)\cdot J_1(\beta_2)$
1	0	1	$J_0(\beta_1)\cdot J_1(\beta_2)$	$J_1(\beta_1)\cdot J_0(\beta_2)$
0	1	1	$J_1(\beta_1)\cdot J_0(\beta_2)$	$J_0(\beta_1)\cdot J_1(\beta_2)$
1	1	2	$J_1(\beta_1)\cdot J_1(\beta_2)$	$J_1(\beta_1)\cdot J_1(\beta_2)$

negative $(l+m<0)$ frequency components of Table 3.1, in conjunction with various other

($l = m = \pm 1, \pm 2 \ldots$ and $N = 1$) bandwidth occupancy cases, a particular relationship indicated by Eq (3.15) emerges

$$u_n = \sum_{y=0}^{2x} \left| \sum_{z=0}^{2x-y} 2\sin\left(\frac{\pi(2x-2z-y) \pm 2\Psi_{os}}{4}\right) \cdot J_{|-x+z|}(\beta_1) \left(\frac{|-x+z+\frac{1}{2}|}{-x+z+\frac{1}{2}}\right)^{|-x+z|} \cdot J_{|x-y-z|}(\beta_2) \left(\frac{|x-y-z+\frac{1}{2}|}{x-y-z+\frac{1}{2}}\right)^{|x-y-z|} \cdot \sin\left(2\pi(f_c + y f_d) + \frac{2\Psi_{os} \pm y\pi}{4}\right) \right|. \quad (3.15)$$

In Eq (3.15), f_d is an integer multiple of the modulation frequency and $2x$ refers to an even number of frequency components of interest. In order to demonstrate the relationship between Eq (3.14) and Eq (3.15), consider the case when $l + m = 2$ and $y = 2$. After using Table 3.1 ($l + m = 2$) obtained from Eq (3.14), for this case it can be shown that

$$\begin{aligned} & J_1(\beta_1) \cdot J_1(\beta_2) \cdot \left(\cos\left(2\pi(f_c + 2f_d) + \Psi_{os} + \frac{\pi}{2}\right) - \cos\left(2\pi(f_c + 2f_d) + \frac{\pi}{2}\right) \right) \\ = \; & 2J_1(\beta_1) \cdot J_1(\beta_2) \cdot \left(\sin\left(\frac{\Psi_{os}}{2}\right) \cdot \sin\left(2\pi(f_c + 2f_d) + \frac{\Psi_{os}}{2} + \frac{\pi}{2}\right) \right). \end{aligned} \quad (3.16)$$

Substituting $2x = 2$ and $y = 2$ into Eq (3.15), results in

$$\begin{aligned} & 2\sin\left(\frac{2\Psi_{os}}{4}\right) \cdot J_1(\beta_1) \left(\frac{|-\frac{1}{2}|}{-\frac{1}{2}}\right) \cdot J_1(\beta_2) \left(\frac{|-\frac{1}{2}|}{-\frac{1}{2}}\right) \cdot \sin\left(2\pi(f_c + 2f_d) + \frac{2\Psi_{os} + 3\pi}{4}\right) \\ = \; & 2J_1(\beta_1) J_1(\beta_2) \sin\left(\frac{\Psi_{os}}{2}\right) \cdot \sin\left(2\pi(f_c + 2f_d) + \frac{\Psi_{os}}{2} + \frac{\pi}{2}\right). \end{aligned} \quad (3.17)$$

This result correlates with that from Eq (3.16), thus validating some of the components of Eq (3.15) with those in Eq (3.14). In a similar manner, all of the other components can be validated. In most cases, the adapted phase deviation (β_1 and β_2) of the signal is not known beforehand; however, a reasonably good approximation can be made, based on

$$\alpha_1 \approx E[max(|\Re(m(t))|)], \quad (3.18)$$

$$\alpha_2 \approx E[max(|\Im(m(t))|)], \quad (3.19)$$

$$\beta_1 \approx \frac{\alpha_1}{\varsigma} \quad \text{and} \quad (3.20)$$

$$\beta_2 \approx \frac{\alpha_2}{\varsigma}. \quad (3.21)$$

In Eq (3.18), Eq (3.19), Eq (3.20) and Eq (3.21), α_1 and α_2, refer to the real and imaginary phase deviations of the OFDM signal respectively and E [.] is the expected value. Typically, there is no interest in all the frequency components, but rather in the more dominant components. Hence, the bandwidth can be defined by considering only those sidebands which contain significant power. Suppose, for explanation purposes, the first two components ($2x = 2$) are of interest and $\beta \approx \beta_1 \approx \beta_2$. After inspecting Eq (3.15), Fig. 3.5 depicts the frequency spectrum and its corresponding amplitude components. This frequency spectrum is different from that of a conventional phase modulated signal.

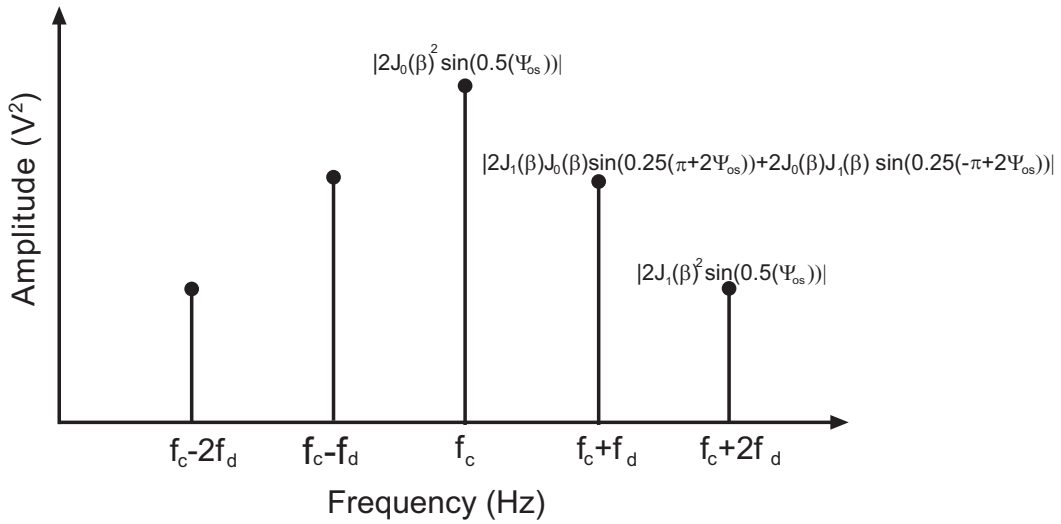

Figure 3.5: Theoretically derived (Eq (3.15)) frequency spectrum of an OM-OFDM signal.

The squaring of the Bessel functions limits the bandwidth occupancy of the signal. If β is sufficiently small ($\beta = 0.02$), it can be seen that a large percentage of the power is constrained within these ($2x = 2$) frequency components. This depiction may serve as a simplistic OM-OFDM bandwidth occupancy description. The dominant frequency component is given by $2J_0(\beta)^2 \sin(2\pi f_c t - \frac{\Psi_{os}}{2})$, provided $\Psi_{os} >> \Phi_2(t) - \Phi_1(t)$. In such a case, the dominant frequency component can be shown to be dependent on the Ψ_{os} term.

This expression also provides some insight into an OM-OFDM transmission, namely the bandwidth expansion is dependent on the ς term. The higher the ς term, the lower the phase β, thus indicating less bandwidth expansion. Ideally an attempt might be made to choose ς as high as possible. However, as the ς term increases, the signal would lose

resolution and this would lead to an increase in the BER. Thus far it has been shown that the dominant frequency component of an OM-OFDM transmission can be predicted by $2J_0(\beta)^2\sin(2\pi f_c t - \frac{\Psi_{os}}{2})$. By subtracting $2\gamma J_0(\beta)^2\sin(2\pi f_c t - \frac{\Psi_{os}}{2}), \quad 0 \leq \gamma < 1$, (where γ is the dominant frequency component control factor) from the dominant frequency component at the transmitter (Fig. 3.2) and re-instating the subtracted term at the receiver (Fig. 3.3), the PAPR may be controlled.

The receiver gains knowledge of the subtracted term by examining the PAPR of the incoming signal, from which the Ψ_{os}, ς and γ terms can be extracted by using a simple look-up table. Since the Ψ_{os} and ς terms are in most cases identical, only the γ term is subsequently extracted from the received signal's PAPR. It might be argued that after a transmission through a multi-path fading channel, the received and transmitted PAPR might differ. However, for an n-tap channel, each path affects both the RMS and peak value of the received signal equally. Therefore the PAPR from each path is equivalent to the originally sent PAPR.

This principle can be demonstrated by using the 8k mode of the DVB-T2 standard [95] to transmit 64-QAM OM-OFDM data through a 5-tap typical-urban area [96] at a low 10 dB SNR (E_b/N_o). The complementary cumulative distribution function (CCDF) of such a transmission, depicted in Fig. 3.6, indicates that the sent and received PAPRs are almost identical. In the next section, the manner in which the dominant frequency component is varied and the resultant BER characteristics are presented.

3.4 SYMBOL AND BIT ERROR RATE CHARACTERISTICS OF OFFSET MODULATION

A received signal under AWGN conditions is expressed as [87, 97]

$$r(t) = u(t) + n(t) = u(t) + N_c(t)\cos(2\pi f_c t) - N_s(t)\sin(2\pi f_c t). \tag{3.22}$$

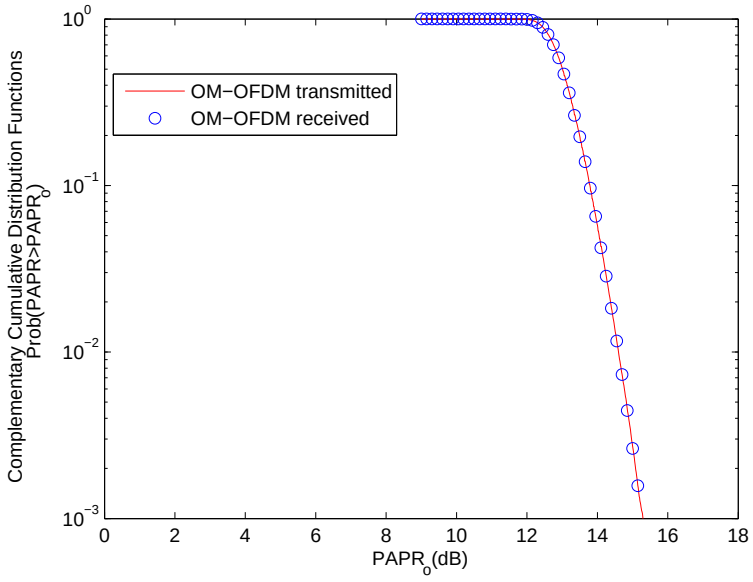

Figure 3.6: Complementary cumulative distribution functions for a 64-QAM constellation, when using the DVB-T2 standard for a 5-tap typical urban area channel at a 10 dB signal-to-noise ratio (E_b/N_o).

In Eq (3.22), $u(t)$ refers to an offset-modulated signal and $n(t)$ represents AWGN. The $N_c(t)$ and $N_s(t)$ expressions refer to the in-phase and the quadrature components of noise respectively. The noise expression can also be written as

$$\begin{aligned} n(t) &= \sqrt{N_c^2(t)+N_s^2(t)}\sin\left(2\pi f_c t + arctan\frac{N_c(t)}{N_s(t)}\right) \\ &= V_n(t)\sin(2\pi f_c t+\Phi_n(t)). \end{aligned} \tag{3.23}$$

In Eq (3.23), $V_n(t)$ and $\Phi_n(t)$ represent the envelope and phase of the band-pass noise. The offset modulated signal $u(t)$ can be expressed as

$$\begin{aligned} u(t) &= 2\sin\left(\frac{\Phi_2(t)-\Phi_1(t)-\Psi_{os}}{2}\right)\cdot\sin\left(2\pi f_c t+\frac{\Phi_1(t)+\Psi_{os}+\Phi_2(t)}{2}\right) \\ &\approx A_c(t)\sin(2\pi f_c t+\Phi(t)), \end{aligned} \tag{3.24}$$

where $A_c(t)$ and $\Phi(t)$ can be seen as the envelope and phase of an offset modulated signal. After using phasor manipulation, depicted in Fig. 3.7, it can be shown that the received signal

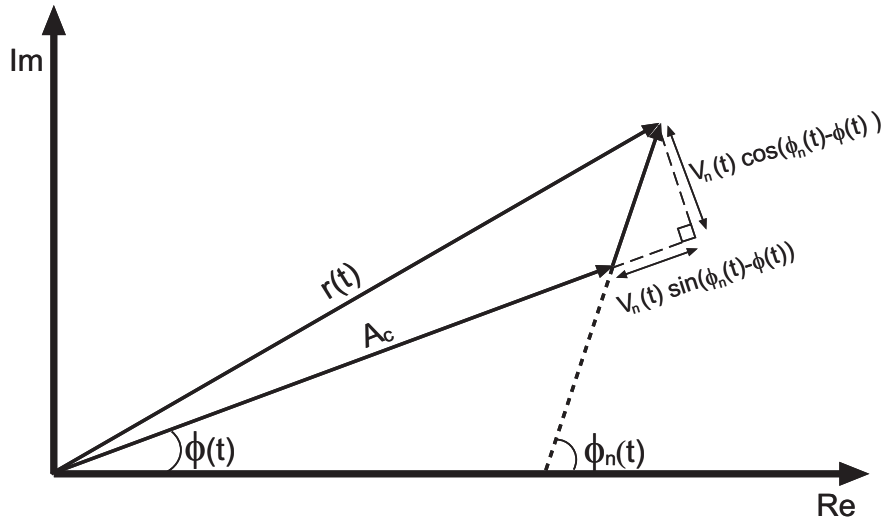

Figure 3.7: OM-OFDM phasor [97]

can be written as

$$\begin{aligned} r(t) &= (A_c(t) + V_n(t)\sin(\Phi_n(t) - \Phi(t))) \cdot \\ &\quad \sin\left(2\pi f_c t + \Phi(t) + arctan\left[\frac{V_n(t)\cos(\Phi_n(t) - \Phi(t))}{A_c + V_n(t)\cos(\Phi_n(t) - \Phi(t))}\right]\right). \end{aligned} \tag{3.25}$$

If the assumption is made that the signal is much larger than the noise, in this case

$$r(t) \approx (A_c(t) + V_n(t)\sin(\Phi_n(t) - \Phi(t))) \cdot \sin\left(2\pi f_c t + \Phi(t) + \frac{V_n(t)\cos(\Phi_n(t) - \Phi(t))}{A_c}\right) \tag{3.26}$$

it can be seen from Eq (3.26), that the noise expression at the y branch of the demodulator can be written as

$$Y_n(t) = \frac{V_n(t)\cos(\Phi_n(t) - \Phi(t))}{A_c}. \tag{3.27}$$

By applying the following identity,

$$\cos(\alpha - \beta) = \cos\alpha\cos\beta + \sin\alpha\sin\beta, \tag{3.28}$$

the noise expression can be represented by

$$Y_n(t) = \frac{V_n(t)\cos(\Phi_n(t))\cos(\Phi(t)) + V_n(t)\sin(\Phi_n(t))\sin(\Phi(t))}{A_c} \tag{3.29}$$

therefore

$$Y_n(t) = \frac{n_c(t)\cos(\Phi(t)) + n_s\sin(\Phi(t))}{A_c}. \tag{3.30}$$

In Eq (3.30), n_c and n_s refer to the noise co-sinusoidal and sinusoidal expressions, respectively. An auto correlation is performed on the noise, in order to study the spectrum characteristics of this expression. This can be expressed as

$$\begin{aligned} E[Y_n(t)Y_n(t+\tau)] = E\Bigg[& \frac{n_c(t)n_c(t+\tau)\cos(\Phi(t))\cos(\Phi(t+\tau))}{{A_c}^2} + \\ & \frac{n_c(t)n_s(t+\tau)\cos(\Phi(t))\sin(\Phi(t+\tau))}{{A_c}^2} + \\ & \frac{n_s(t)n_c(t+\tau)\sin(\Phi(t))\cos(\Phi(t+\tau))}{{A_c}^2} + \\ & \frac{n_s(t)n_s(t+\tau)\sin(\Phi(t))\sin(\Phi(t+\tau))}{{A_c}^2}\Bigg]. \end{aligned} \tag{3.31}$$

According to [97], for stationary white symmetric noise

$$n_c(t)n_s(t+\tau) = n_c(t)n_s(t+\tau) = 0 \tag{3.32}$$

$$R_{nc}(\tau) = n_c(t)n_c(t+\tau) \tag{3.33}$$

$$R_{ns}(\tau) = n_s(t)n_s(t+\tau) \tag{3.34}$$

$$R_{ns}(\tau) = R_{nc}(\tau) \tag{3.35}$$

where $R_{nc}(\tau)$ and $R_{ns}(\tau)$ are band-pass signals. Substituting Eq (3.32), Eq (3.33), Eq (3.34) and Eq (3.35) into Eq (3.31), results in the following expression

$$E[Y_n(t)Y_n(t+\tau)] = E\left[\frac{R_{nc}(\tau)\cos(\Phi(t))\cos(\Phi(t+\tau))}{{A_c}^2} + \frac{R_{ns}(\tau)\sin(\Phi(t))\sin(\Phi(t+\tau))}{{A_c}^2}\right]. \tag{3.36}$$

After using the identity presented in Eq (3.28) in conjunction with Eq (3.35), Eq (3.36) simplifies to

$$E[Y_n(t)Y_n(t+\tau)] = \frac{R_{nc}(\tau)}{{A_c}^2}E[\cos(\Phi(t+\tau)-\Phi(t))]. \tag{3.37}$$

According to [97], at any fixed time t, a random variable $Z(t,\tau)=\Phi(t+\tau)-\Phi(t)$ is the difference between two jointly Gaussian random variables. This is itself a Gaussian random variable with mean equal to zero and a variance given by

$$\begin{aligned} {\sigma_Z}^2 &= E[(\Phi(t+\tau)-\Phi(t))^2] \\ &= E[\Phi^2(t+\tau)]+E[\Phi^2(t)]-2R_\Phi(\tau) \\ &= 2(R_\Phi(0)-R_\Phi(\tau)), \end{aligned} \tag{3.38}$$

where, as previously mentioned, $2R_\Phi(\tau)$ is a band-pass signal. Substituting Eq (3.38) into Eq (3.37) results in

$$\begin{aligned} E[Y_n(t)Y_n(t+\tau)] &= \frac{R_{nc}(\tau)}{{A_c}^2}E[\cos(\Phi(t+\tau)-\Phi(t))] \\ &= \frac{R_{nc}(\tau)}{{A_c}^2}\Re\left(E\left[e^{j(\Phi(t+\tau)-\Phi(t))}\right]\right) \\ &= \frac{R_{nc}(\tau)}{{A_c}^2}\Re\left(E\left[e^{j(Z(t,\tau))}\right]\right) \\ &= \frac{R_{nc}(\tau)}{{A_c}^2}\Re\left(e^{-\left(\frac{{\sigma_Z}^2}{2}\right)}\right) \\ &= \frac{R_{nc}(\tau)}{{A_c}^2}\Re\left(e^{-(R_\Phi(0)-R_\Phi(\tau))}\right) \\ &= \frac{R_{nc}(\tau)}{{A_c}^2}\left(e^{-(R_\Phi(0)-R_\Phi(\tau))}\right). \end{aligned} \tag{3.39}$$

From the autocorrelation of the noise, the power spectral density of the noise can be written as

$$\begin{aligned} S_Y(f) &= \mathscr{F}[R_Y(\tau)] \\ &= \mathscr{F}\left[\frac{R_{nc}(\tau)}{{A_c}^2}\left(e^{-(R_\Phi(0)-R_\Phi(\tau))}\right)\right] \end{aligned}$$

$$\begin{aligned} &= \frac{e^{-R_\Phi(0)}}{A_c^2}\mathscr{F}\left[R_{nc}(\tau)e^{R_\Phi(\tau)}\right] \\ &= \frac{e^{-R_\Phi(0)}}{A_c^2}\mathscr{F}\left[R_{nc}(\tau)g(\tau)\right] \\ &= \frac{e^{-R_\Phi(0)}}{A_c^2}S_{nc}(f)\star G(f), \end{aligned} \tag{3.40}$$

where $G(f)$ is the Fourier transform ($\mathscr{F}$) of $g(\tau) = e^{R_\Phi(\tau)}$, $S_{nc}(f)$ is the Fourier transform of R_{nc} and the $\star$ refers to a convolutional process. Now suppose the discussion is confined to a specific bandwidth of $-\frac{B_c}{2}$ to $\frac{B_c}{2}$. For this case suppose, $S_{nc}(f) = N_o$, here N_o is the power spectral density of the additive noise. The power spectral density may now be expressed as

$$\begin{aligned} S_Y(f) &= \frac{e^{-R_\Phi(0)}}{A_c^2}N_o\int_{-\frac{B_c}{2}}^{\frac{B_c}{2}} G(f)\,df \\ &\approx \frac{e^{-R_\Phi(0)}}{A_c^2}N_o\int_{-\infty}^{\infty} G(f)\,df \\ &= \frac{e^{-R_\Phi(0)}}{A_c^2}N_o g(\tau)\Big|_{\tau=0} \\ &= \frac{e^{-R_\Phi(0)}}{A_c^2}N_o e^{R_\Phi(0)} \\ &= \frac{N_o}{A_c^2}. \end{aligned} \tag{3.41}$$

Suppose $A_c \approx 2\ \sin\left(\frac{-\varphi}{2}\right)$ (from Eq (3.24)) where φ refers to a constant term. With the use of Eq (3.41) and by following a similar methodology, the Y and X output power-spectral density of the noise component can be shown to be written as

$$S_Y(f) \approx \frac{N_o}{4\sin^2\left(\frac{-\varphi}{2}\right)} \tag{3.42}$$

and

$$S_X(f) \approx N_o. \tag{3.43}$$

After band limiting (B_c) the transmission ($0 > B > \frac{B_c}{2}$), the noise variance at the output of the various branches of the demodulator (Fig. 3.1) is given by

$$\sigma_Y^2 \approx \frac{N_o}{8\sin^2\left(\frac{-\varphi}{2}\right)} \quad \text{and} \quad \sigma_X^2 \approx \frac{N_o}{2} \tag{3.44}$$

where, by inspection, φ may be approximated by Table 3.2. In Table 3.2, γ is the dominant

Table 3.2: Selection of a φ term, based on γ and α

	$0 < \alpha < 0.1$	$0.1 \leq \alpha < 0.2$	$0.2 \leq \alpha < 0.3$
$\varphi \approx \frac{\beta\sin(\Psi_{os})}{4(1-\gamma)}$	$0 \leq \gamma < 0.988$	$0 \leq \gamma < 0.97$	$0 \leq \gamma < 0.96$
$\varphi \approx \frac{\beta\sin(\Psi_{os})}{5(1-\gamma)}$	$0.988 \leq \gamma < 1$	$0.97 \leq \gamma < 1$	$0.96 \leq \gamma < 1$

frequency component control factor and the α ($\alpha \approx \alpha_1 \approx \alpha_2$) and β ($\beta \approx \beta_1 \approx \beta_2$) terms originate from Eq (3.18), Eq (3.19), Eq (3.20) and Eq (3.21). The proposed φ term is obtained, based on a number of observations, provided $0 \leq \varphi \leq \frac{\pi}{2}$, namely

$$N_o \propto \frac{1}{\sin(\Psi_{os})} \tag{3.45}$$

$$N_o \propto \varsigma \tag{3.46}$$

$$N_o \propto [1-\gamma]. \tag{3.47}$$

From these observations the φ term in Table 3.2 is proposed. Therefore, from the γ and α term of a particular transmission (shown in Table 3.2), either the

$$\varphi \approx \frac{\beta\sin(\Psi_{os})}{4(1-\gamma)} \quad \text{or} \tag{3.48}$$

$$\varphi \approx \frac{\beta\sin(\Psi_{os})}{5(1-\gamma)} \tag{3.49}$$

term, can be used to describe the noise properties. In the sub-sections which follow the BER and symbol error rate (SER) expression for an OM-OFDM transmission will be derived by using the noise variance expression (Eq (3.44)).

3.4.1 A 4-PAM symbol and bit error rate derivation

Consider a 4-PAM baseband signal, depicted in Fig. 3.8, with signal points $s_0 = -3d\sqrt{\frac{\xi_s}{\xi_{av}}}$, $s_1 = -d\sqrt{\frac{\xi_s}{\xi_{av}}}$, $s_2 = d\sqrt{\frac{\xi_s}{\xi_{av}}}$ and $s_3 = 3d\sqrt{\frac{\xi_s}{\xi_{av}}}$, where d is the Euclidean distance, ξ_s is the energy per symbol and ξ_{av} is the average energy per symbol. Suppose the received signal at

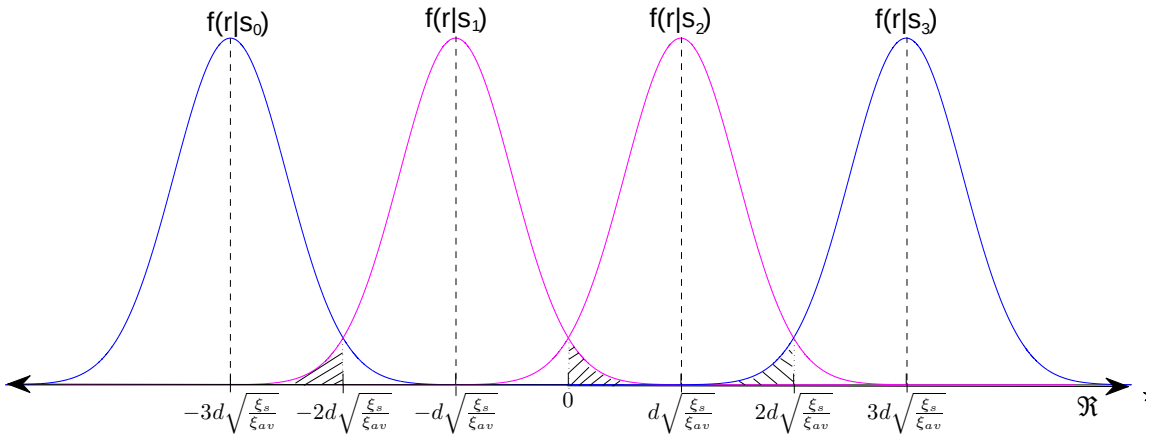

Figure 3.8: Conditional PDFs of four signals

the output of the demodulator is

$$r = s_3 + n = 3d\sqrt{\frac{\xi_s}{\xi_{av}}} + n. \tag{3.50}$$

In Eq (3.50), n represents AWGN. The decision rule compares the received signal (r) with a threshold. If $r > 2d\sqrt{\frac{\xi_s}{\xi_{av}}}$, a decision is made in favour of s_3, if $r < 2d\sqrt{\frac{\xi_s}{\xi_{av}}}$, the decision is made in favour of s_2. The conditional probability density functions for r are

$$\begin{aligned} f(r|s_0) &= \frac{1}{\sqrt{2\pi}\sigma} e^{\frac{-\left(r+3d\sqrt{\frac{\xi_s}{\xi_{av}}}\right)^2}{2\sigma^2}} \\ f(r|s_1) &= \frac{1}{\sqrt{2\pi}\sigma} e^{\frac{-\left(r+d\sqrt{\frac{\xi_s}{\xi_{av}}}\right)^2}{2\sigma^2}} \\ f(r|s_2) &= \frac{1}{\sqrt{2\pi}\sigma} e^{\frac{-\left(r-d\sqrt{\frac{\xi_s}{\xi_{av}}}\right)^2}{2\sigma^2}} \end{aligned}$$

$$f(r|s_3) = \frac{1}{\sqrt{2\pi}\sigma} e^{\frac{-\left(r-3d\sqrt{\frac{\xi_s}{\xi_{av}}}\right)^2}{2\sigma^2}} \tag{3.51}$$

where σ is the variance of the noise. Given that s_3 was transmitted, the probability of a symbol error is

$$\begin{aligned} p(e|s_3) &= \int_{-\infty}^{2d\sqrt{\frac{\xi_s}{\xi_{av}}}} p(r|s_3) \quad dr \\ &= \frac{1}{\sqrt{2\pi}\sigma} \int_{-\infty}^{2d\sqrt{\frac{\xi_s}{\xi_{av}}}} e^{\frac{-\left(r-3d\sqrt{\frac{\xi_s}{\xi_{av}}}\right)^2}{2\sigma^2}} \quad dr \\ &= \frac{1}{\sqrt{\pi}} \int_{-\infty}^{-d\sqrt{\frac{\xi_s}{2\sigma^2\xi_{av}}}} e^{-t^2} \quad dt \\ &= \frac{1}{\sqrt{\pi}} \int_{d\sqrt{\frac{\xi_s}{2\sigma^2\xi_{av}}}}^{\infty} e^{-t^2} \quad dt \\ &= \frac{1}{2}\text{erfc}\left(d\sqrt{\frac{\xi_s}{2\sigma^2\xi_{av}}}\right) \end{aligned} \tag{3.52}$$

in Eq (3.52), erfc is the error function. It can similarly be shown that $p(e|s_0) = p(e|s_3) = \frac{1}{2}\text{erfc}\left(d\sqrt{\frac{\xi_s}{2\sigma^2\xi_{av}}}\right)$. Given that s_1 was transmitted, the probability of a symbol error is

$$\begin{aligned} p(e|s_1) &= \int_{-\infty}^{-2d\sqrt{\frac{\xi_s}{\xi_{av}}}} p(r|s_1)dr + \int_0^{\infty} p(r|s_1)dr \\ &= \frac{1}{\sqrt{2\pi}\sigma} \int_{-\infty}^{-2d\sqrt{\frac{\xi_s}{\xi_{av}}}} e^{\frac{-\left(r+d\sqrt{\frac{\xi_s}{\xi_{av}}}\right)^2}{2\sigma^2}} dr + \frac{1}{\sqrt{2\pi}\sigma} \int_0^{\infty} e^{\frac{-\left(r+d\sqrt{\frac{\xi_s}{\xi_{av}}}\right)^2}{2\sigma^2}} dr \\ &= \frac{1}{\sqrt{\pi}} \int_{-\infty}^{-d\sqrt{\frac{\xi_s}{2\sigma^2\xi_{av}}}} e^{-t^2} dt + \frac{1}{\sqrt{\pi}} \int_{d\sqrt{\frac{\xi_s}{2\sigma^2\xi_{av}}}}^{\infty} e^{-t^2} dt \\ &= \frac{1}{2}\text{erfc}\left(d\sqrt{\frac{\xi_s}{2\sigma^2\xi_{av}}}\right) + \frac{1}{2}\text{erfc}\left(d\sqrt{\frac{\xi_s}{2\sigma^2\xi_{av}}}\right) \\ &= \text{erfc}\left(d\sqrt{\frac{\xi_s}{2\sigma^2\xi_{av}}}\right). \end{aligned} \tag{3.53}$$

Similarly, it can be shown that $p(e|s_2) = p(e|s_1) = \text{erfc}\left(d\sqrt{\frac{\xi_s}{2\sigma^2\xi_{av}}}\right)$. The SER is then

$$P_{SER} = p(s_0)p(e|s_0) + p(s_1)p(e|s_1) + p(s_2)p(e|s_2) + p(s_3)p(e|s_3) \tag{3.54}$$

where $p(s_0)$, $p(s_1)$, $p(s_2)$ and $p(s_3)$ are the probabilities of the s_0, s_1, s_2 and s_3 symbols respectively. If it is assumed that each symbol is equally probable i.e. $p(s_0) = p(s_1) = p(s_2) = p(s_3) = \frac{1}{4}$, the SER for a 4-PAM constellation can be written as

$$\begin{aligned} SER_{4PAM} &= \frac{1}{4}\text{erfc}\left(d\sqrt{\frac{\xi_s}{2\sigma^2\xi_{av}}}\right) + \frac{2}{4}\text{erfc}\left(d\sqrt{\frac{\xi_s}{2\sigma^2\xi_{av}}}\right) \\ &= \frac{3}{4}\text{erfc}\left(d\sqrt{\frac{\xi_s}{2\sigma^2\xi_{av}}}\right). \end{aligned} \tag{3.55}$$

A particular symbol s_1 is comprised of a number of bits. The number of bits denoted by k is dependent on the constellation and can be written as $k = \log_2 M$. When the constellation is Gray-coded and $(p(s_0|s_1)|p(s_2|s_1)) >> p(s_3|s_1)$, the subsequent number of bits in error can be written as

$$BER_{4PAM} = \frac{3}{4k}\text{erfc}\left(d\sqrt{\frac{kE_b}{2\sigma^2\xi_{av}}}\right) \tag{3.56}$$

where E_b is the energy per bit and $\frac{\xi_s}{\sigma^2} = \frac{kE_b}{\sigma^2}$.

3.4.2 A 4-QAM symbol and bit error rate derivation

Similarly for a 4-QAM constellation, depicted in Fig. 3.9, the symbol s_1 is correctly detected only if r falls within the following region

$$p(c|s_1) = p\big(\Re_r > 0\big|s_1\big)\,p\big(\Im_r > 0\big|s_1\big). \tag{3.57}$$

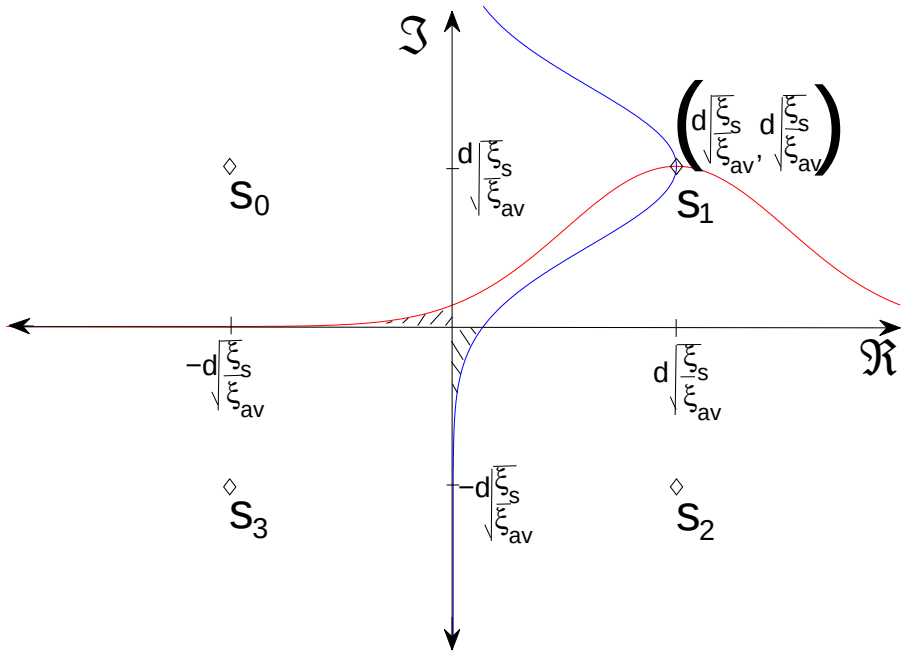

Figure 3.9: 4-QAM constellation

In Eq (3.57), $\Re_r$ and $\Im_r$ are the received real and imaginary components. The probability of the real component of r being greater than 0, given that s_1 was transmitted, is

$$\begin{aligned} p(\Re_r > 0|s_1) &= 1 - \frac{1}{\sqrt{2\pi}\sigma_x}\int_{-\infty}^{0} e^{\frac{-\left(\Re_r - d\sqrt{\frac{\xi_s}{\xi_{av}}}\right)^2}{2\sigma_x^2}} dr \\ &= 1 - \frac{1}{2}\text{erfc}\left(d\sqrt{\frac{\xi_s}{2\sigma_x^2\xi_{av}}}\right) \end{aligned} \tag{3.58}$$

where, σ_x is the variance of the x component of the noise. Similarly, the probability of the imaginary component of r being greater than 0, given that s_1 was transmitted, is

$$\begin{aligned} p(\Im_r > 0|s_1) &= 1 - \frac{1}{\sqrt{2\pi}\sigma_y}\int_{-\infty}^{0} e^{\frac{-\left(\Im_r - d\sqrt{\frac{\xi_s}{\xi_{av}}}\right)^2}{2\sigma_y^2}} dr \\ &= 1 - \frac{1}{2}\text{erfc}\left(d\sqrt{\frac{\xi_s}{2\sigma_y^2\xi_{av}}}\right). \end{aligned} \tag{3.59}$$

In Eq (3.59), σ_y is the variance of the y component of the noise. The probability of s_1 being detected correctly is

$$p(c|s_1) = \left[1-\frac{1}{2}\text{erfc}\left(d\sqrt{\frac{\xi_s}{2\sigma_x^2\xi_{av}}}\right)\right]\left[1-\frac{1}{2}\text{erfc}\left(d\sqrt{\frac{\xi_s}{2\sigma_y^2\xi_{av}}}\right)\right]. \quad (3.60)$$

As previously stated in Eq (3.44), for an OM-OFDM transmission

$$\sigma_X^2 \approx \frac{N_o}{2} \quad \text{and} \quad \sigma_Y^2 \approx \frac{N_o}{8\sin^2\left(\frac{-\varphi}{2}\right)} \quad (3.61)$$

after substituting Eq (3.61) into Eq (3.60), this results in

$$p(c|s_1) = \left[1-\frac{1}{2}\text{erfc}\left(d\sqrt{\frac{\xi_s}{N_0\xi_{av}}}\right)\right]\left[1-\frac{1}{2}\text{erfc}\left(d\sqrt{\frac{4\sin^2(-\frac{\varphi}{2})\xi_s}{\xi_{av}N_o}}\right)\right]. \quad (3.62)$$

Now let

$$p = \text{erfc}\left(d\sqrt{\frac{\xi_s}{\xi_{av}N_o}}\right) \quad \text{and} \quad l = \text{erfc}\left(d\sqrt{\frac{4\sin^2(-\frac{\varphi}{2})\xi_s}{\xi_{av}N_o}}\right). \quad (3.63)$$

The resultant probability of symbol s_1 being incorrectly detected is

$$\begin{aligned} p(e|s_1) &= 1-p(c|s_1) \\ &= 1-\left[1-\frac{p}{2}\right]\left[1-\frac{l}{2}\right] \\ &= \frac{2l+2p-p\cdot l}{4}. \end{aligned} \quad (3.64)$$

It can similarly be shown that $p(e|s_1) = p(e|s_2) = p(e|s_3) = p(e|s_0)$. The SER is then

$$P_{SER} = p(s_0)p(e|s_0)+p(s_1)p(e|s_1)+p(s_2)p(e|s_2)+p(s_3)p(e|s_3) \quad (3.65)$$

where $p(s_0)$, $p(s_1)$, $p(s_2)$ and $p(s_3)$ are the probabilities of the s_0, s_1, s_2 and s_3 symbols respectively. If it is assumed that each symbol is equally probable i.e. $p(s_0) = p(s_1) =$

$p(s_2) = p(s_3) = \frac{1}{4}$, then the symbol error probability for this 4-QAM constellation is

$$SER_{4QAM} = \frac{2l + 2p - p \cdot l}{4}. \tag{3.66}$$

If the particular constellation is Gray-coded and $(p(s_0|s_1) \mid p(s_2|s_1)) >> p(s_3|s_1)$ for this 4-QAM constellation, the subsequent bit error rate probability, when symbol s_1 is incorrectly detected, can be written as

$$p(e|b_1) = 1 - \left[1 - \frac{1}{2k}\text{erfc}\left(d\sqrt{\frac{kE_b}{\xi_{av}N_0}}\right)\right]\left[1 - \frac{1}{2k}\text{erfc}\left(d\sqrt{\frac{4k\sin^2(-\frac{\varphi}{2})E_b}{\xi_{av}N_o}}\right)\right] \tag{3.67}$$

where E_b is the energy per bit and $\frac{\xi_s}{N_0} = \frac{kE_b}{N_0}$. Now let

$$\wp = \text{erfc}\left(d\sqrt{\frac{kE_b}{\xi_{av}N_o}}\right) \tag{3.68}$$

and

$$\ell = \text{erfc}\left(d\sqrt{\frac{4k\sin^2(-\frac{\varphi}{2})E_b}{\xi_{av}N_o}}\right). \tag{3.69}$$

The subsequent bit error rate probability when symbol s_1 is incorrectly detected can be written as

$$\begin{aligned} p(e|b_1) &= 1 - \left[1 - \frac{\wp}{2k}\right]\left[1 - \frac{\ell}{2k}\right] \\ &= \frac{2k \cdot \ell + 2\wp \cdot k - \wp \cdot \ell}{4k^2}. \end{aligned} \tag{3.70}$$

It can similarly be shown that $p(e|b_1) = p(e|b_2) = p(e|b_3) = p(e|b_0)$. The BER for this 4-QAM constellation is

$$\begin{aligned} BER_{4QAM} &= p(s_0)p(e|b_0) + p(s_1)p(e|b_1) + p(s_2)p(e|b_2) + p(s_3)p(e|b_3) \\ &= \frac{2k \cdot \ell + 2\wp \cdot k - \wp \cdot \ell}{4k^2}. \end{aligned} \tag{3.71}$$

3.4.3 A 16-QAM symbol and bit error rate derivation

3.4.3.1 Symbols in the centre of a constellation

For a 16-QAM constellation, depicted in Fig. 3.10, the symbol s_5 is correctly detected only

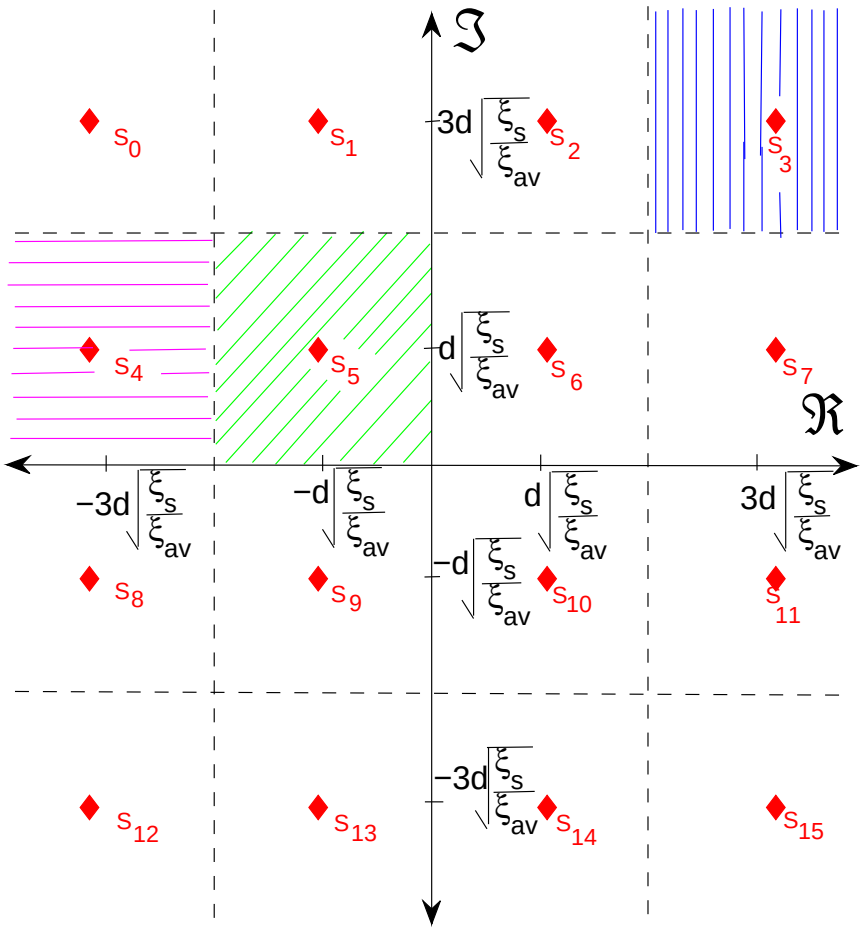

Figure 3.10: 16-QAM constellation

if r falls in the forward hashed green region as indicated by the following expression

$$p(c|s_5) = p\left(\Re_r \leq 0, \Re_r > -2d\sqrt{\frac{\xi_s}{\xi_{av}}}\middle| s_5\right) p\left(\Im_r > 0, \Im_r \leq 2d\sqrt{\frac{\xi_s}{\xi_{av}}}\middle| s_5\right). \quad (3.72)$$

By making use of Eq (3.53) for a 4-PAM constellation

$$p(c|s_5) = \left[1 - \text{erfc}\left(d\sqrt{\frac{\xi_s}{2\sigma_x^2\xi_{av}}}\right)\right]\left[1 - \text{erfc}\left(d\sqrt{\frac{\xi_s}{2\sigma_y^2\xi_{av}}}\right)\right]. \tag{3.73}$$

After substituting Eq (3.61) into Eq (3.73), this results in

$$p(c|s_5) = \left[1 - \text{erfc}\left(d\sqrt{\frac{\xi_s}{N_0\xi_{av}}}\right)\right]\left[1 - \text{erfc}\left(d\sqrt{\frac{4\sin^2(-\frac{\varphi}{2})\xi_s}{\xi_{av}N_o}}\right)\right]. \tag{3.74}$$

After substituting Eq (3.63) into Eq (3.74), the resultant probability of symbol s_5 being incorrectly detected is

$$\begin{aligned} p(e|s_5) &= 1 - p(c|s_5). \\ &= l + p - p \cdot l. \end{aligned} \tag{3.75}$$

In addition, it can be shown that $p(e|s_5) = p(e|s_6) = p(e|s_9) = p(e|s_{10})$. The subsequent bit error rate probability when symbol s_5 is incorrectly detected can be written as

$$\begin{aligned} p(e|b_5) &= 1 - \left[1 - \frac{1}{k}\text{erfc}\left(d\sqrt{\frac{kE_b}{\xi_{av}N_0}}\right)\right]\left[1 - \frac{1}{k}\text{erfc}\left(d\sqrt{\frac{4k\sin^2(-\frac{\varphi}{2})E_b}{\xi_{av}N_o}}\right)\right] \\ &= \frac{k\cdot\ell + \wp\cdot k - \wp\cdot\ell}{k^2}. \end{aligned} \tag{3.76}$$

Similarly it can be shown that $p(e|b_5) = p(e|b_6) = p(e|b_9) = p(e|b_{10})$.

3.4.3.2 Symbols in the corner of a constellation

In Fig. 3.10, the symbol s_3 is correctly detected only if r falls in the vertical blue region, as indicated by the following expression

$$p(c|s_3) = p\left(\Re_r > 2d\sqrt{\frac{\xi_s}{\xi_{av}}}\middle| s_3\right) p\left(\Im_r > 2d\sqrt{\frac{\xi_s}{\xi_{av}}}\middle| s_3\right). \tag{3.77}$$

By making use of Eq (3.60) for a 4-QAM constellation and Eq (3.61)

$$\begin{aligned} p(c|s_3) &= \left[1-\frac{1}{2}\text{erfc}\left(d\sqrt{\frac{\xi_s}{2\sigma_x^2\xi_{av}}}\right)\right]\left[1-\frac{1}{2}\text{erfc}\left(d\sqrt{\frac{\xi_s}{2\sigma_y^2\xi_{av}}}\right)\right] \\ &= \left[1-\frac{1}{2}\text{erfc}\left(d\sqrt{\frac{\xi_s}{N_0\xi_{av}}}\right)\right]\left[1-\frac{1}{2}\text{erfc}\left(d\sqrt{\frac{4\sin^2(-\frac{\varphi}{2})\xi_s}{\xi_{av}N_o}}\right)\right]. \end{aligned} \quad (3.78)$$

From Eq (3.63) the probability of symbol s_3 being detected incorrectly is

$$\begin{aligned} p(e|s_3) &= 1-p(c|s_3) \\ &= \frac{2l+2p-p\cdot l}{4}. \end{aligned} \quad (3.79)$$

It can also be shown that $p(e|s_3)=p(e|s_0)=p(e|s_{12})=p(e|s_{15})$. As previously mentioned, from Eq (3.68) and Eq (3.69), the subsequent bit error rate probability, when symbol s_3 is incorrectly detected, can be written as

$$\begin{aligned} p(e|b_3) &= 1-\left[1-\frac{1}{2k}\text{erfc}\left(d\sqrt{\frac{kE_b}{\xi_{av}N_0}}\right)\right]\left[1-\frac{1}{2k}\text{erfc}\left(d\sqrt{\frac{4k\sin^2(-\frac{\varphi}{2})E_b}{\xi_{av}N_o}}\right)\right] \\ &= \frac{2k\cdot\ell+2\wp\cdot k-\wp\cdot\ell}{4k^2}. \end{aligned} \quad (3.80)$$

Similarly it can be shown that $p(e|b_3)=p(e|b_0)=p(e|b_{12})=p(e|b_{15})$.

3.4.3.3 Symbols at the edge of a constellation

From Fig. 3.10, the symbol s_4 is correctly detected only if r falls in the horizontal pink region as indicated by the following expression

$$p(c|s_4)=p\left(\Re_r<-2d\sqrt{\frac{\xi_s}{\xi_{av}}}\middle|s_4\right)p\left(\Im_r\geq 0,\Im_r<2d\sqrt{\frac{\xi_s}{\xi_{av}}}\middle|s_4\right). \quad (3.81)$$

After substituting part of Eq (3.73) and part of Eq (3.78) into Eq (3.81), this results in

$$p(c|s_4) = \left[1-\frac{1}{2}\text{erfc}\left(d\sqrt{\frac{\xi_s}{2\sigma_x^2\xi_{av}}}\right)\right]\left[1-\text{erfc}\left(d\sqrt{\frac{\xi_s}{2\sigma_y^2\xi_{av}}}\right)\right]$$

$$= \left[1-\frac{1}{2}\text{erfc}\left(d\sqrt{\frac{\xi_s}{N_0\xi_{av}}}\right)\right]\left[1-\text{erfc}\left(d\sqrt{\frac{4\sin^2(-\frac{\varphi}{2})\xi_s}{\xi_{av}N_o}}\right)\right]. \quad (3.82)$$

After using Eq (3.63), the probability of symbol s_4 being detected incorrectly is

$$\begin{aligned} p(e|s_4) &= 1-p(c|s_4) \\ &= \frac{2l+p-p\cdot l}{2}. \end{aligned} \quad (3.83)$$

In addition, it can be shown that $p(e|s_4) = p(e|s_1) = p(e|s_2) = p(e|s_7) = p(e|s_8) = p(e|s_{11}) = p(e|s_{13}) = p(e|s_{14})$. The subsequent bit error rate probability when symbol s_4 is incorrectly detected can be written as

$$\begin{aligned} p(e|b_4) &= 1-\left[1-\frac{1}{2k}\text{erfc}\left(d\sqrt{\frac{kE_b}{\xi_{av}N_0}}\right)\right]\left[1-\frac{1}{k}\text{erfc}\left(d\sqrt{\frac{4k\sin^2(-\frac{\varphi}{2})E_b}{\xi_{av}N_o}}\right)\right] \\ &= \frac{2k\cdot\ell+\wp\cdot k-\wp\cdot\ell}{2k^2}. \end{aligned} \quad (3.84)$$

Similarly it can be shown that $p(e|b_4) = p(e|b_1) = p(e|b_2) = p(e|b_7) = p(e|b_8) = p(e|b_{11}) = p(e|b_{13}) = p(e|b_{14})$.

3.4.3.4 Combination of all symbols

From Eq (3.75), Eq (3.76), Eq (3.79), Eq (3.80), Eq (3.83) and Eq (3.84), assuming that all the symbols are equally probable (4 centre symbols, 4 corner symbols and 8 edge symbols), the SER and BER expressions for a 16-QAM constellation are given as

$$\begin{aligned} SER_{16QAM} &= \frac{4}{16}\left(\frac{l+p-p\cdot l}{1}\right)+\frac{4}{16}\left(\frac{2l+2p-p\cdot l}{4}\right)+\frac{8}{16}\left(\frac{2l+p-p\cdot l}{2}\right) \\ &= \left(\frac{14\cdot l+10p-9p\cdot l}{16}\right) \end{aligned} \quad (3.85)$$

and

$$BER_{16QAM} = \frac{4}{16}\left(\frac{k\cdot\ell+\wp\cdot k-\wp\cdot\ell}{k^2}\right)+\frac{4}{16}\left(\frac{2k\cdot\ell+2\wp\cdot k-\wp\cdot\ell}{4k^2}\right)+\frac{8}{16}\left(\frac{2k\cdot\ell+\wp\cdot k-\wp\cdot\ell}{2k^2}\right) = \frac{1}{16}\left(\frac{14k\cdot\ell+10\wp\cdot k-9\wp\cdot\ell}{k^2}\right). \quad (3.86)$$

3.4.3.5 A 64-QAM symbol and bit error rate derivation

A 64-QAM constellation, partially depicted in Fig. 3.11, is composed of four quadrants. Each quadrant contains 16 symbol points; consider one of these quadrants. Assuming that

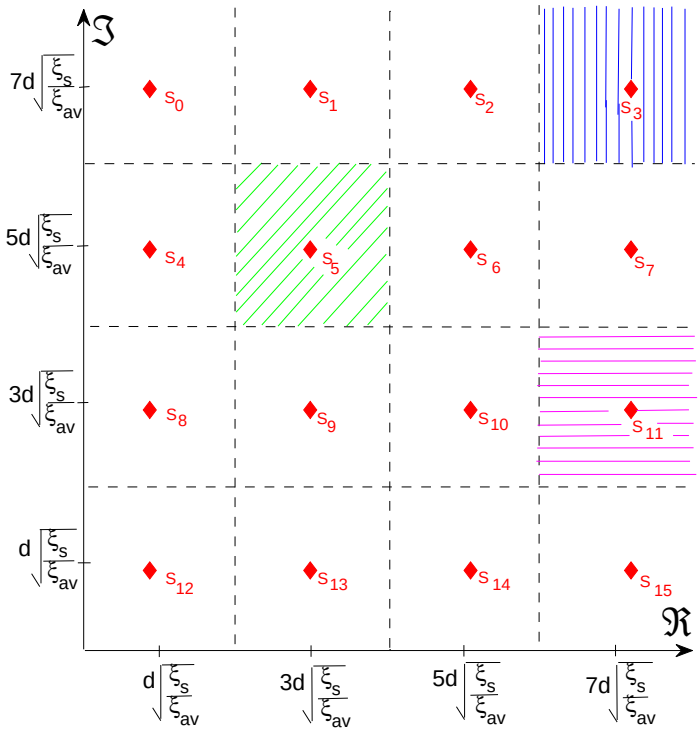

Figure 3.11: 64-QAM constellation

all the symbols of a 64-QAM constellation are equally probable (9 centre symbols in each of the 4 quadrants; 1 corner symbols in each of the 4 quadrants and 6 edge symbols in each

of the 4 quadrants), thereafter by using Eq (3.75), Eq (3.76), Eq (3.79), Eq (3.80), Eq (3.83) and Eq (3.84) the total probability of a symbol error and bit error are given as

$$\begin{aligned} SER_{64QAM} &= \frac{4\cdot 9}{64}\left(\frac{l+p-p\cdot l}{1}\right)+\frac{4\cdot 1}{64}\left(\frac{2l+2p-p\cdot l}{4}\right)+\frac{4\cdot 6}{64}\left(\frac{2l+p-p\cdot l}{2}\right) \\ &= \frac{1}{64}\left(\frac{62l+50p-49p\cdot l}{1}\right) \end{aligned} \tag{3.87}$$

and

$$\begin{aligned} BER_{64QAM} &= \frac{4\cdot 9}{64}\left(\frac{k\cdot \ell+\wp\cdot k-\wp\cdot \ell}{k^2}\right)+\frac{4\cdot 1}{64}\left(\frac{2k\cdot \ell+2\wp\cdot k-\wp\cdot \ell}{4k^2}\right)+ \\ &\quad \frac{4\cdot 6}{64}\left(\frac{2k\cdot \ell+\wp\cdot k-\wp\cdot \ell}{2k^2}\right) \\ &= \frac{1}{64}\left(\frac{62k\cdot \ell+50\wp\cdot k-49\wp\cdot \ell}{k^2}\right). \end{aligned} \tag{3.88}$$

This type of analysis can be extended further to investigate various other M-ary QAM constellations.

3.4.4 M-ary QAM symbol and bit error rate derivation

The previous sub-section has demonstrated the relationship between BER and SER. In this sub-section closed-form SER and BER expressions for M-ary QAM constellations are presented.

From the previous sub-sections, Table 3.3 and Table 3.4 present some of the results obtained. The remaining results were obtained after following a similar methodology. After studying these particular SER and BER expressions in Table 3.3 and Table 3.4, a particular relationship emerges which can be encapsulated by the following equations

$$SER_{EVEN} \approx \frac{l(M-2)+p\cdot(M-2\sqrt{M}+2)}{M}+\frac{p\cdot l(2\sqrt{M}-M-1)}{M}, \tag{3.89}$$

Table 3.3: Summarised SER QAM expressions

$QAM_{k=EVEN}$	**SER expressions**	$QAM_{k=ODD}$	**SER expressions**
4	$\frac{2l+2p-p\cdot l}{4}$	8	$\frac{6l+4p-3p\cdot l}{8}$
16	$\frac{14l+10p-9p\cdot l}{16}$	32	$\frac{30l+22p-21p\cdot l}{32}$
64	$\frac{62l+50p-49p\cdot l}{64}$	128	$\frac{126l+106p-105p\cdot l}{128}$
256	$\frac{254l+226p-225p\cdot l}{256}$	512	$\frac{510l+466p-465p\cdot l}{256}$

Table 3.4: Summarised BER QAM expressions

$QAM_{k=EVEN}$	**BER expressions**	$QAM_{k=ODD}$	**BER expressions**
4	$\frac{2k\cdot\ell+2\wp\cdot k-\wp\cdot\ell}{4k^2}$	8	$\frac{6k\cdot\ell+4\wp\cdot k-3\wp\cdot\ell}{8k^2}$
16	$\frac{14k\cdot\ell+10\wp\cdot k-9\wp\cdot\ell}{16k^2}$	32	$\frac{30k\cdot\ell+22\wp\cdot k-21\wp\cdot\ell}{32k^2}$
64	$\frac{62k\cdot\ell+50\wp\cdot k-49\wp\cdot\ell}{64k^2}$	128	$\frac{126k\cdot\ell+106\wp\cdot k-105\wp\cdot\ell}{128k^2}$
256	$\frac{254k\cdot\ell+226\wp\cdot k-225\wp\cdot\ell}{256k^2}$	512	$\frac{510k\cdot\ell+466\wp\cdot k-465\wp\cdot\ell}{256k^2}$

$$SER_{ODD} \approx \frac{\left(M-2-\left[\frac{3\sqrt{2}M-8\sqrt{M}}{2\sqrt{M}}\right]\right)p}{M} + \frac{(M-2)\cdot l-\left(M-3-\left[\frac{3\sqrt{2}M-8\sqrt{M}}{2\sqrt{M}}\right]\right)p\cdot l}{M}, \tag{3.90}$$

$$BER_{EVEN} \approx \frac{k\cdot\ell(M-2)+\wp\cdot k(M-2\sqrt{M}+2)}{M\cdot k^2}+\frac{\wp\cdot\ell(2\sqrt{M}-M-1)}{M\cdot k^2} \tag{3.91}$$

and

$$BER_{ODD} \approx \frac{\left(M-2-\left[\frac{3\sqrt{2}M-8\sqrt{M}}{2\sqrt{M}}\right]\right)\wp\cdot k}{M\cdot k^2} + \frac{(M-2)k\cdot\ell-\left(M-3-\left[\frac{3\sqrt{2}M-8\sqrt{M}}{2\sqrt{M}}\right]\right)\wp\cdot\ell}{M\cdot k^2}. \quad (3.92)$$

The subsequent expressions presented in Eq (3.89), Eq (3.90), Eq (3.91) and Eq (3.92) can be used to determine the SER and BER characteristics for any M-ary QAM OM-OFDM transmission.

3.4.5 M-ary PSK symbol and bit error rate derivation

In this sub-section an M-ary SER and BER expression for a PSK constellation is derived. In order to simplify the discussion the 16-PSK case will be discussed. This 16-PSK constellation, depicted in Fig. 3.12, can be adapted to include any M-ary PSK constellation.

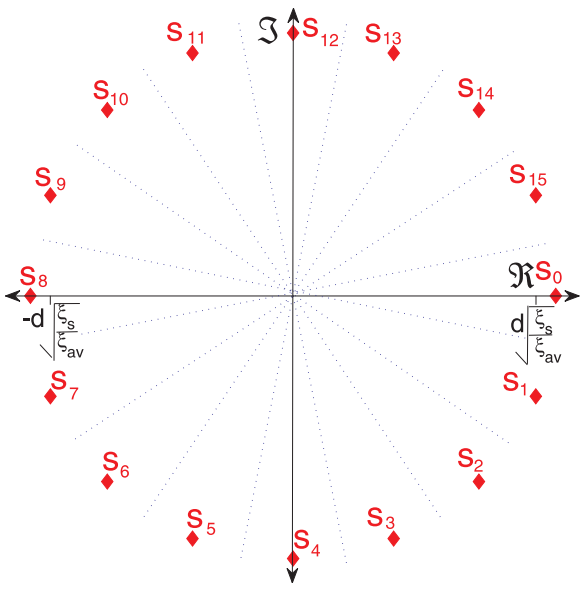

Figure 3.12: 16-PSK constellation

Consider symbol s_0, depicted in Fig. 3.12, on the real axis

$$s_0 = d\sqrt{\frac{\xi_s}{\xi_{av}}}. \tag{3.93}$$

The received symbol is $r = d\sqrt{\frac{\xi_s}{\xi_{av}}} + n$, where n is the AWGN noise. For a high SNR, the real part of the received signal, depicted in Fig. 3.13, should be correctly detected. As seen

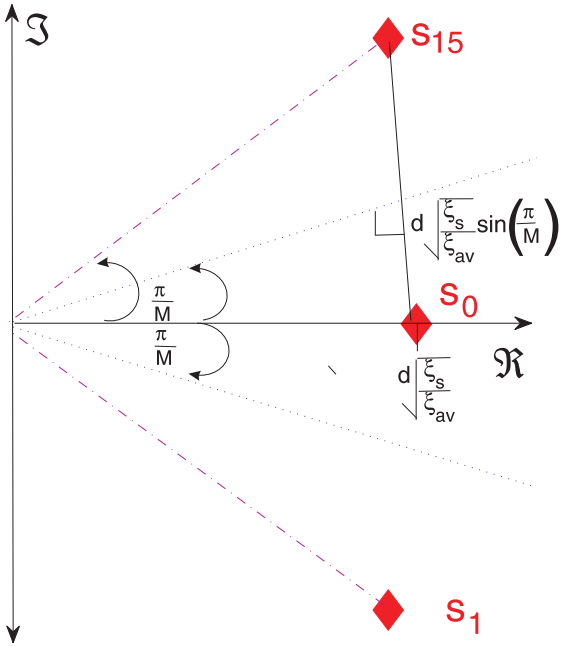

Figure 3.13: Distance between PSK constellation points

in Fig. 3.13, the symbol s_0 is incorrectly detected only if r falls outside the boundary region defined by the dotted blue lines. This may be expressed as

$$p(e|s_0) = p\left(\Im_r > d\sqrt{\frac{\xi_s}{\xi_{av}}}\sin\left(\frac{\pi}{M}\right)\middle| s_0\right) + p\left(\Im_r < -d\sqrt{\frac{\xi_s}{\xi_{av}}}\sin\left(\frac{\pi}{M}\right)\middle| s_0\right) \tag{3.94}$$

where

$$p\left(\Im_r > d\sqrt{\frac{\xi_s}{\xi_{av}}}\sin\left(\frac{\pi}{M}\right)\middle| s_0\right) = \frac{1}{\sqrt{2\pi}\sigma_y}\int_{d\sqrt{\frac{\xi_s}{\xi_{av}}}\sin(\frac{\pi}{M})}^{\infty} e^{\frac{-\Im_r{}^2}{2\sigma_y^2}}\, dr. \tag{3.95}$$

Let $u = \frac{-\Im_r}{\sqrt{2\sigma_y^2}}$, then

$$p\left(\Im_r > d\sqrt{\frac{\xi_s}{\xi_{av}}}\sin\left(\frac{\pi}{M}\right)\middle| s_0\right) = \frac{1}{\sqrt{\pi}}\int_{d\sqrt{\frac{\xi_s}{2\sigma_y\xi_{av}}}\sin(\frac{\pi}{M})}^{\infty} e^{-u^2}du$$
$$= \frac{1}{2}\text{erfc}\left(d\sqrt{\frac{\xi_s}{2\sigma_y\xi_{av}}}\sin\left(\frac{\pi}{M}\right)\right). \quad (3.96)$$

After substituting Eq (3.61) into Eq (3.96), this results in

$$p\left(\Im_r > d\sqrt{\frac{\xi_s}{\xi_{av}}}\sin\left(\frac{\pi}{M}\right)\middle| s_0\right) = \frac{1}{2}\text{erfc}\left(d\sqrt{\frac{4\xi_s}{N_0\xi_{av}}}\sin\left(\frac{\pi}{M}\right)\sin\left(\frac{-\varphi}{2}\right)\right). \quad (3.97)$$

The symbol s_0 is incorrectly detected if the imaginary component of the received real component is less than $-d\sqrt{\frac{\xi_s}{\xi_{av}}}\sin(\frac{\pi}{M})$. The probability of s_0 being incorrectly detected can be written as

$$p\left(\Im_r < -d\sqrt{\frac{\xi_s}{\xi_{av}}}\sin\left(\frac{\pi}{M}\right)\middle| s_0\right) = \frac{1}{\sqrt{\pi}}\int_{-\infty}^{-d\sqrt{\frac{\xi_s}{2\sigma_y\xi_{av}}}\sin(\frac{\pi}{M})} e^{-u^2}du$$
$$= \frac{1}{2}\text{erfc}\left(d\sqrt{\frac{4\xi_s}{N_0\xi_{av}}}\sin\left(\frac{\pi}{M}\right)\sin\left(\frac{-\varphi}{2}\right)\right). \quad (3.98)$$

The total conditional probability of an error, given that s_0 was transmitted, is

$$p(e|s_0) = \text{erfc}\left(d\sqrt{\frac{4\xi_s}{N_0\xi_{av}}}\sin\left(\frac{\pi}{M}\right)\sin\left(\frac{-\varphi}{2}\right)\right). \quad (3.99)$$

If it is assumed that each of M-PSK symbols are equally probable. The total symbol error probability for a M-PSK constellation is

$$SER_{PSK} = \text{erfc}\left(d\sqrt{\frac{4\xi_s}{N_0\xi_{av}}}\sin\left(\frac{\pi}{M}\right)\sin\left(\frac{-\varphi}{2}\right)\right). \quad (3.100)$$

For a Gray-coded constellation, when $(p(s_1|s_0)|p(s_{15}|s_0)) >> (p(s_2|s_0)|p(s_{14}|s_0))$ the sub-

sequent bit error rate can be written as

$$BER_{PSK} = \frac{1}{k}\text{erfc}\left(d\sqrt{\frac{4k\cdot E_b \sin^2\left(\frac{-\varphi}{2}\right)\sin^2\left(\frac{\pi}{M}\right)}{N_o}}\right). \tag{3.101}$$

The expressions presented in Eq (3.100) and Eq (3.101) can be used to determine the SER and BER characteristics for an M-ary PSK OM-OFDM transmission.

3.5 OM-OFDM PARAMETER SELECTION

In this section the manner in which the selection of the Ψ_{os}, ς and γ terms influences the derived 64-QAM BER expression, at a SNR=7 dB (E_b/N_o), will be investigated. Although this discussion may seem confined to this particular case (64-QAM, SNR=7 dB), it can be extended to include various other constellations. For the choice of Ψ_{os}, ς and γ terms, both Eq (3.44) and Table 3.2 (provided $0 \leq \varphi \leq \frac{\pi}{2}$) offer guidelines for these parameters. In order

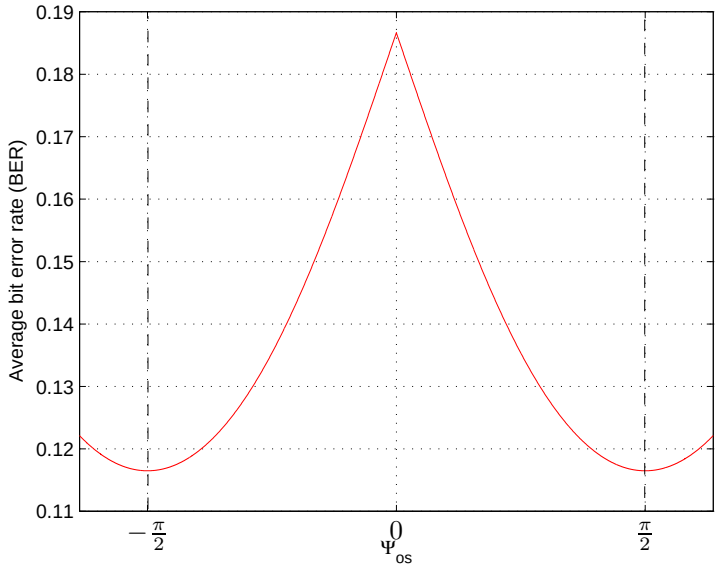

Figure 3.14: Ψ_{os} Parameter choice when $\gamma = 0.95$ and $\varsigma = 44000/16384$ in an AWGN channel for a 64-QAM constellation, with SNR=7 dB (E_b/N_o).

to obtain the relationship between BER and Ψ_{os}; the ς and γ terms are kept constant and the Ψ_{os} term is varied. As shown in Fig. 3.14, as Ψ_{os} approaches the limits ($\Psi_{os} = -\frac{\pi}{2}, \frac{\pi}{2}$),

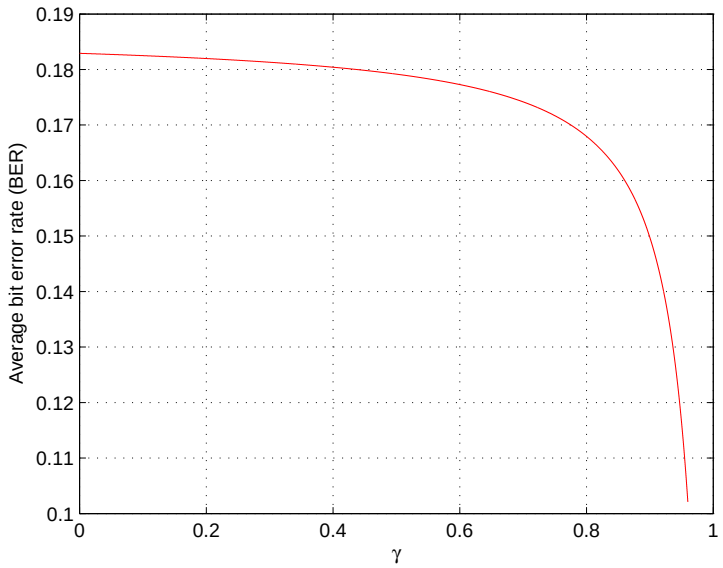

Figure 3.15: γ Parameter choice when $\Psi_{os} = 1.59$ and $\varsigma = 44000/16384$ in an AWGN channel for a 64-QAM constellation, with SNR=7 dB (E_b/N_o).

the noise components are lowered. As shown in Fig. 3.14, an increase in BER degradation is evident as the Ψ_{os} term moves away from these limits. It is also noted that as the ς term increases, the signal would lose resolution, which will affect the BER performance of the system.

Similarly in Fig. 3.15, in order to obtain the relationship between BER and γ; the Ψ_{os} and ς terms are kept constant and the γ term is varied. As shown in Fig. 3.15, as the γ term approaches 1, the noise decreases, since the PAPR is being sacrificed to obtain this BER performance improvement.

3.6 VALIDATION OF THE DERIVATION

Using these guidelines, the commonly used theoretically derived expressions needed to be validated. It should be noted that the theoretical expressions do not accept a $\gamma = 1$; if such a term arises, then $\varphi = 1$ (SER_{EVEN}, BER_{EVEN}), $\varphi = 1.5$ (SER_{ODD}, BER_{ODD}) and $\varphi = 1.23$ (SER_{PSK}, BER_{PSK}). These values simplify Eq (3.89), Eq (3.90), Eq (3.91), Eq (3.92), Eq (3.100) and Eq (3.101) into a SER and BER expression for an AWGN transmission.

By means of a simulation (the 2k or the 8k mode of the DVB-T2 standard [95]), offset modulated 4-QAM, 16-QAM and 64-QAM, as well as QPSK and 8-PSK Gray-coded signal constellations, were used to transmit data through an AWGN channel. The parameters used for the 4-QAM, 16-QAM, 64-QAM, QPSK and 8-PSK OM-OFDM transmission are given in Table 3.5, Table 3.6, Table 3.7, Table 3.8 and Table 3.9, respectively.

In these Tables the φ term is calculated by substituting the α, ς, Ψ_{os} and γ terms into the φ expression in Table 3.2. The specific terms (ς and Ψ_{os}) are chosen (as previously discussed in Section 3.5) such that they minimise the BER degradation, and the α term is obtained as indicated in Eq (3.18) and Eq (3.19).

In all these Tables the various parameters for a 7 dB - 13 dB PAPR range are presented. The γ term can be further varied, until an average PAPR in the range of 3 dB - 13 dB is reached. The lower bound (3 dB) is the ideal average PAPR [87] and the upper bound (12 dB or 13 dB) indicates the average PAPR of a traditional OFDM transmission [98] (since an attempt is made to reduce this PAPR).

Various BER comparisons between the theoretically derived and simulated OM-OFDM transmissions for various constellations are shown in Fig. 3.16, Fig. 3.17, Fig. 3.18, Fig. 3.19 and Fig. 3.20.

Table 3.5: Parameters for an 4-QAM OM-OFDM system ($\alpha = 0.036$)

PAPR	Ψ_{os}	ς	γ	φ
7 dB	1.5	10000/4096	0.9835	0.22
8 dB	1.5	10000/4096	0.9882	0.31
9 dB	1.5	10000/4096	0.992	0.4
10 dB	1.5	10000/4096	0.994	0.5
11 dB	1.5	10000/4096	0.996	0.7
12 dB	1.5	10000/4096	1	1

Table 3.6: Parameters for an 16-QAM OM-OFDM system($\alpha = 0.07408$)

PAPR	Ψ_{os}	ς	γ	φ
7 dB	1.5	10000/4096	0.963	0.205
8 dB	1.5	10000/4096	0.973	0.280
9 dB	1.5	10000/4096	0.98	0.378
10 dB	1.5	10000/4096	0.985	0.505
11 dB	1.5	10000/4096	0.988	0.631
12 dB	1.5	10000/4096	1	1.0

Table 3.7: Parameters for an 64-QAM OM-OFDM system ($\alpha = 0.27$)

PAPR	Ψ_{os}	ς	γ	φ
7 dB	1.596	44000/16384	0.86	0.2
8 dB	1.596	44000/16384	0.9	0.251
9 dB	1.596	44000/16384	0.925	0.34
10 dB	1.596	44000/16384	0.943	0.44
11 dB	1.596	44000/16384	0.962	0.53
12 dB	1.596	44000/16384	0.97	0.67
13 dB	1.596	44000/16384	1	1

Table 3.8: Parameters for QPSK OM-OFDM system ($\alpha = 0.027$)

PAPR	Ψ_{os}	ς	γ	φ
7 dB	1.5	10000/4096	0.98845	0.24
8 dB	1.5	10000/4096	0.992	0.3
9 dB	1.5	10000/4096	0.99418	0.4674
10 dB	1.5	10000/4096	0.996	0.55
11 dB	1.5	10000/4096	0.997	0.7
12 dB	1.5	10000/4096	1	1

Table 3.9: Parameters for 8-PSK OM-OFDM system ($\alpha = 0.027$)

PAPR	Ψ_{os}	ς	γ	φ
7 dB	1.5	10000/4096	0.9889	0.2485
8 dB	1.5	10000/4096	0.992	0.3
9 dB	1.5	10000/4096	0.9941	0.4674
10 dB	1.5	10000/4096	0.996	0.55
11 dB	1.5	10000/4096	0.997	0.7
12 dB	1.5	10000/4096	1	1

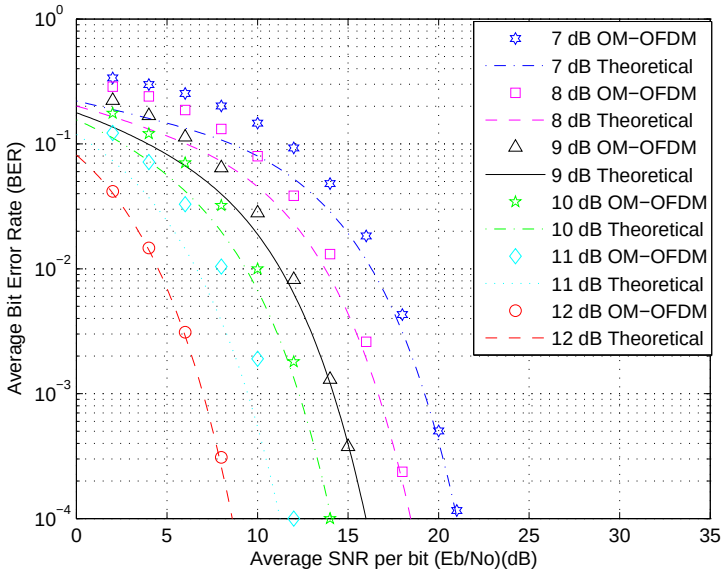

Figure 3.16: Theoretically derived (Eq (3.91)) and simulated BER comparisons for an OM-OFDM transmission in an AWGN channel for a 4-QAM constellation.

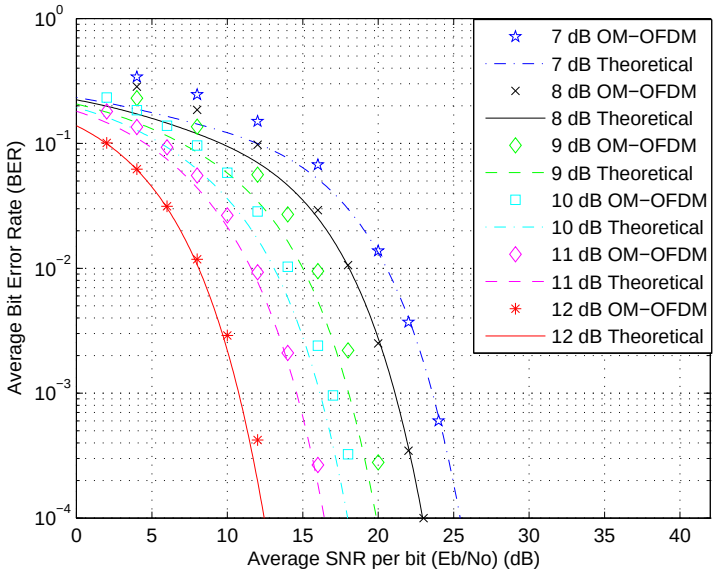

Figure 3.17: Theoretically derived (Eq (3.91)) and simulated BER comparisons for an OM-OFDM transmission in an AWGN channel for a 16-QAM constellation.

From this comparison, it is seen that the theoretically predicted results (Eq (3.91) and Eq (3.101)) and the simulated results correlate reasonably well, thus validating the theoretically derived expression. The slight difference between the simulated and theoretical results is due to the fact that the theoretical analysis does not take into account certain errors (e.g.

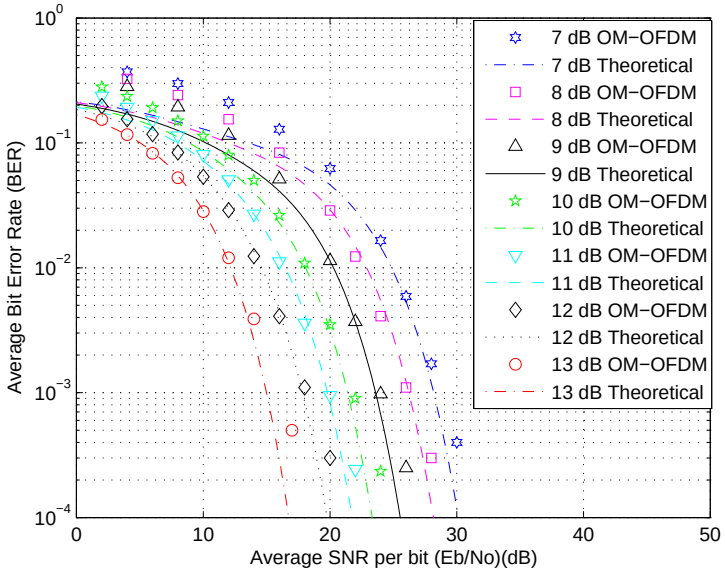

Figure 3.18: Theoretically derived (Eq (3.91)) and simulated BER comparisons for an OM-OFDM transmission in an AWGN channel for a 64-QAM constellation.

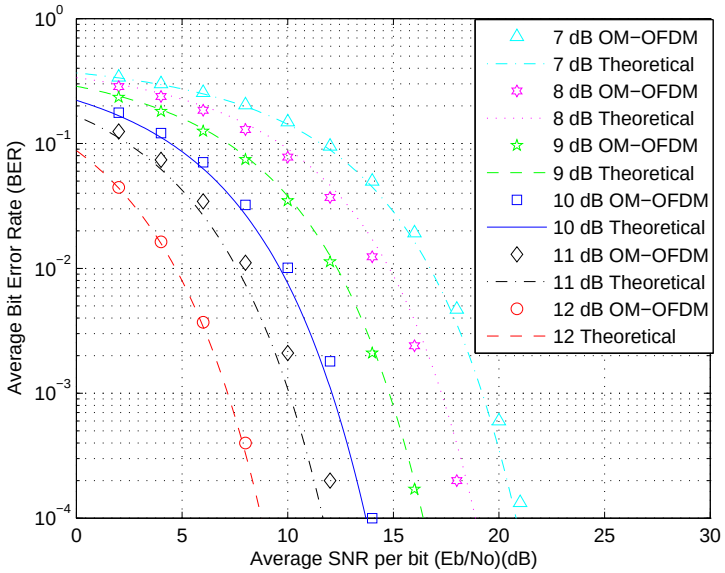

Figure 3.19: Theoretically derived (Eq (3.101)) and simulated BER comparisons for an OM-OFDM transmission in an AWGN channel for a QPSK constellation.

filter effects and quantisation effects, amongst others). Furthermore, Fig. 3.21, Fig. 3.22, Fig. 3.23, Fig. 3.24 and Fig. 3.25 depict the complementary cumulative distribution function for a 4-QAM, 16-QAM, 64-QAM, QPSK and 8-PSK OM-OFDM transmission, respectively.

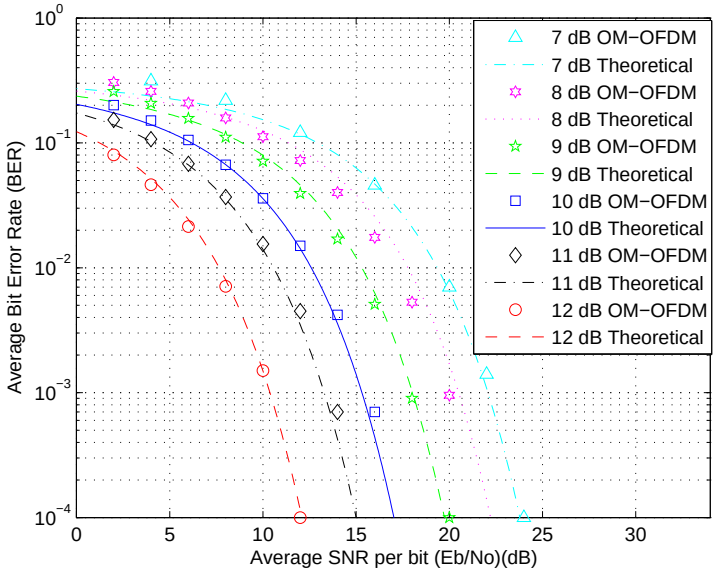

Figure 3.20: Theoretically derived (Eq (3.101)) and simulated BER comparisons for an OM-OFDM transmission in an AWGN channel for an 8-PSK constellation.

This CCDF graph can be interpreted as the probability of the various transmissions having a PAPR value above a certain threshold ($PAPR_o$). In the next section a decision metric is presented, which will later be used to determine the optimum OM-OFDM operating point.

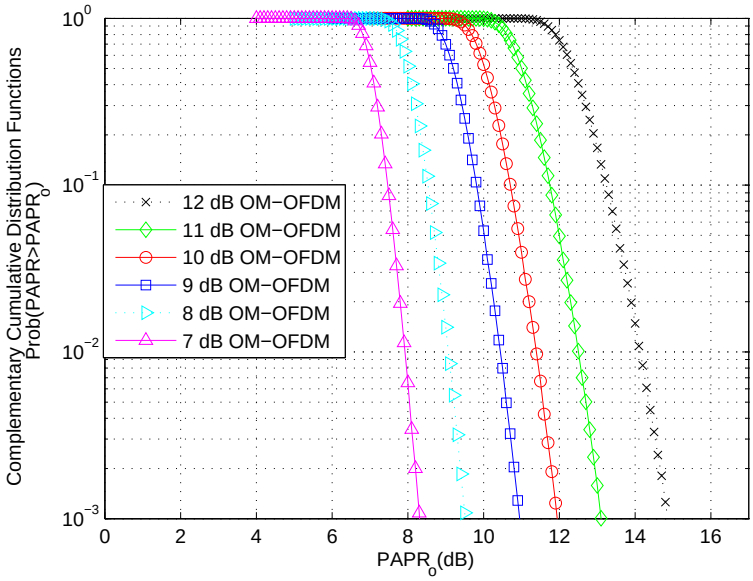

Figure 3.21: Complementary cumulative distribution functions for a 4-QAM constellation.

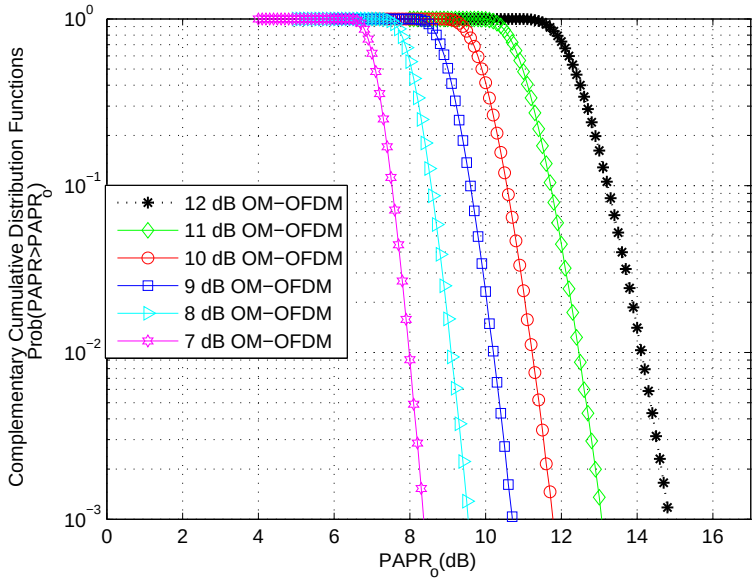

Figure 3.22: Complementary cumulative distribution functions for a 16-QAM constellation.

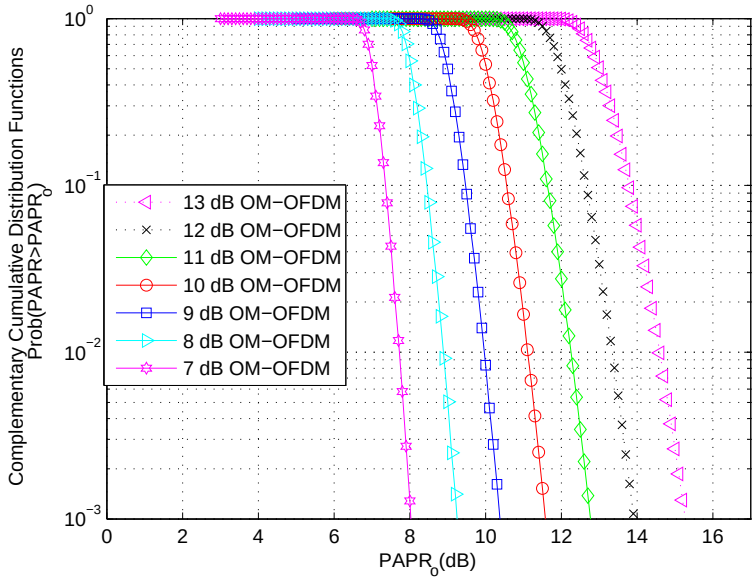

Figure 3.23: Complementary cumulative distribution functions for a 64-QAM constellation.

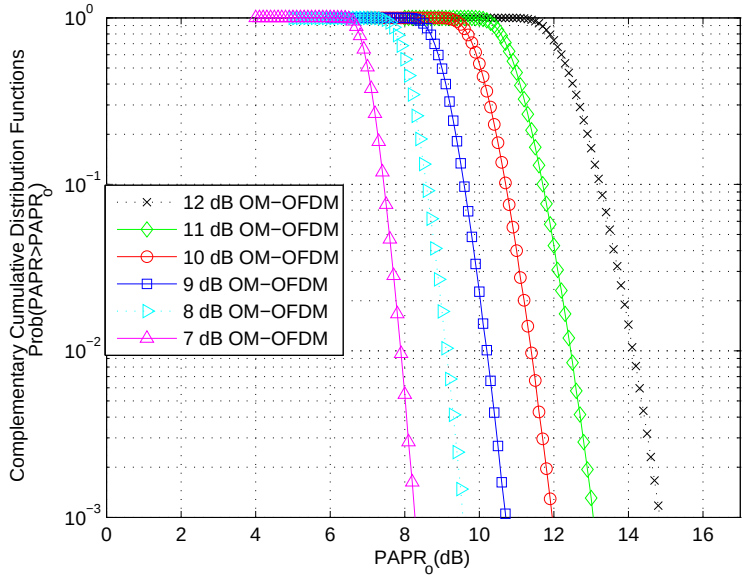

Figure 3.24: Complementary cumulative distribution functions for a QPSK constellation.

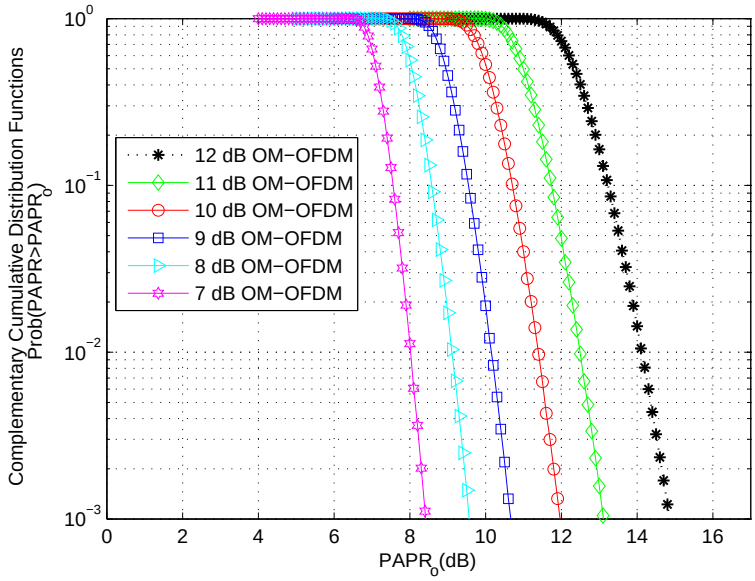

Figure 3.25: Complementary cumulative distribution functions for an 8-PSK constellation.

3.7 DECISION METRIC

The conventional metric used to describe a communication system is BER, which is usually a function of $\frac{E_b}{N_o}$. The relationship between energy per bit E_b, average received power $\overline{P_r}$ and data rate R_b is given by [99]

$$E_b \quad (joules/bit) \quad = \quad \frac{\overline{P_r} \quad (joules/s)}{R_b \quad (bits/s)}. \tag{3.102}$$

The E_b only takes into account the received energy per bit and offers no indication of the actual total energy required (e.g. dc power consumption of the amplifier) for transmission of an information bit. To obtain an indication of this, consider the instantaneous power-added efficiency (PAE) of the amplifier given by

$$P_{ae} \quad = \quad \frac{P_{rf}(t) - P_{in}(t)}{P_{dc}(t)} \tag{3.103}$$

where $P_{dc}(t)$ is the dc power supplied to the amplifier, P_{in} and P_{rf} are the input and output RF powers of the amplifier, respectively. The average total power $\overline{P_t}$ consumed by an amplifier, after using Eq (3.103), can be written as

$$\begin{aligned} \overline{P_t} &= \overline{P_{dc}} + \overline{P_{in}} \\ &= \overline{P_{rf}}\left(1 + \frac{\overline{P_{dc}}(1-\overline{P_{ae}})}{\overline{P_{rf}}}\right) \\ &= \overline{P_{rf}}(1+w) \end{aligned} \tag{3.104}$$

where $\overline{X}$ denotes the average power of X and w refers to the fractional average power not converted to RF power. The total energy per bit E_t for a given BER and N_o can be written as

$$\begin{aligned} E_t &= \frac{\overline{P_t}}{R_b} \\ &= \frac{\overline{P_r}(1+w)}{R_b} \\ &= E_b + E_w. \end{aligned} \tag{3.105}$$

In Eq (3.105), $\overline{P_r}$ is the average received power and $\overline{P_{rf}} = \overline{P_r}$. In addition E_w is the wasted energy per bit due to the inefficient power amplifier utilisation. As the input drive level increases, the E_w decreases. Increasing the input drive level improves efficiency; however, if an optimum back-off is not maintained, this distorts the signal waveform, which results in a BER trade-off. Another metric used to describe spectral efficiency is

$$\frac{R_b}{W} \quad (bits/s/Hz), \tag{3.106}$$

where R_b is the data rate and W refers to the bandwidth occupancy. Liang et al. [99] have proposed a decision metric (D), which combines two metrics and is given by

$$D = \frac{E_t}{N_o} \cdot \frac{W}{R_b}, \tag{3.107}$$

Unlike traditional approaches, which only take into account the received energy per bit (E_b) and often ignore the total energy consumption (e.g. dc power consumption of the amplifier), here, E_t incorporates the total energy per bit and as discussed (Eq (3.105)) can be written as

$$E_t = E_b + E_w, \tag{3.108}$$

where, E_w is the wasted energy per bit due to inefficient power amplifier utilisation. In order to determine E_t, the PAE of the amplifier which is to be used, is required. Liang et al. [99] have used this metric to investigate the trade-offs between amplifier efficiency, amplifier distortion, signal bandwidth occupation, throughput and power consumption. The purpose of the decision metric was to investigate an optimum combination of these factors to minimise the energy required. This metric can be adapted to investigate whether the proposed OM-OFDM transmission has an optimum solution and whether a net gain exists for such a solution. This adaptation involves considering that typically during fair comparisons, identical throughput and bandwidth occupancies are used, thus $\frac{W}{R_b}$ remains constant and the metric simplifies to

$$D \propto \frac{E_t}{N_o}. \tag{3.109}$$

This metric can also be utilised to compare various PAPR methods in the field. In addition, if both the BER compromise and the efficiency effects of the PAPR reduction, when using OM-OFDM, are considered, an optimum total energy per bit and PAPR value may be found. Thus an optimal solution for an OM-OFDM transmission may be obtained. In the rest of this thesis this metric is applied to various amplifiers.

3.8 CONCLUDING REMARKS

In this chapter a novel method, called offset modulation, is proposed to control the PAPR of an OFDM signal. The theoretical bandwidth occupancy of the proposed offset modulated signal is derived. Using these bandwidth occupancy results, a closed-form theoretical BER expression for an offset modulated transmission is derived and validated. A newly applied power performance decision metric is also introduced, which can be utilised to compare various PAPR methods.

CHAPTER 4

COMPARISON OF OM-OFDM AND CE-OFDM

4.1 INTRODUCTION

In this thesis, an offset modulation method has been proposed to control the PAPR of an OFDM transmission. The proposed OM-OFDM method may appear to be similar if not identical to phase modulation of an OFDM transmission, which is well known [82–90]. In this chapter the differences between an OM-OFDM and CE-OFDM methods are evaluated and the benefits of the OM-OFDM method are presented.

4.2 STRUCTURAL COMPARISON

Consider the discrete complex output of an N-point inverse fast Fourier transformed OFDM signal, given by

$$m_n = \frac{1}{\sqrt{N}} \sum_{k=0}^{N-1} X_k e^{j\frac{2\pi nk}{N}}, \qquad n = 0, 1, ..., N-1. \tag{4.1}$$

In Eq (4.1), X_k represents the complex signal output $(a_k + jb_k)$ of the IFFT. This signal may be modulated using the method which follows

$$\Phi_{1n} = \frac{\Re(m_n)}{\varsigma} \quad \text{and} \quad \Phi_{2n} = \frac{\Im(m_n)}{\varsigma}. \tag{4.2}$$

In Eq (4.2), m_n denotes the discrete complex OFDM signal, ς refers to a constant division term, $\Re$ and $\Im$ refer to the real and imaginary parts of an OFDM signal respectively. In addition, Φ_{1n} and Φ_{2n} represent the equivalent discrete real and imaginary OFDM phase mapping. These Φ_{1n} and Φ_{2n} terms are passed through a DAC and may now be combined into a co-sinusoid, given by

$$s(t) = \cos(2\pi f_c t + \Phi_1(t) + \Psi_{os}) - \cos(2\pi f_c t + \Phi_2(t)) \tag{4.3}$$

here, Ψ_{os} refers to an offset term, $\Phi_1(t)$ and $\Phi_2(t)$ represent the equivalent real and imaginary OFDM phase mapping. The Ψ_{os} and ς terms ensure that the receiver can successfully detect the originally transmitted signal. The proposed offset modulation method may appear to be similar, if not identical, to CE-OFDM. A CE-OFDM transmission is ideally suited for constellations without imaginary components (e.g. BPSK). In cases where imaginary components exist (e.g. such as in 16-QAM), as depicted in Fig. 4.1(a), this constellation is uniquely mapped onto a constellation without imaginary components (e.g. 16-QAM to 16-PAM mapping). This mapping process results in a severe BER degradation. After the mapping process, depicted in Fig. 4.1(a), an IFFT is performed on the mapped signal. The resultant OFDM signal, denoted by $\phi(t)$ in Fig. 4.1(a), is phase modulated as shown below

$$S(t) \quad = \quad A_c \cos(2\pi f_c t + 2\pi h \phi(t)). \tag{4.4}$$

In Eq (4.4), A_c is the signal amplitude, f_c is the carrier frequency and h denotes the modulation index. On the contrary, an OM-OFDM transmission modulates a constellation containing both real and imaginary components without a mapping process. The OM-OFDM transmission may appear to be a phase modulated signal, therefore losing its attractive OFDM properties. However, the OM-OFDM system's transmitter receiver structure (Fig. 4.1(b)) maintains the fundamental OFDM building blocks. The OM-OFDM equalisation process is identical to that employed in OFDM. Channel state information is extracted from the pilot symbols and used during the equalisation process to mitigate the effects of fading. Thus, OM-OFDM still maintains the ease of equalisation, whereas the CE-OFDM transmission re-

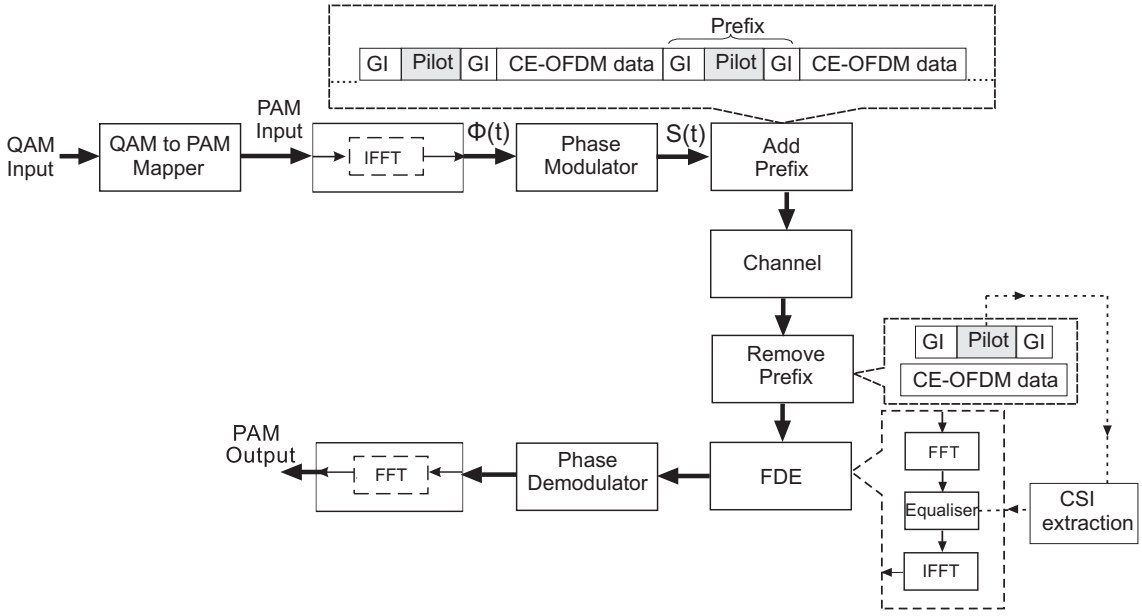

(a) CE-OFDM structure [100]

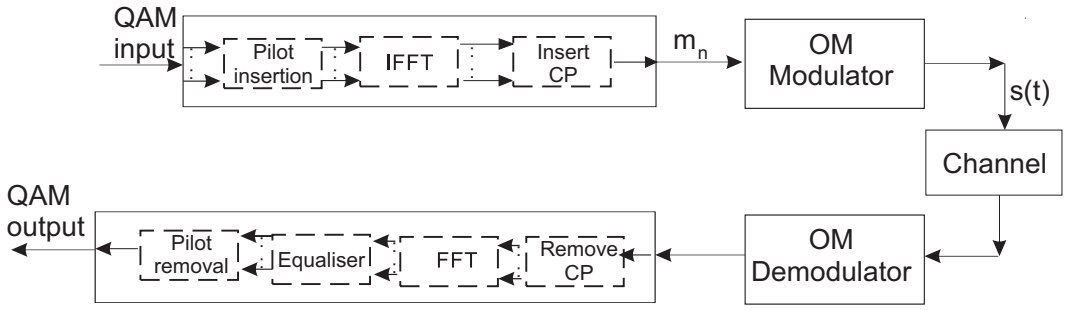

(b) OM-OFDM structure

Figure 4.1: A CE-OFDM (a) and OM-OFDM (b) transmitter-receiver structure comparison.

quires a more complex equalisation process. During a CE-OFDM transmission, as depicted in Fig. 4.1(a), a frequency-domain equaliser (FDE) is used to mitigate the effects of a channel. The FDE extracts CSI from the prefix (pilot and guard intervals (GI)), which are inserted between successive CE-OFDM blocks. During the FDE process either a zero-forcing or minimum mean-squared error equaliser can be used. The CE-OFDM equalisation process requires additional overhead (pilot and GI) and an increase in computational complexity when compared to an OM-OFDM transmission. A comparison between Fig. 4.1(b) and Fig. 4.1(a) demonstrates the structural difference between an OM-OFDM and CE-OFDM transmission, in particular the placement of the equaliser. The only similarity that OM-OFDM and CE-OFDM share is that both methods involve a form of phase modulation, other than that the two methods are significantly different.

4.3 BANDWIDTH COMPARISON

The bandwidth occupancy for $N = 1$, of an OM-OFDM transmission can be written as (Eq (3.15))

$$u_n = \sum_{y=0}^{2x} \left| \sum_{z=0}^{2x-y} 2\sin\left(\frac{\pi(2x-2z-y) \pm 2\Psi_{os}}{4}\right) \cdot J_{|-x+z|}(\beta_1) \left(\frac{|-x+z+\frac{1}{2}|}{-x+z+\frac{1}{2}}\right)^{|-x+z|} \cdot J_{|x-y-z|}(\beta_2) \left(\frac{|x-y-z+\frac{1}{2}|}{x-y-z+\frac{1}{2}}\right)^{|x-y-z|} \cdot \sin\left(2\pi(f_c + y f_d) + \frac{2\Psi_{os} \pm y\pi}{4}\right) \right|. \quad (4.5)$$

Then by inspection of Eq (4.5), Fig. 4.2 depicts the frequency spectrum of an OM-OFDM and CE-OFDM transmission, where A_c refers to the envelope of the phase modulated signal. The frequency spectrum of an OM-OFDM transmission is different from that of a conventional phase modulated signal. The squaring of the Bessel functions limits the bandwidth

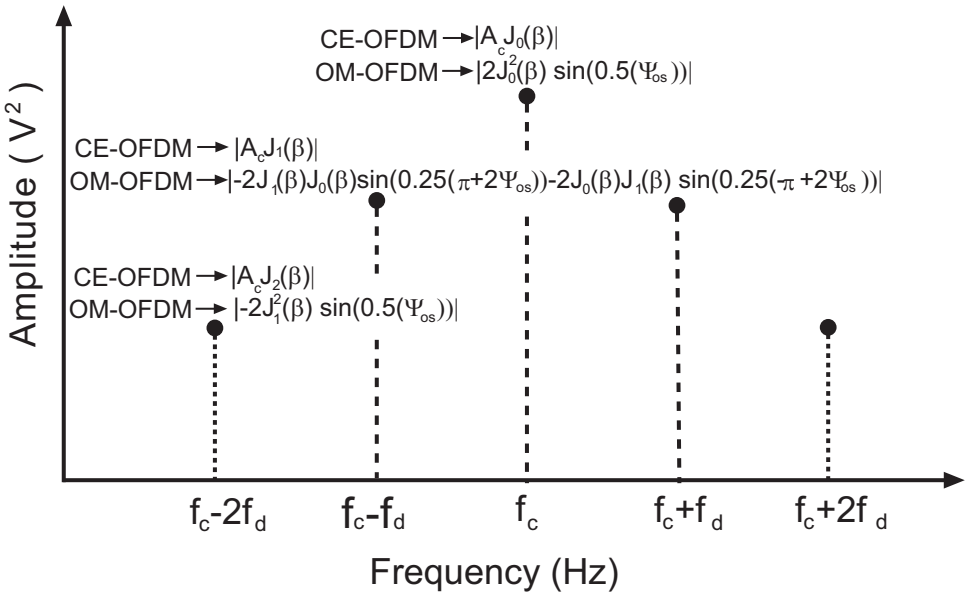

Figure 4.2: A CE-OFDM and OM-OFDM theoretical derived frequency spectrum comparison.

occupancy of an OM-OFDM signal. This indicates that the OM-OFDM transmission is spectrally more efficient than a CE-OFDM transmission. In order to further validate this mathematical analysis, in Fig. 4.3 the bandwidth occupancies of an OM-OFDM, OFDM and CE-OFDM transmission are compared. The bandwidth occupancies of an OM-OFDM,

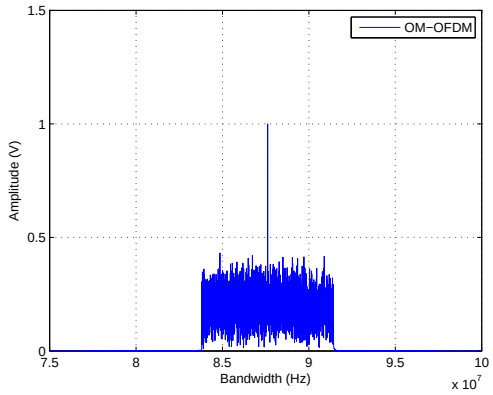

(a) Normalised OM-OFDM bandwidth occupancy

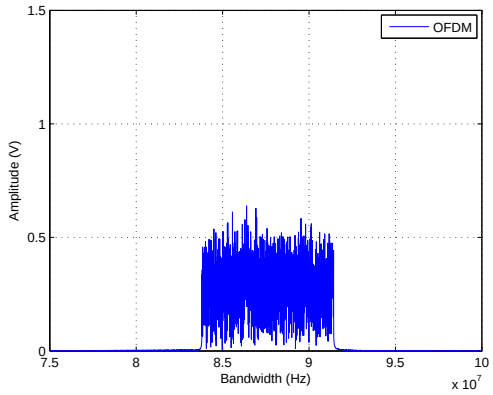

(b) OFDM bandwidth occupancy

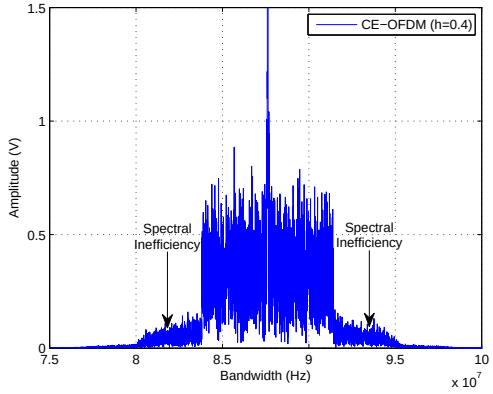

(c) CE-OFDM bandwidth occupancy

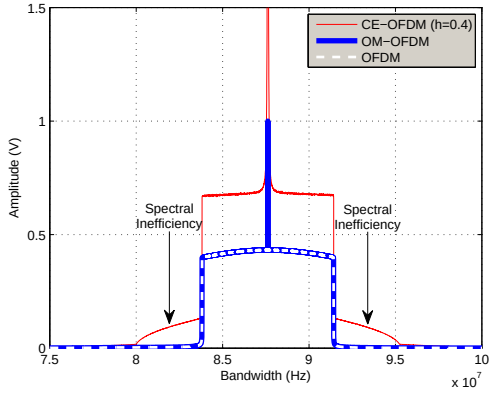

(d) Averaged OM-OFDM, OFDM and CE-OFDM bandwidth occupancy

Figure 4.3: An OM-OFDM, OFDM and CE-OFDM bandwidth comparison.

OFDM and CE-OFDM transmission are presented in Fig. 4.3(a), Fig. 4.3(b) and Fig. 4.3(c), respectively. Both the OM-OFDM (Fig. 4.3(a)) and OFDM (Fig. 4.3(b)) methods appear to be spectrally efficient, whereas in Fig. 4.3(c), for the CE-OFDM method, spectral inefficiencies are noticed. Furthermore, in Fig. 4.3(d), the average bandwidth occupancy of the OM-OFDM, OFDM and CE-OFDM transmissions are compared. This OM-OFDM and OFDM comparison further highlights their spectral efficiency and the CE-OFDM method depicts its spectral inefficiencies. The mathematical reasoning for this type of result has been discussed previously (Fig. 4.2).

In addition, by subtracting $2\gamma J_0(\beta)^2 \sin(2\pi f_c t - \frac{\Psi_{os}}{2}), \quad 0 \leq \gamma < 1$ (where γ is the dominant frequency component control factor) from the dominant frequency of an OM-OFDM

transmission, the PAPR of such a transmission (Eq (4.3)) may be controlled in order to improve the BER characteristic. This is not the case in a CE-OFDM transmission, where the PAPR is fixed at a desirable 3 dB PAPR, but at the expense of a severe BER degradation. The BER characteristics of a CE-OFDM transmission may be improved by increasing the bandwidth occupancy (modulation index) of such a transmission. This involves frequency domain spreading of the signal. However, in certain instances spreading the CE-OFDM signal into a noise floor worsens the BER characteristics instead of improving them.

4.4 RESULTS AND DISCUSSION

In all the results which follow, the 2k mode of the DVB - T2 standard [95] was used to transmit OFDM, OM-OFDM and CE-OFDM (16-QAM Gray-coded) data through a 3-tap bad-urban frequency selective fading channel, the channel was obtained from [96]. Identical throughput and bandwidth occupancies were used to ensure a fair comparison between the various methods. The OM-OFDM method as well as the other methods, conforms to both the throughput and the spectrum mask properties imposed by the DVB-T2 standard. Perfect carrier and timing synchronisation is assumed. The parameters used for the OM-OFDM transmission are given in Table 4.1, and the modulation index of a CE-OFDM transmission is $2\pi h = 0.0628$.

Table 4.1: Parameters for a 16-QAM OM-OFDM system ($\alpha = 0.07408$)

PAPR	Ψ_{os}	ς	γ	φ
3 dB	1.7	20000/4096	1.00E-05	3.76E-03
4 dB	1.5	10000/4096	0.807	3.92E-02
5 dB	1.5	10000/4096	0.91	8.41E-02
6 dB	1.5	10000/4096	0.945	1.38E-01
7 dB	1.5	10000/4096	0.963	0.205
8 dB	1.5	10000/4096	0.973	0.280
9 dB	1.5	10000/4096	0.98	0.378
10 dB	1.5	10000/4096	0.985	0.505
11 dB	1.5	10000/4096	0.988	0.631
12 dB	1.5	10000/4096	1	1.0

4.4.1 Bit error rate performance analysis

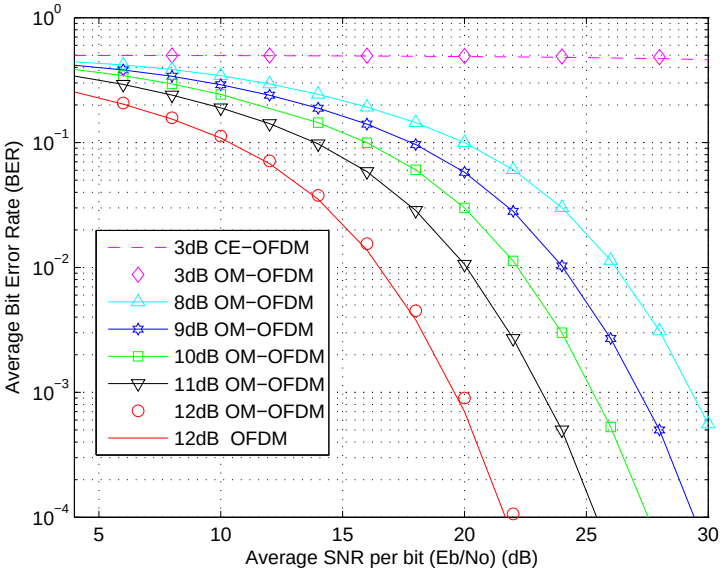

Figure 4.4: A BER comparison between an OM-OFDM, OFDM and a CE-OFDM transmission in a 3-tap bad-urban frequency selective fading channel.

The averaged PAPR of an OFDM transmission when using the DVB-T2 standard, according to simulations, is 12 dB. This PAPR is fixed for an OFDM transmission, whereas OM-OFDM allows the PAPR of the signal to be varied, while maintaining identical throughput and bandwidth occupancy as an OFDM transmission. Hence, from a direct BER comparison between OM-OFDM and OFDM, depicted in Fig. 4.4, it is noted that both methods offered similar BER characteristics at a PAPR of 12 dB. A further BER comparison between OM-OFDM and CE-OFDM, partially depicted in Fig. 4.4, indicates that for a similar PAPR (3 dB) both methods offered similar BER characteristics. At a BER of 10^{-4} the SNR of a CE-OFDM transmission is 68.85 dB. This indicates the extent of the severe BER degradation for a fixed PAPR of 3 dB.

4.4.2 Decision metric performance analysis

In order to facilitate a direct comparison between OFDM, OM-OFDM and CE-OFDM transmissions, the decision metric discussed in Section 3.7, together with a standard OTS AN10858 RF power amplifier, was employed. When using this decision metric, as depicted

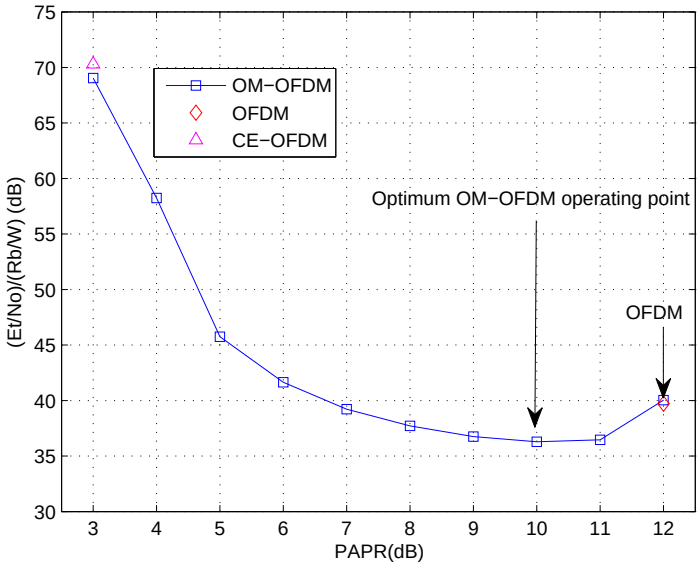

Figure 4.5: System performance at a BER of 10^{-4} for an AN10858 amplifier.

in Fig. 4.5, the optimum operating point for an OM-OFDM transmission is at a PAPR of 10 dB (where a minimum decision metric occurs). At this optimum operating point, depicted in Fig. 4.5, the OM-OFDM transmission is shown to offer a net power performance gain of 34 dB and 3.44 dB (at a BER of 10^{-4}) when compared to CE-OFDM and traditional OFDM transmissions, respectively. Furthermore, the decision metric suggests that the OM-OFDM method's average PAPR value may be lowered to 8 dB (thus a 4 dB average PAPR reduction when compared to the original OFDM transmission), while maintaining a performance improvement when compared to an OFDM transmission. A comparison between OM-OFDM and CE-OFDM indicates the significant power performance improvements offered by OM-OFDM.

This decision metric result might appear to be misleading, since at a BER of 10^{-4}, shown in Fig. 4.4, a 3.44 dB net gain is not expected. This 3.44 dB net power performance gain is attributed to the fact that there is an exponential relationship between PAPR (dB) and PAE (Fig. 2.9), instead of a linear relationship. Thus as the PAPR decreases, efficiency increases exponentially; this relationship is valid within a certain PAPR range. It is this association which leads to the 3.44 dB net power performance gain.

4.5 CONCLUSIONS

The proposed OM-OFDM method appears to be similar to a well-known CE-OFDM transmission. In this chapter, the significant differences between an OM-OFDM and CE-OFDM method are demonstrated. Thereafter, by using a decision metric, OM-OFDM is shown to offer a phenomenal 34 dB improvement when compared to a CE-OFDM transmission and a 3.44 dB (54.7%) net performance gain (at a BER of 10^{-4}) when compared to a traditional OFDM transmission for frequency selective fading channel conditions.

CHAPTER 5

OFFSET MODULATION RESULTS AND DISCUSSION

5.1 INTRODUCTION

In this chapter, in order to demonstrate the benefits of OM-OFDM, the proposed OM-OFDM method is compared to an OFDM transmission, as well as existing PAPR reduction methods. A 64-QAM Gray-coded 8k mode of the DVB-T2 standard [95] was used to compare OFDM, active constellation extended OFDM, tone reserved OFDM, OM-OFDM and classically clipped OFDM transmissions.

The clipping method was chosen, since to the best of the author's knowledge this method, in conjunction with the OM-OFDM method, are the only methods currently in the PAPR field which allow for the accurate control of the PAPR of an OFDM transmission. The ACE and TR methods were selected since the DVB-T2 standard has recommended that these methods be used to reduce the PAPR of an OFDM transmission.

5.2 METHODOLOGY

When classically clipping a signal, both in-band and out-of-band distortions are introduced. In order to minimise the in-band distortion, the clipped OFDM signal was oversampled by a factor of 4. To limit the out-of-band distortion, the clipped OFDM signal was filtered

before transmission with an 7^{th} order Butterworth band-pass filter with a 9 dB ripple in the pass-band and a 42 dB stop attenuation.

The ACE method made use of the projection onto convex sets (POCS) [69, 73] approach. This iterative filtering and clipping ACE process involves using an oversampled signal (oversampled by a factor of 4), which is clipped with a clipping threshold of 7.8 dB and thereafter filtered with a 14^{th} order Butterworth band-pass filter with a 9 dB ripple in the pass-band and a 42 dB stop attenuation.

The outer constellation points of this clipped and filtered signal, which lie within a certain region that does not affect the BER, are left unaltered, hence the constellation is said to be extended. The remaining constellation points are returned to their original position (before the clipping and filtering process). The outer constellation points have a maximum constellation extension limit (L) and the limit for this particular case is $L = 1.4$ (as recommended in the DVB-T2 standard). This iterative POCS approach was terminated after 30 iterations, since this proved to be a convergence point. The clipping threshold and filter parameters were determined after an exhaustive search.

Similarly, the POCS approach was used in the TR method. Each sub-carrier in the TR method is limited to 10 times the average power of the data carriers (as recommended in the DVB-T2 standard). The TR signal is oversampled by a factor of 4, with a clipping threshold of 7.8 dB. This iterative POCS approach, used for the TR method, was terminated after 60 iterations, since this proved to be a convergence point.

Furthermore, in all the BER results which follow, a 64-QAM Gray-coded 8k mode of the DVB-T2 standard was used to transmit OM-OFDM, OFDM and clipped OFDM data through a 5-tap typical-urban frequency selective fading channel. For an OM-OFDM, OFDM and clipped OFDM transmission, CSI is extracted from the pilot symbols and used during the equalisation process to mitigate the effects of fading. The pilot symbol placement, as well as tone reserved sub-carrier (used in TR), can be found in the DVB-T2 standard. Similarly the 5-tap typical-urban area model was obtained from Patzold [96] (which origin-

ates from the COST 207 models). Identical throughput and bandwidth occupancies were used to ensure a fair comparison between the various methods. The OM-OFDM method as well as the other methods, conforms to both the throughput and the spectrum mask properties imposed by the DVB-T2 standard. Perfect carrier and timing synchronisation is assumed. In Table 5.1, the parameters used for the OM-OFDM transmission are presented.

Table 5.1: Parameters for an 64-QAM OM-OFDM system ($\alpha = 0.27$)

PAPR	Ψ_{os}	ς	γ	φ
7 dB	1.596	44000/16384	0.86	0.2
8 dB	1.596	44000/16384	0.9	0.251
9 dB	1.596	44000/16384	0.925	0.34
10 dB	1.596	44000/16384	0.943	0.44
11 dB	1.596	44000/16384	0.962	0.53
12 dB	1.596	44000/16384	0.97	0.67
13 dB	1.596	44000/16384	1	1

5.3 BIT ERROR RATE PERFORMANCE ANALYSIS

OM-OFDM, OFDM and clipped OFDM data were sent through a 5-tap typical-urban area by using the parameters previously mentioned. The averaged PAPR of an OFDM transmission when using the 8k mode of the DVB-T2 standard, according to simulations, is 13 dB. This PAPR value has also been verified independently by [98]. This PAPR is fixed for an OFDM transmission and may only be changed, as discussed in Section 2.8, by adopting one or some of the PAPR reduction methods. For the same DVB-T2 standard OM-OFDM allows the PAPR of the signal to be varied, while maintaining identical throughput and bandwidth occupancy as an OFDM transmission.

A direct BER comparison, as shown in Fig. 5.1, between OFDM and OM-OFDM can be made when both methods offer the same PAPR (13 dB). From this OM-OFDM and

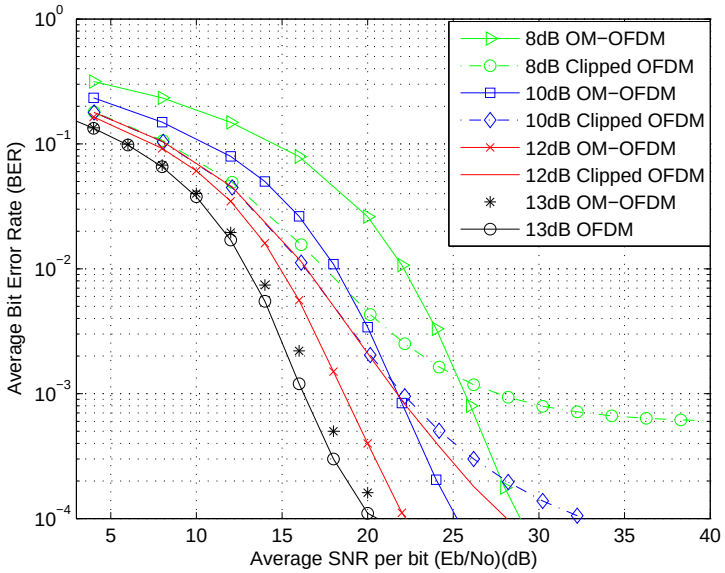

Figure 5.1: A 64-QAM constellation, BER comparison between an OM-OFDM, OFDM and a clipped OFDM transmission in a 5-tap typical-urban area.

OFDM comparison, it is noted that both methods offered similar BER characteristics at a PAPR of 13 dB. The OM-OFDM method, in addition, allows the designer to vary the PAPR until a desired BER is achieved. A further comparison between OM-OFDM and a clipped OFDM transmission shows that the clipped OFDM transmission reaches a BER plateau (PAPR $\leq$ 9 dB), whereas OM-OFDM does not result in a BER plateau for this case.

When a signal is clipped, information about the signal is permanently removed. Methods such as DAR clipping [28], as previously discussed, have been recommended to be used to reconstruct the clipped method, i.e. restore missing information about the signal. However this DAR method does not work well under frequency selective fading conditions. This permanent removal of information about the signal during clipping results in the BER plateau effect (PAPR $\leq$ 9 dB). A combination of the removal of information about the signal and the channel effects results in these subsequent clipping BER characteristics. OM-OFDM, on the other hand, does not remove information about the transmission, hence no BER plateau effect occurs. For the ACE and TR method the resultant fixed average PAPR is 12 dB and 12.7 dB, respectively. The BER performance of the ACE and TR methods is not presented, since it resembles that of an OFDM transmission.

5.4 DECISION METRIC PERFORMANCE ANALYSIS

In order to facilitate a direct comparison between OM-OFDM, OFDM, ACE, TR and a clipped OFDM transmission, the decision metric discussed in Section 3.7 was utilised. The decision metric employed a standard OTS FPD2000AS [101] RF power amplifier. A 10^{th} degree polynomial was used to describe the PAE for this particular amplifier. In Fig. 5.2, the PAE, as well as the input-output characteristics of such an amplifier, are depicted. The results depicted in Fig. 5.3 were obtained when using the decision metric.

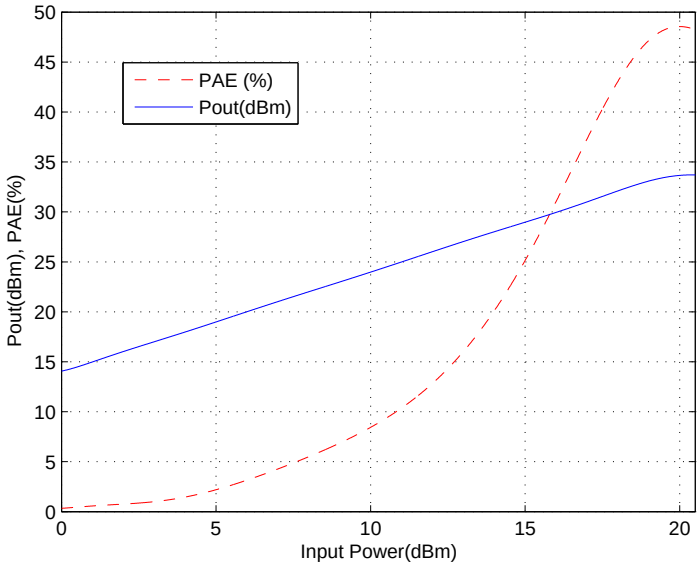

Figure 5.2: Power compression curves of an FPD2000AS amplifier [101].

When using this standard OTS power amplifier, as depicted in Fig. 5.3, the optimum operating point for an OM-OFDM transmission is at a PAPR of 10 dB (where a minimum decision metric occurs) and for the ACE and clipped OFDM transmission the optimum operating points are 12 dB. Similarly, the TR transmission has an optimum operating point at 12.7 dB.

At these optimum operating points OM-OFDM offers a net power performance gain of 1.2 dB (23.6%), 2 dB (36.8%), 2.2 dB (39.8%) and 4.1 dB (60.8%), at a BER of 10^{-4}, when compared to an ACE, TR, OFDM and clipped OFDM transmission respectively.

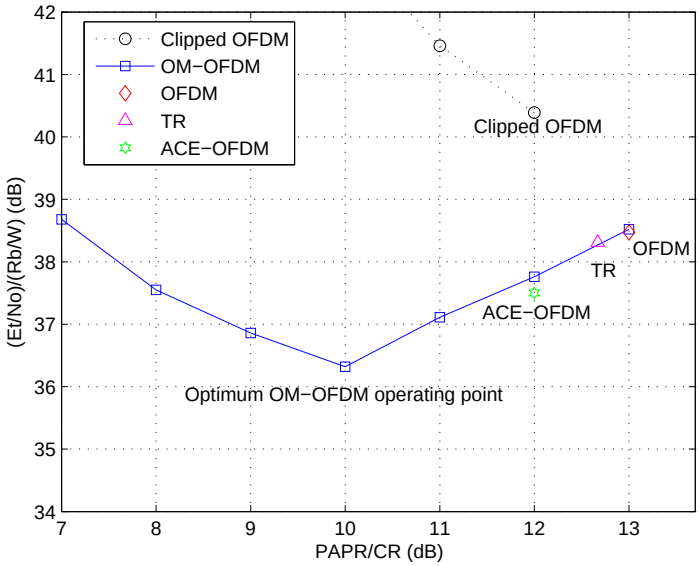

Figure 5.3: System performance for a 64-QAM constellation at a BER of 10^{-4} for a FPD2000AS RF power amplifier.

Hence, the OM-OFDM method offers a performance improvement when compared to an ACE and TR method, without the need for an iterative (30-60 iterations) process. Furthermore the decision metric suggests that the OM-OFDM method's PAPR value may be lowered to 8 dB (thus a 5 dB PAPR reduction when compared to the original OFDM transmission), while maintaining a performance improvement when compared to an ACE, TR, OFDM and clipped OFDM transmissions.

This decision metric result might appear to be misleading, since from Fig. 5.1 at a BER of 10^{-4}, a 2.2 dB net gain is not expected, as proposed by the decision metric. This 2.2 dB net power performance gain is attributed to the fact that the PAE curve of a typical amplifier is exponentially shaped, depicted in Fig. 5.2, instead of linear. Hence, there is an exponential relationship between PAPR (dB) and PAE, instead of a linear relationship. As the PAPR decreases, there is an exponential increase in efficiency; this relationship is valid within a certain PAPR range. It is this association which leads to the 2.2 dB net power performance gain.

In order to validate the results further, another standard OTS AN10858 [98] RF power amplifier, manufactured by a different supplier, was used. A 2nd degree polynomial was used to describe the PAE of this particular amplifier. Similar to the previous case for this

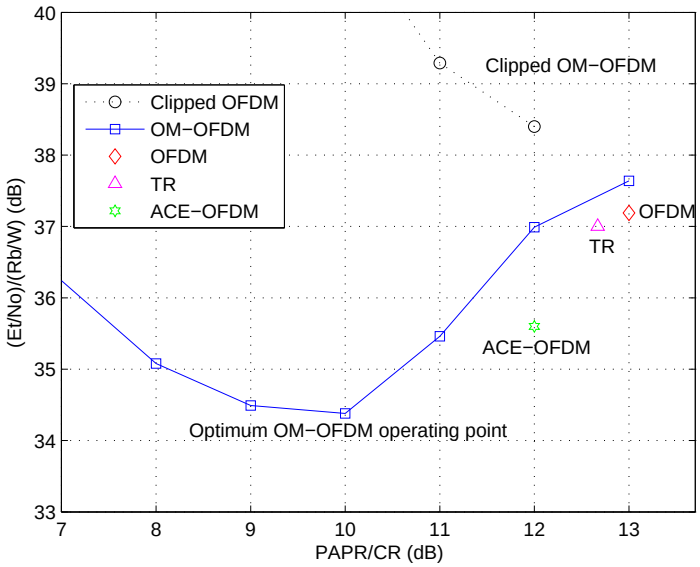

Figure 5.4: System performance for a 64-QAM constellation at a BER of 10^{-4} for a AN10858 RF power amplifier.

AN10858 standard OTS power amplifier, depicted in Fig. 5.4, at the optimum operating points OM-OFDM offers a net power performance gain of 1.2 dB (23.6%), 2.7 dB (45.3%), 2.8 dB (47.6%) and 4 dB (60.4%), at a BER of 10^{-4}, when compared to an ACE, TR, OFDM and clipped OFDM transmissions respectively. Hence, the OM-OFDM method again offers a performance improvement when compared to an ACE and TR method. Furthermore, the decision metric suggests that the OM-OFDM method's PAPR value may be lowered to 8 dB, while maintaining a performance improvement.

In Table 5.2, the decision metric improvements obtained when using OM-OFDM for the FPD2000AS and AN10858 RF power amplifiers are summarised. From these comparisons, it is noted that OM-OFDM offers a performance improvement of between 4 dB - 1.2 dB (60.4%-23.6%) and between 4.1 dB - 1.2 dB (60.8%-23.6%) for the AN10858 and FPD2000AS RF power amplifiers respectively, when compared to an ACE, TR, OFDM

Table 5.2: Decision metric performance improvement obtained when using OM-OFDM at a BER of 10^{-4}

Method	**Amplifiers**	
	AN10858	**FPD**2000**AS**
OFDM	2.8 dB (47.6%)	2.2 dB (39.8%)
Clipping	4.0 dB (60.4%)	4.1 dB (60.8%)
ACE	1.2 dB (23.6%)	1.2 dB (23.6%)
TR	2.7 dB (45.3%)	2.0 dB (36.8%)

and a clipped OFDM transmissions. Furthermore, at the optimum operating point of an OM-OFDM transmission (10 dB), the FPD2000AS and AN10858 RF power amplifiers produce decision metric results of 36.32 dB and 34.38 dB respectively. This comparison indicates that the AN10858 amplifier offers a 1.94 dB improvement over the FPD2000AS amplifier, thus making it a better amplifier for this particular application. This result was intuitively expected, since the AN10858 RF power amplifier has been specifically designed for this current application (8k mode of the DVB - T standard).

5.5 COMPLEMENTARY CUMULATIVE DISTRIBUTION FUNCTION PERFORMANCE ANALYSIS

Based on the optimum operating points obtained from the decision metric in the previous section, the complementary cumulative distribution function, depicted in Fig. 5.5, was used to compare the PAPR characteristics of an OM-OFDM, OFDM, clipped OFDM, TR and ACE transmission. At these optimum operating points OM-OFDM is shown to offer a PAPR reduction of 2.27 dB, 2.56 dB, 2.75 dB and 3.19 dB (at a CCDF of 10^{-1}) when compared to a clipped OFDM, ACE, TR and OFDM transmission respectively. Although the clipping

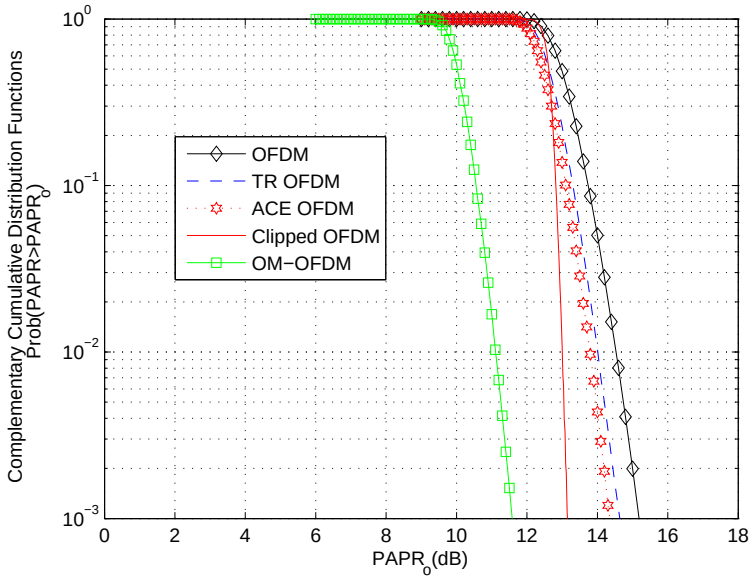

Figure 5.5: Complementary cumulative distribution functions of an OM-OFDM, clipped OFDM, ACE, TR and OFDM transmissions for a 64-QAM constellation.

method offers attractive CCDF results, the subsequent BER characteristics are not attractive. From these comparisons, it is noted that OM-OFDM offers a significant PAPR reduction when compared to the various methods.

5.6 CONCLUSIONS

In this chapter, the proposed OM-OFDM method was compared to OFDM, as well as existing PAPR reduction methods. A BER comparison between OM-OFDM and OFDM, at a PAPR value of 13 dB, indicates that both methods offer similar BER characteristics for frequency selective fading channel conditions. The OM-OFDM method is also able to control the PAPR of a transmission accurately for a targeted BER.

When utilising the decision metric, OM-OFDM is shown to offer a net power performance gain of between 4 dB - 1.2 dB (60.4%-23.6%) and 4.1 dB - 1.2 dB (60.8%-23.6%), at a BER of 10^{-4}, for a AN10858 and FPD2000AS RF power amplifier respectively, when compared to clipped OFDM, OFDM, TR and ACE transmissions, in a frequency selective fading channel. These results can be further summarised, as depicted in Fig. 5.6. In Fig. 5.6, the

normalised decision metric results for an AN10858 and a FPD2000AS RF power amplifier, when comparing clipped OFDM, OFDM, OM-OFDM, TR and ACE transmissions, in frequency selective fading channel is presented. This graphically illustration, depicted in Fig. 5.6, indicates the significant power performance offered by OM-OFDM when compared to various other methods. By utilising a complementary cumulative distribution

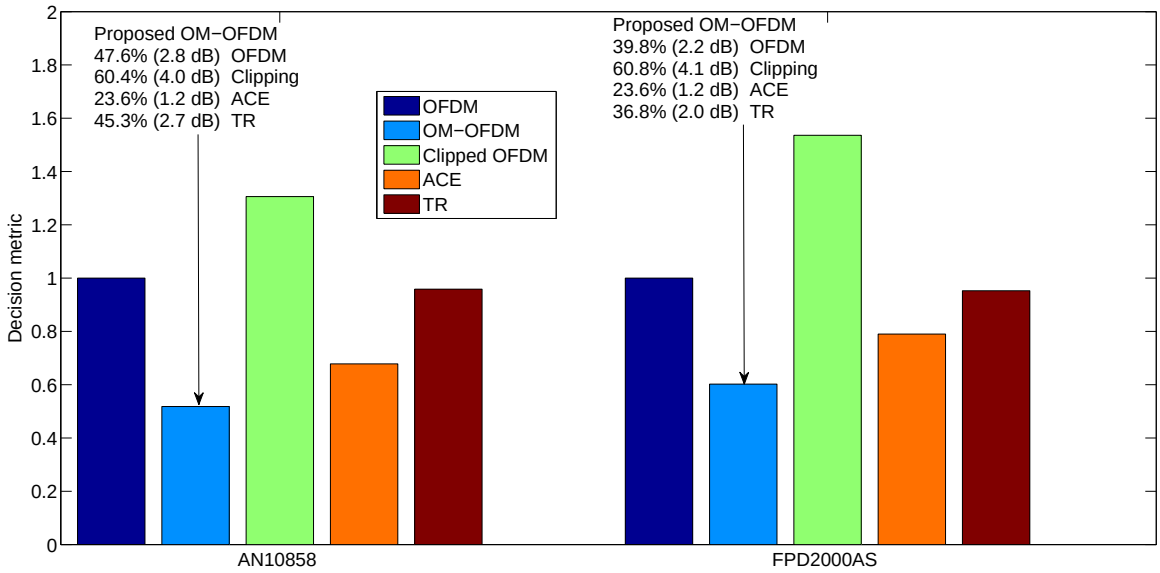

Figure 5.6: Summarised normalised decision metric performance results for a 64-QAM constellation at a BER of 10^{-4} for AN10858 and FPD2000AS RF power amplifiers under frequency selective fading conditions.

function, the OM-OFDM method is further shown to offer a PAPR reduction of between 3.2 dB - 2.3 dB (at a CCDF of 10^{-1}) when compared to an OFDM, TR, clipped and ACE OFDM transmissions. Hence, the proposed OM-OFDM method has offered performance improvements when compared to simple (clipping) as well as more well-established (ACE and TR) iterative (30-60 iterations) methods.

CHAPTER 6

HYBRID OM-ACE TRANSMISSION

6.1 INTRODUCTION

In this chapter, the ease with which an ACE method, which is a well-established PAPR reduction method recommended by the DVB - T2 standard [95], may be incorporated into an OM-OFDM transmission is discussed. The PAPR benefits derived from both the OM-OFDM and ACE methods are inherited by this offset modulation with the active constellation extension (OM-ACE) method. Although this chapter confines its discussion to this particular case, it demonstrates the manner in which the various other PAPR reduction methods may be incorporated into an OM-OFDM transmission. This chapter begins by introducing this hybrid OM-ACE method.

6.2 PROPOSED OM-ACE METHOD

Consider the complex output of an N-point inverse fast Fourier transformed OFDM signal, given by

$$m_n = \frac{1}{\sqrt{N}} \sum_{k=0}^{N-1} X_k e^{j\frac{2\pi nk}{N}}, \qquad n = 0, 1, ..., N-1. \tag{6.1}$$

In Eq (6.1), X_k represents the complex signal output $(a_k + jb_k)$ of the IFFT. This signal may be modulated using the method which follows.

$$\Phi_{1n} = \frac{\Re(m(t))}{\varsigma} \quad \text{and} \quad \Phi_{2n} = \frac{\Im(m(t))}{\varsigma} \tag{6.2}$$

In Eq (6.2), $\Re$ and $\Im$, refer to the real and imaginary parts of the OFDM message signal and ς refers to a constant division term. These Φ_{1n} and Φ_{2n} terms are passed through a DAC and may now be combined into a unique co-sinusoid

$$\cos(2\pi f_c t + \Phi_1(t) + \Psi_{os}) - \cos(2\pi f_c t + \Phi_2(t)) \tag{6.3}$$

where, $\Phi_1(t)$ and $\Phi_2(t)$ represent the equivalent real and imaginary OFDM phase mapping. When $\Phi_1(t) + \Psi_{os} \leq \pi/2$, this allows the original $\Phi_1(t)$ expression to be accurately extracted at the receiver. In order to maintain this limit, the ACE method can be used. A block

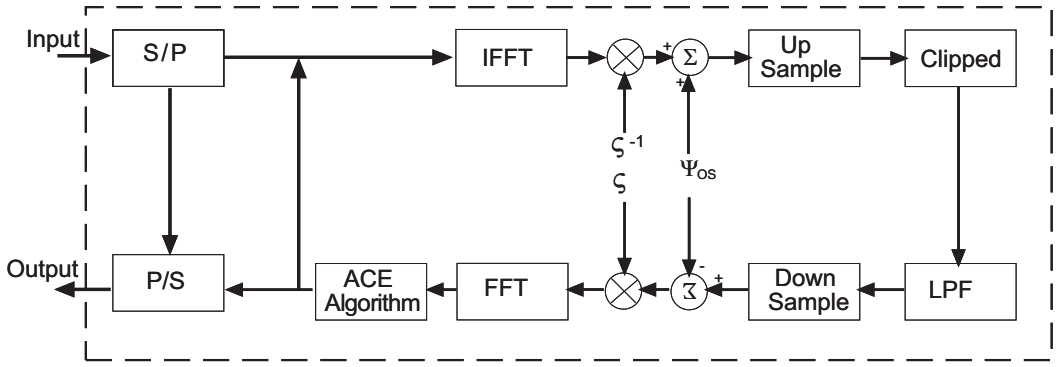

Figure 6.1: ACE structure

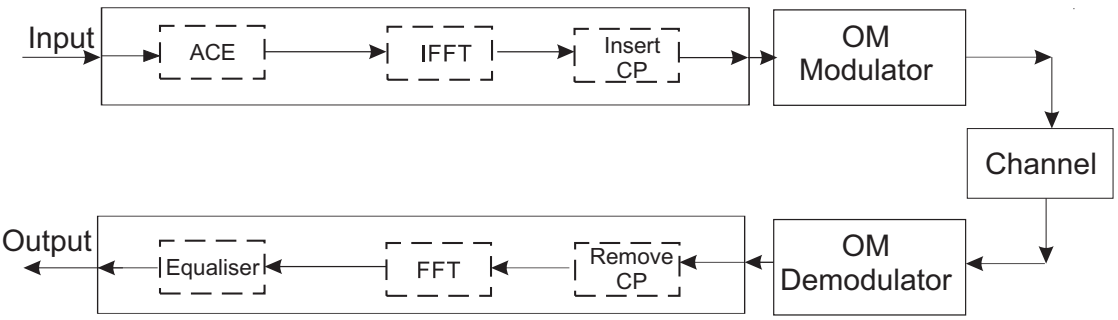

Figure 6.2: OM-ACE transmitter receiver structure

diagram, depicted in Fig. 6.1 and Fig. 6.2, shows the processes involved during an OM-ACE transmission. The incoming constellation is intelligently extended by using the ACE method (Fig. 6.1) such that $\Phi_1(t) + \Psi_{os} \leq \pi/2$. The message signal is inverse fast Fourier transformed and a cyclic prefix is amended to the OFDM signal. Thereafter, the signal is modulated using an OM modulator (Fig. 3.2), after which the signal is passed through a channel. The subsequent incoming signal is passed through an OM demodulator (Fig. 3.3) to recover the OFDM signal. The cyclic prefix is removed and a FFT is performed. Thereafter, equalisation is performed to mitigate the channel effects. The equalisation process is identical to that used for an OFDM transmission; CSI is extracted from the pilot symbols and used during the equalisation process to mitigate the channel effects.

6.3 BIT ERROR RATE CHARACTERISTICS OF AN OM-ACE TRANSMISSION

In this section the reasoning for the inclusion of the ACE method in an OM-OFDM transmission will be addressed. Based on work from Chapter 3 (Eq (3.91)), suppose the QAM theoretical BER for an OM-ACE transmission through an AWGN channel can be written as

$$BER_{QAM} \approx \frac{k \cdot \ell(M-2) + \wp \cdot k(M - 2\sqrt{M} + 2)}{M \cdot k^2} + \frac{\wp \cdot \ell(2\sqrt{M} - M - 1)}{M \cdot k^2} \tag{6.4}$$

where

$$\wp = \operatorname{erfc}\left(\sqrt{\frac{k\xi_b}{\xi_{av}N_o}}\right) \quad \text{and} \quad \ell = \operatorname{erfc}\left(\sqrt{\frac{4k\sin^2(-\frac{\varphi}{2})\xi_b}{\xi_{av}N_o}}\right). \tag{6.5}$$

As previously mentioned in Section 6.2, $\Phi_1(t) + \Psi_{os} \leq \pi/2$, this allows the original $\Phi_1(t)$ expression (adapted real phase deviation) to be accurately extracted at the receiver. The ACE method, or any alternate method discussed in Section 2.8, may be used to reduce the adapted real phase deviations. A traditional ACE transmission makes use of an iterative process, which is used to find an optimum real and imaginary constellation extension. When using the ACE method in an OM-ACE transmission and limiting its application to only the

adapted real phase deviations, the iterative nature of the process is reduced when compared to a traditional ACE transmission, which involves extending both the real and imaginary constellation. The inclusion of the ACE method in an OM-OFDM method should allow both the Ψ_{os} and γ term to approach the optimum operating point closely. This would improve the BER characteristics of an OM-ACE transmission.

With these guidelines, the theoretically presented BER expression for an OM-ACE transmission needed to be validated. By means of a simulation (the 2k mode of the DVB - T2 standard [95]), 16-QAM Gray-coded OM-OFDM and OM-ACE data were transmitted through an AWGN channel. The parameters used for the 16-QAM OM-OFDM and OM-ACE transmission are given in Table 6.1 and Table 6.2, respectively. In both Table 6.1 and Table 6.2 the φ term is calculated, as indicated in Table 3.2, by substituting α, ς, Ψ_{os} and γ terms into the φ expression. The specific terms (ς and Ψ_{os}) are chosen to minimise the BER degradation and the α ($\alpha \approx \alpha_1 \approx \alpha_2$) term is obtained as indicated in Eq (3.18) and Eq (3.19).

Table 6.1: Parameters for a 16-QAM OM-OFDM system ($\alpha = 0.07408$))

PAPR	Ψ_{os}	ς	γ	φ
8 dB	1.5	10000/4096	0.973	0.3
9 dB	1.5	10000/4096	0.98	0.4
10 dB	1.5	10000/4096	0.985	0.5
11 dB	1.5	10000/4096	0.988	0.6
12 dB	1.5	10000/4096	1	1.0

Table 6.2: Parameters for a 16-QAM OM-ACE system ($\alpha = 0.07408$)

PAPR	Ψ_{os}	ς	γ	φ
8 dB	1.55	10000/4096	0.975	0.3
9 dB	1.55	10000/4096	0.982	0.4
10 dB	1.55	10000/4096	0.988	0.5
11 dB	1.55	10000/4096	0.9919	0.7
11.4 dB	1.55	10000/4096	1	1.0

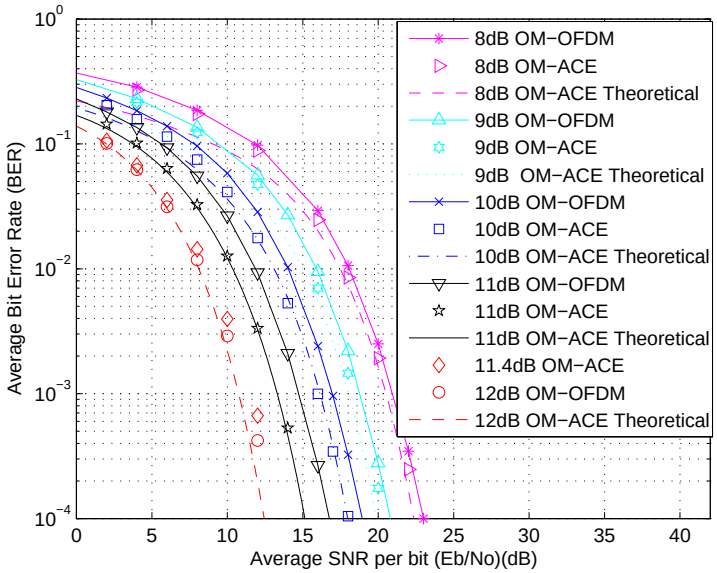

Figure 6.3: A BER comparison between an OM-ACE, theoretically predicted OM-ACE (Eq (6.4)) and OM-OFDM transmission in an AWGN channel.

From the BER comparison depicted in Fig. 6.3, it can be seen that the theoretically predicted OM-ACE results and the simulated OM-ACE results correlate reasonably well, thus validating the theoretical expression. Furthermore, a comparison between Table 6.1 and Table 6.2 indicates that the Ψ_{os} term has increased. This is possible because of the introduction of the ACE method. The γ term has also increased and the combination of an increase in the Ψ_{os} and γ term should result in an improvement in the OM-ACE BER characteristics, when compared to an OM-OFDM transmission (without ACE). This observation is corroborated, as depicted in Fig. 6.3, by the results presented.

6.4 RESULTS AND DISCUSSION

In this section, a 16-QAM Gray-coded 2k mode of the DVB-T2 [95] standard was used to compare OFDM, OM-OFDM, ACE, OM-ACE and a classically clipped OFDM transmission. When classically clipping a signal to limit the out-of-band distortion, the clipped OFDM signal was filtered before transmission with an 9^{th} order Butterworth low-pass filter.

The ACE method made use of the POCS [69, 73] approach, which involved clipping the signal with a 7 dB clipping threshold and thereafter using a 4^{th} order Butterworth low-pass filter. This iterative POCS approach was terminated after 30 iterations, since this proved to be a convergence point. After an exhaustive search, all the clipping thresholds and filter parameters used in this section were found to be optimal solutions.

In all the BER results which follow, a 16-QAM Gray-coded 2k mode of the DVB-T2 standard was used to transmit OM-ACE, OM-OFDM, OFDM and clipped OFDM data through a 5-tap typical-urban frequency selective fading channel. For the OM-ACE, OM-OFDM, OFDM and clipped OFDM transmissions, CSI is extracted from the pilot symbols and used during the equalisation process to mitigate the effects of fading. The pilot symbol placement can be found in the DVB-T2 standard. Similarly, the 5-tap typical-urban area model was obtained from Patzold [96]. Identical throughputs were used to ensure a fair comparison between the various methods and perfect carrier and timing synchronisation is assumed. All the methods conform to both the spectrum mask and throughput requirements imposed by the DVB-T2 standard. The parameters used for the OM-OFDM and OM-ACE transmission are given in Table 6.1 and Table 6.2 respectively.

6.4.1 Bit error rate performance analysis

OFDM, clipped OFDM, OM-OFDM and OM-ACE data were sent through a 5-tap typical-urban area by using the parameters previously mentioned. The average PAPR of an OFDM transmission when using the 2k mode of the DVB-T2 standard, according to simulations, is 12 dB. This PAPR is fixed for an OFDM transmission and as discussed in Section 2.8, may only be changed by adopting one or some of the PAPR reduction methods. For the ACE and OM-ACE method, the initial averaged PAPRs are 11.83 and 11.37 respectively; these are from henceforth referred to as an ACE and an OM-ACE transmission.

Unlike the OFDM and ACE transmission, both the OM-OFDM and OM-ACE methods allow the PAPR of the signal to be varied, while maintaining identical throughput

and bandwidth occupancy as an OFDM and ACE transmission. A direct comparison, as

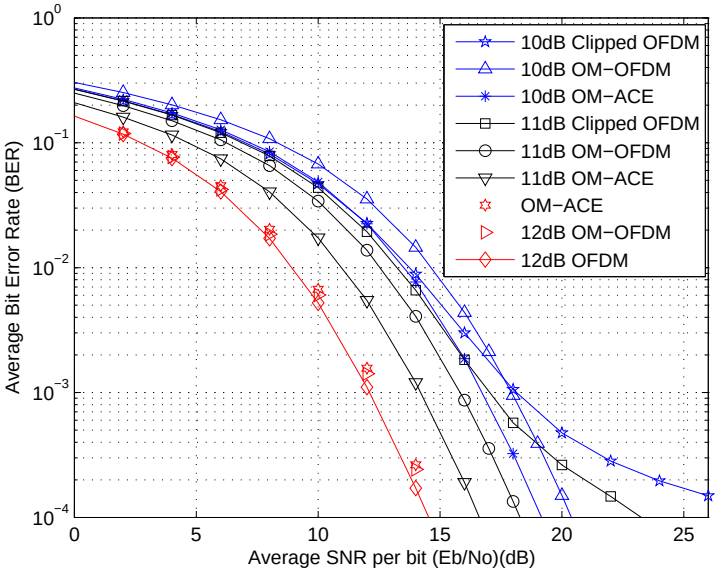

Figure 6.4: BER comparisons for a 16-QAM transmission through a 5-tap typical-urban area.

shown in Fig. 6.4, between an OFDM, OM-OFDM and OM-ACE transmission shows that all three methods offered similar BER characteristics. However, a comparison between an OM-ACE (PAPR 11.37 dB), OFDM (PAPR 12 dB) and OM-OFDM (PAPR 12 dB) transmission, indicates that the OM-ACE (PAPR 11.37 dB) transmission offers on average a 0.63 dB PAPR reduction for similar BER characteristics. Another comparison, depicted in Fig. 6.4, between OM-ACE and a clipped OFDM transmission shows that the clipped OFDM transmission reaches a BER plateau (PAPR $\leq$ 10 dB), whereas the OM-ACE does not result in this BER effect in this case. The BER performance of the ACE methods is not presented, since it resembles that of an OM-ACE and OFDM transmission.

6.4.2 Power performance decision metric performance analysis

A direct comparison between OM-ACE, OM-OFDM, ACE, OFDM and clipped OFDM transmissions is facilitated by utilising the power performance decision metric discussed in Section 3.7. The results from such an implementation, depicted in Fig. 6.5, used a standard OTS AN10858 [98] RF power amplifier. From this comparison it should be noted that the

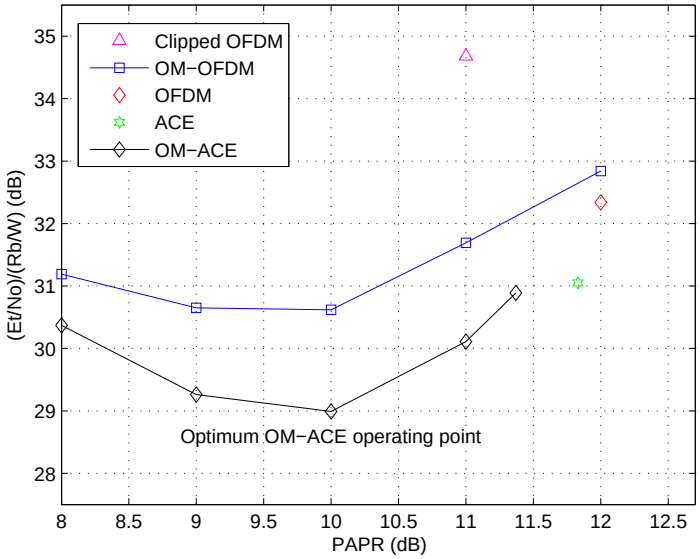

Figure 6.5: System performance for a 16-QAM constellation at a BER of 10^{-4} for a AN10858 RF power amplifier.

clipped OFDM results have been abridged because the clipped OFDM BER plateaued, thus it was unable to produce the specific BER. When using this standard OTS power amplifier, the optimum operating point for an OM-ACE and OM-OFDM transmission is at a PAPR of 10 dB, where a minimum decision metric occurs. For the ACE and clipped OFDM transmission the optimum operating points are 11.83 dB and 11 dB respectively.

At these optimum operating points, the OM-ACE transmission is shown to offer a net power performance gain of 1.6 dB (31.62%), 2 dB (37.71%), 3 dB (50.83%) and 5.7 dB (73.02%), at a BER of 10^{-4}, when compared to OM-OFDM, ACE, OFDM and clipped OFDM transmissions, respectively. The decision metric also suggests that the OM-ACE method's average PAPR value may be lowered to 8 dB (thus a 4 dB average PAPR reduction when compared to the original OFDM transmission), while maintaining a performance improvement over OM-OFDM, ACE, OFDM and clipped OFDM transmissions.

This power performance decision metric result might appear to be misleading, since at a BER of 10^{-4}, as shown in Fig. 6.4, this 3 dB net gain is not expected. The 3 dB net power performance gain is attributed to the fact that the PAE curve of a typical amplifier

is exponentially shaped [98], instead of being linear. Hence, the exponential relationship between PAPR (dB) and PAE, instead of a linear relationship, results in this exponential increase in efficiency.

6.4.3 Complementary cumulative distribution function performance analysis

Using the optimum operating points obtained from the power performance decision metric in the previous sub-section, the complementary cumulative distribution function, depicted in Fig. 6.6, was used to compare the PAPR characteristics of clipped OFDM, OFDM, ACE and OM-ACE transmissions. At the optimum operating points, the OM-ACE transmission

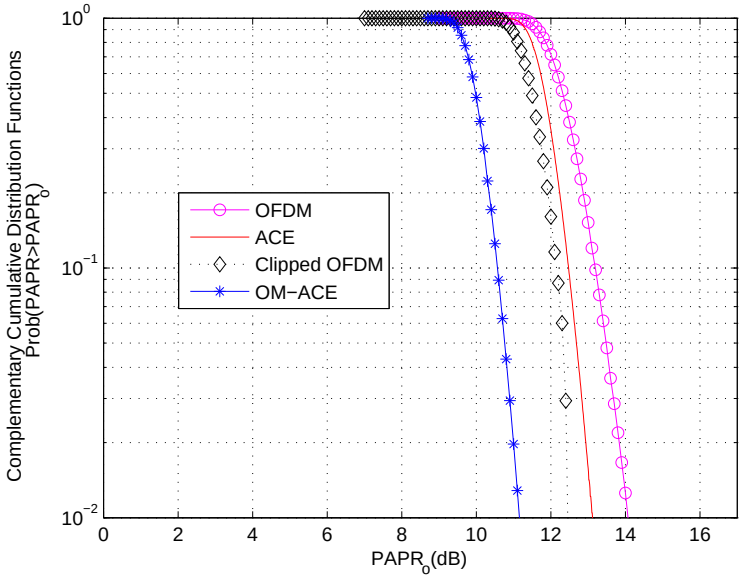

Figure 6.6: Complementary cumulative distribution functions for a 16-QAM constellation.

is shown to offer a PAPR reduction of 2.6 dB, 1.9 dB and 1.6 dB (at a CCDF of 10^{-1}) when compared to OFDM, ACE and clipped OFDM transmissions respectively. Although the clipping method offers attractive CCDF results, the subsequent BER characteristics are not attractive.

6.5 CONCLUSIONS

In this chapter, an OM-ACE method has been proposed to control the PAPR of an OFDM DVB-T2 transmission, for a targeted BER. A closed-form theoretical BER expression for this OM-ACE transmission is presented. This mathematical BER expression has been shown to agree with the simulated results, thus further validating the derivation.

Thereafter, when utilising the power performance decision metric, the OM-ACE transmission is shown to offer a net power performance gain of between 5.7 dB-1.6 dB (73.02%-31.62%), at a BER of 10^{-4}, when compared to clipped OFDM, OFDM, OM-OFDM and ACE transmissions, in a frequency selective fading channel. By using a CCDF, the OM-ACE method is shown to offer a PAPR reduction of between 2.6 dB - 1.6 dB (at a CCDF of 10^{-1}) when compared to OFDM, ACE and clipped OFDM transmissions.

CHAPTER 7

A COGNITIVE RADIO APPLICATION OF OM-OFDM

7.1 INTRODUCTION

In November 2002, the federal communications commission (FCC) published a report, which contained results obtained from limited spectrum measurements in urban areas [102]. This report suggested that there was some evidence indicating that the shortage of spectrum is often a spectrum access problem. That is, the spectrum resource is available, but its use is compartmented by traditional policies based on traditional technologies. In August 2005 [103], during spectrum occupancy measurements at six locations, it was shown that the average occupancy over all of the locations was 5.2%. As the demand for bandwidth increases, the natural approach would be the better utilisation of such bandwidth by spectrum sharing. It is these factors which have made cognitive radio (CR) a promising concept. In this chapter [104] the detection characteristics of OM-OFDM and OFDM transmissions are investigated for cognitive radio applications.

7.2 COGNITIVE RADIO

The word cognitive radio was proposed by Mitola [105] [106], although the cognitive concept was already previously known [107]. Thereafter, the Defence Advanced Research Project Agency (DARPA) was the first to launch an initiative employing CR called neXt

Generation communication systems, aimed at developing technologies to dynamically manage the spectrum [108]. The cognitive concept currently involves thinking of frequency spectrum in terms of spectrum holes. A spectrum hole is a band of frequencies assigned to a primary user (the owner of the spectrum), but at a particular time and geographic location not being occupied by this user. A secondary user is allowed to access this spectrum hole, and later vacate it, provided that it does not interfere with the primary user. This process exploits spectrum holes and ultimately leads to efficient bandwidth utilisation. While the cognitive radio concept is still in its conceptual stage, the benefits of spectrum sharing with interference avoidance has already been demonstrated by the co-existence between the IEEE 802.11 (Wi-Fi) and IEEE 802.15 (bluetooth) networks. Regulators are willing to go further by experimenting with spectrum sharing of the TV band in the development of the IEEE 802.22 standard. A technical proof and feasibility of this concept would further clear the way for regulatory approval for spectrum-sharing licensing.

Thus far the secondary user is seen as an opportunistic user, which continuously senses different spectrums and when it identifies a spectrum hole, accesses it. The secondary user later vacates the spectrum, such that it does not interfere with the primary user. Various sensing methods such as matched filtering, energy detection and cyclostationary feature detection [109, 110], amongst others, have been recommended. Of the three methods mentioned, energy detection requires the lowest complexity and requires no prior information about the signal.

In this chapter, the energy detection method will be used to detect a DVB-T2 [95] OFDM transmission. This type of energy detection would typically be employed by a secondary user in the spectrum sensing of a TV band in the development of the IEEE 802.22 standard. The problem associated with such an OFDM transmission is its high PAPR. As previously stated, OM-OFDM has been proposed to control the PAPR of an OFDM transmission. This OM-OFDM method has been shown to offer a significant power performance improvement when compared to a traditional OFDM transmission. In this chapter, the ability of a secondary user to detect OM-OFDM and OFDM transmissions will be investigated.

7.3 BANDWIDTH OCCUPANCY OF OFFSET MODULATION

In this section the bandwidth occupancy of an OM-OFDM transmission will be investigated to highlight its attractive detection characteristics. As previously described (Eq (3.15)), the bandwidth occupancy of an OM-OFDM transmission can be written as

$$u_n = \sum_{y=0}^{2x} \left| \sum_{z=0}^{2x-y} 2\sin\left(\frac{\pi(2x-2z-y)\pm 2\Psi_{os}}{4}\right) \cdot J_{|-x+z|}(\beta_1) \left(\frac{|-x+z+\frac{1}{2}|}{-x+z+\frac{1}{2}}\right)^{|-x+z|} \cdot J_{|x-y-z|}(\beta_2) \left(\frac{|x-y-z+\frac{1}{2}|}{x-y-z+\frac{1}{2}}\right)^{|x-y-z|} \cdot \sin\left(2\pi(f_c+yf_d)+\frac{2\Psi_{os}\pm y\pi}{4}\right) \right|. \quad (7.1)$$

Then by inspection of Eq (7.1) for this particular case, as depicted in Fig. 7.1, the frequency spectrum and its corresponding amplitude components are shown. The dominant frequency

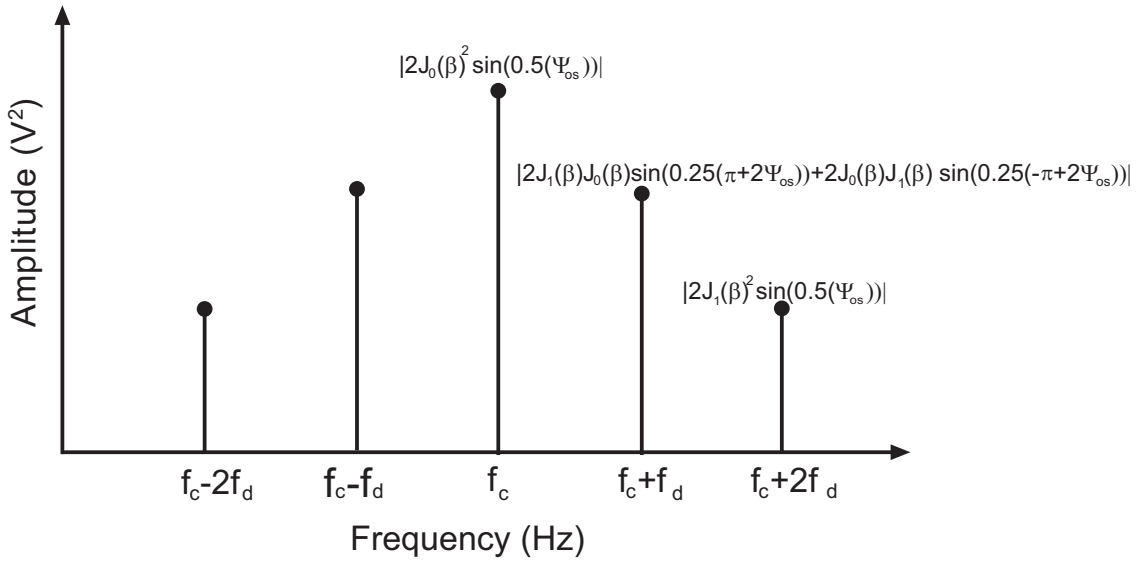

Figure 7.1: Theoretically derived (Eq (7.1)) frequency spectrum of an OM-OFDM signal.

component is given by $2J_0(\beta)^2\sin(2\pi f_c t - \frac{\Psi_{os}}{2})$, provided $\Psi_{os} >> \Phi_2(t) - \Phi_1(t)$. It is the prominence of this dominant frequency component that should significantly aid in the detection of an OM-OFDM transmission by a secondary user, when using energy detection.

7.4 RECEIVER OPERATING CHARACTERISTIC DERIVATION

During energy detection as described in [111] (depicted in Fig. 7.2), the received signal is first pre-filtered by a band-pass filter. The output of this filter is then squared and integrated to produce a measure of the energy of the received waveform. The subsequent output of the

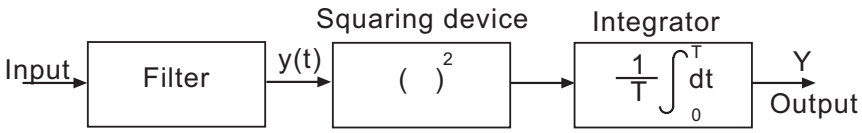

Figure 7.2: Energy detection [111]

integrator, denoted by Y, will act as a detection test for the

$$\begin{aligned} H_0, &\quad \text{the input is noise alone and} \\ H_1, &\quad \text{the input is a signal plus noise} \end{aligned} \tag{7.2}$$

hypothesis. The probability of a detection (P_d) and the probability of a false alarm can be determined by

$$P_d = P(Y > \lambda | H_1) \tag{7.3}$$

$$P_{fa} = P(Y > \lambda | H_o) \tag{7.4}$$

where λ is the decision threshold, Y has a chi-square distribution for both the H_0 (central chi-square distribution) and H_1 (non-central chi-square distribution) cases. The subsequent probability density function (PDF) of Y [3, Eq (2.1-110) and Eq (2.1-118)], when $y \geq 0$ can be written as

$$f_Y(y) = \begin{cases} \frac{y^{u-1} e^{\frac{-y}{2\sigma^2}}}{\sigma^{2u} 2^u \Gamma(u)} \\ \frac{1}{2\sigma^2} \left(\frac{y}{a \cdot \Upsilon^2} \right)^{\frac{u-1}{2}} e^{-\frac{a \cdot \Upsilon^2 + y}{2\sigma^2}} J_{u-1} \left(\frac{\sqrt{y \cdot a \cdot \Upsilon^2}}{\sigma^2} \right) \end{cases} \tag{7.5}$$

where u refers to an even number of degrees of freedom, σ^2 is the variance, $\Gamma(.)$ is the gamma function, Υ is the signal-to-noise ratio $\left(\Upsilon = \frac{E_s}{N_0} \right.$, where E_s is the signal energy and N_0 is the

one-sided power spectral density$\Big)$ and a is the non-centrality parameter of the distribution. After using [3, Eq (2.1-124)], the P_d can be shown to be written as

$$P_d = Q_u\left(\frac{\sqrt{a\cdot\Upsilon^2}}{\sigma},\frac{\sqrt{\lambda}}{\sigma}\right) \tag{7.6}$$

in Eq (7.6), $Q_u(.,.)$ is the Marcum Q-function [3]. From Eq (7.5), it can be shown that

$$P_{fa} = \int_{\frac{\lambda}{2\sigma^2}}^{\infty}\frac{e^{-t}t^{u-1}}{\Gamma(u)}dt. \tag{7.7}$$

Consider the upper incomplete gamma function $\Gamma(.,.)$, and the lower incomplete gamma function $\chi(.,.)$, defined as [91, Eq (6.5.3), Eq (6.5.2)]

$$\Gamma(u,x) = \Gamma(u)-\chi(u,x) = \int_x^{\infty}e^{-t}t^{u-1}dt \quad \text{and} \tag{7.8}$$

$$\chi(u,x) = \int_0^{x}e^{-t}t^{u-1}dt. \tag{7.9}$$

Using Eq (7.8) to evaluate Eq (7.7), results in

$$P_{fa} = \frac{\Gamma(u,\frac{\lambda}{2\sigma^2})}{\Gamma(u)} = \frac{\Gamma(u)-\chi(u,\frac{\lambda}{2\sigma^2})}{\Gamma(u)}. \tag{7.10}$$

If the received signal strength follows a Rician distribution, the PDF ($\Upsilon \geq 0$) can be written as

$$f(\Upsilon) = \frac{2\Upsilon(K+1)}{\overline{\Upsilon}}J_0\Big(2\sqrt{\frac{K(K+1)}{\overline{\Upsilon}}}\Upsilon\Big)e^{-K-\frac{(K+1)\Upsilon^2}{\overline{\Upsilon}}}. \tag{7.11}$$

In Eq (7.11), K is the Rician distribution factor and $\overline{\Upsilon}$ is the average signal-to-noise ratio. This equation (Eq (7.11)) is slightly different from that introduced by Digham et al. [112, Eq (24)] since the errors made in [112] have been corrected. The expression for the average $\overline{P_d}$ in a Rician environment is calculated by averaging the expression for P_d in AWGN (Eq (7.6)) over the Rician fading PDF (Eq (7.11)), this results in

$$F(\Upsilon) = \frac{2(K+1)}{\overline{\Upsilon}}\int_0^{\infty}\Upsilon\cdot Q_u\left(\frac{\sqrt{a\cdot\Upsilon^2}}{\sigma},\frac{\sqrt{\lambda}}{\sigma}\right)\cdot e^{\left(-K-\frac{(K+1)\Upsilon^2}{\overline{\Upsilon}}\right)}\cdot J_0\left(2\sqrt{\frac{K(K+1)}{\overline{\Upsilon}}}\Upsilon\right)d\Upsilon. \tag{7.12}$$

After using [113, Eq (45)], Eq (7.12) simplifies into

$$\overline{P_{d_{Ric}}} = Q\left(\sqrt{\frac{2aK\overline{\Upsilon}}{2\sigma^2(K+1)+a\overline{\Upsilon}}}, \sqrt{\frac{2\lambda(K+1)}{2\sigma^2(K+1)+a\overline{\Upsilon}}}\right). \tag{7.13}$$

An equation relating the P_{md} to P_{fa} for a Rician fading channel can be obtained by solving for λ in Eq (7.10). When $u = 1$, and Eq (7.8), Eq (7.9) and Eq (7.10) are used, this results in

$$P_{fa} = 1 - \frac{\chi\left(1, \frac{\lambda}{2\sigma^2}\right)}{\int_0^\infty e^{-t}dt} = 1 - \int_0^{\frac{\lambda}{2\sigma^2}} e^{-t}dt = e^{-\frac{\lambda}{2\sigma^2}}. \tag{7.14}$$

From Eq (7.14) it can be shown that $\lambda = -2\sigma^2\ln(P_{fa})$; substituting this into Eq (7.13) results in

$$\overline{P_{md\,Ric}}|_{u=1} = 1 - Q\left(\sqrt{\frac{2aK\overline{\Upsilon}}{2\sigma^2(K+1)+a\overline{\Upsilon}}}, \sqrt{\frac{-4\sigma^2(K+1)\ln P_{fa}}{2\sigma^2(K+1)+a\overline{\Upsilon}}}\right). \tag{7.15}$$

When $K = 0$, the above expression reduces to the average $\overline{P_d}$ for a Rayleigh fading channel, which can be written as

$$\begin{aligned}\overline{P_{md\,Ray}}|_{u=1} &= 1 - Q\left(0, \sqrt{\frac{-4\sigma^2\ln P_{fa}}{2\sigma^2+a\overline{\Upsilon}}}\right) \\ &= 1 - \exp\left[\frac{2\sigma^2\ln P_{fa}}{2\sigma^2+a\overline{\Upsilon}}\right].\end{aligned} \tag{7.16}$$

As previously mentioned, the σ and a term in Eq (7.15) and Eq (7.16) are signal-dependent. For an OFDM transmission it can be shown that $\sigma^2 \approx 1$ and $a \approx 2$, while similarly, for an OM-OFDM transmission

$$\sigma^2 \approx \frac{1}{\sin^2\left(\frac{-\varphi}{2}\right)} \quad \text{and} \quad a \approx 2\sqrt{2} \tag{7.17}$$

where, φ is a constant term and has been calculated as presented in Table 3.2. Previous expressions have been derived, which relate the P_{md} to P_{fa} [109, 112, 114]. However, to

Table 7.1: Parameters for a 16-QAM OM-OFDM system ($\alpha = 0.07408$)

PAPR	Ψ_{os}	ς	γ	φ
10 dB	1.5	$10000/4096$	0.985	0.505

the best of the author's knowledge, they have not been presented in such a closed-form expression, which can be used for any generic unknown deterministic signal (for instance OFDM and OM-OFDM). In order to validate the theoretical results, 16-QAM Gray-coded OFDM and OM-OFDM data were transmitted through a Rician (K=5dB) and Rayleigh fading channel by using the 2k mode of the DVB-T2 standard. In Table 7.1 the parameters used for the 16-QAM OM-OFDM transmission are given.

When using the DVB-T2 standard, OM-OFDM allows the PAPR of the signal to be varied, while maintaining identical throughput and bandwidth occupancy as an OFDM transmission. The optimum operating point for such an OM-OFDM transmission is at a 10 dB PAPR (Section 4.4). In order to offer a fair comparison, the PAPR of an OFDM transmission was reduced from 12 dB PAPR to 10 dB PAPR by using the clipping method. The ROC of a 10 dB PAPR and 12 dB PAPR clipped OFDM transmission are almost identical. When classically clipping a signal to limit the out-of-band distortion, the clipped OFDM signal was filtered before transmission with an 9^{th} order Butterworth low-pass filter. The ROC results depicted in Fig. 7.3 and Fig. 7.4 were obtained by using an energy detector. These results offer a comparison between simulated and theoretical (Eq (7.15) and Eq (7.16)) OFDM and OM-OFDM transmissions through a Rician (K=5dB) and Rayleigh fading channel, respectively.

From these comparisons, in Fig. 7.3 and Fig. 7.4, it can be seen that the theoretically predicted and simulated results correlate reasonably well, validating the derivation process. The differences between the simulated and theoretical results at high $\overline{\Upsilon}$ can be attributed to the signal being theoretically assumed to have a non-centrality chi-square distribution, for a high $\overline{\Upsilon}$ under the H_1 condition. In order to determine the assumed non-centrality chi-square distribution, various parameters (a, σ^2 and u) were used. There is a slight difference between the actual signal distribution and assumed non-centrality chi-square distribution, which

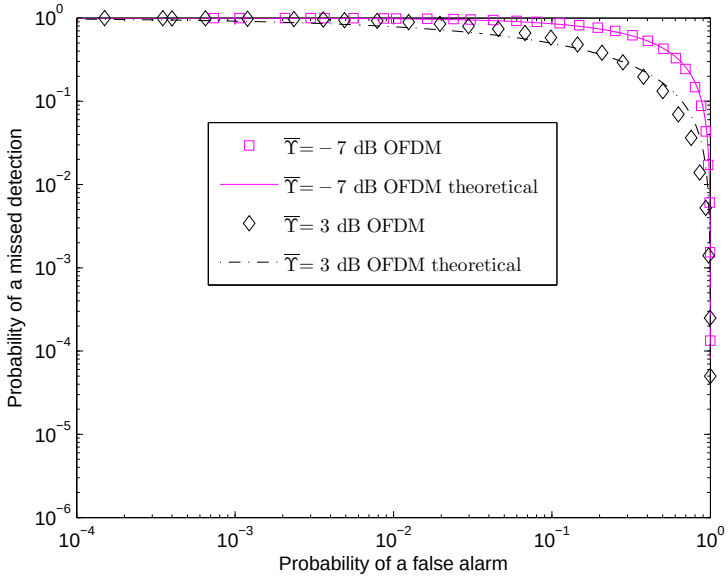

(a) A 12 dB PAPR OFDM transmission

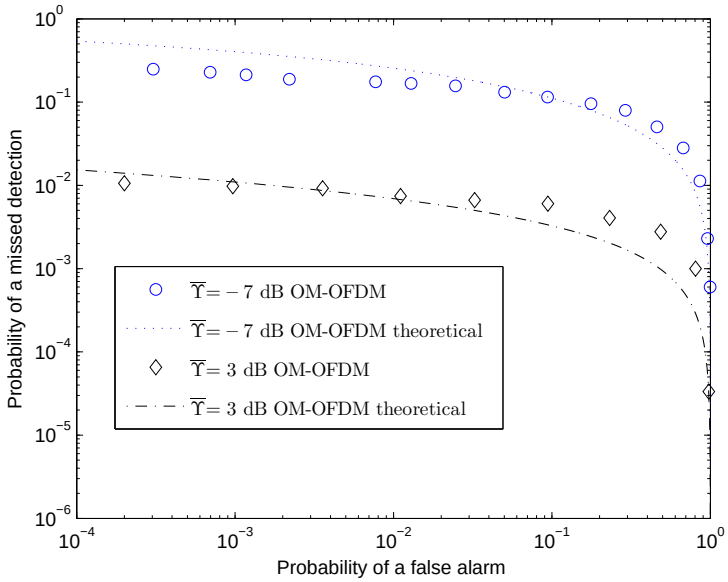

(b) OM-OFDM transmission

Figure 7.3: A ROC comparison between a theoretically predicted (Eq (7.15)) and simulated OFDM and OM-OFDM transmission through a Rician fading (K=5dB) channel.

contributes to the difference between the simulated and theoretical results. A comparison between Fig. 7.3(a) and Fig. 7.3(b) indicates that the OM-OFDM method with a $\overline{\Upsilon} = -7$ dB and $\overline{\Upsilon} = 3$ dB offers better detection characteristics than an OFDM transmission. Similarly, for a Rayleigh fading channel, depicted in Fig. 7.4(a) and Fig. 7.4(b), for a $\overline{\Upsilon} = -7$ dB and

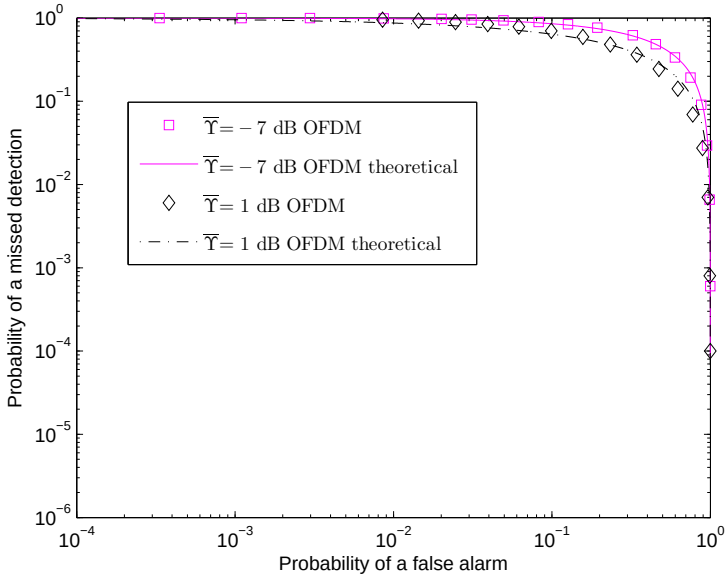

(a) A 12 dB PAPR OFDM transmission

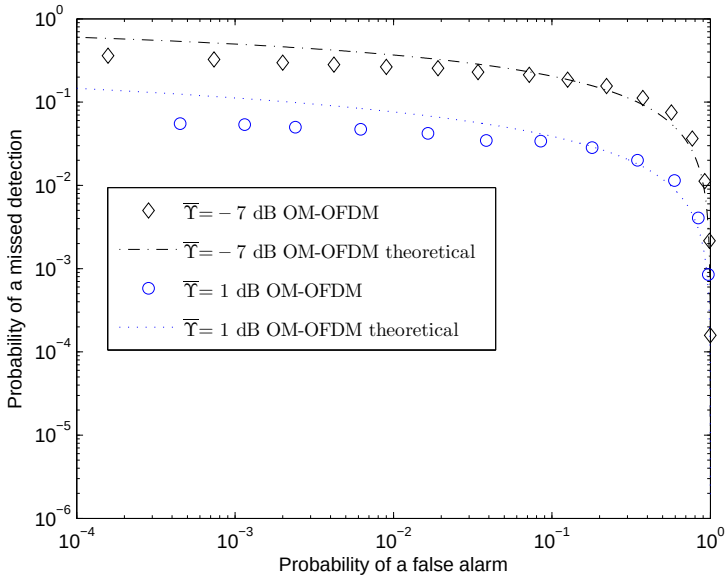

(b) OM-OFDM transmission

Figure 7.4: A ROC comparison between a theoretically predicted (Eq (7.16)) and simulated OFDM and OM-OFDM transmission through a Rayleigh fading channel.

$\overline{\Upsilon} = 1$ dB, OM-OFDM offers better detection characteristics than an OFDM transmission. In the next section a more comprehensive comparison is provided.

7.5 RESULTS AND DISCUSSION

In this section, by using the 2k mode of the DVB-T2 standard, 16-QAM Gray-coded OFDM and OM-OFDM data were transmitted through a Rician, (K=5dB), Rayleigh and a 3-tap typical-urban frequency selective fading channel. The pilot symbol placement for both OM-OFDM and OFDM, can be found in the DVB-T2 standard. Similarly, the 3-tap typical-urban area model was obtained from Patzold [96]. Identical throughputs were used to ensure a fair comparison between the various methods and perfect carrier and timing synchronisation was assumed. Both methods conform to the spectrum mask and throughput requirements imposed by the DVB-T2 standard. This OFDM type of transmissions would typically be encountered in the development of the IEEE 802.22 standard in the spectrum sharing of the TV band. For a Rician channel, depicted in Fig. 7.5, the P_{md} of an OM-OFDM ($\overline{\Upsilon}$=−7 dB)

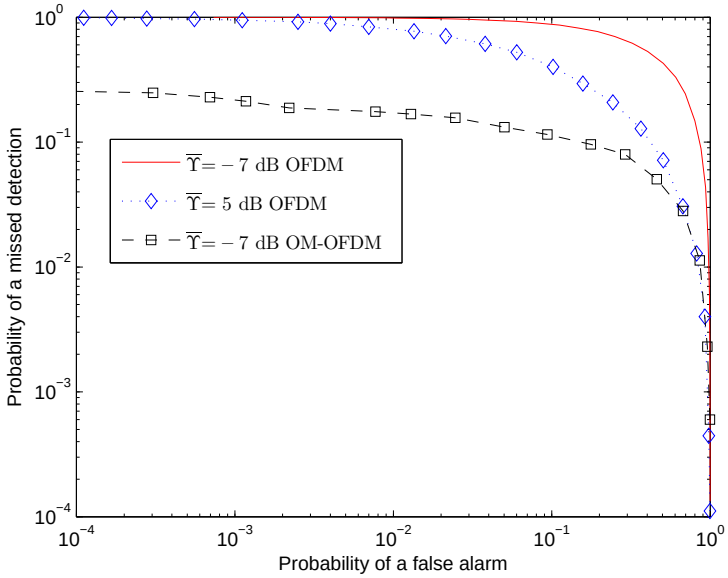

Figure 7.5: ROC comparison over a Rician fading (K=5dB) channel.

transmission is 9.6×10^{-2} and the P_{md} for both OFDM ($\overline{\Upsilon}$=−7 dB and $\overline{\Upsilon}$=5 dB) transmissions are 0.86 and 0.4 (at a $P_{fa} = 10^{-1}$), respectively. Similarly for a Rayleigh channel, depicted in Fig. 7.6, the P_{md} of an OM-OFDM transmission is 1.8×10^{-1} and the P_{md} for both OFDM ($\overline{\Upsilon}$=−7 dB and $\overline{\Upsilon}$=5 dB) transmissions are 0.84 and 0.4 (at a $P_{fa} = 10^{-1}$), respectively. In addition, for a 3-tap typical urban frequency selective fading channel, depicted in Fig. 7.7, the P_{md} of an OM-OFDM transmission is 1×10^{-1} and the P_{md} of both OFDM

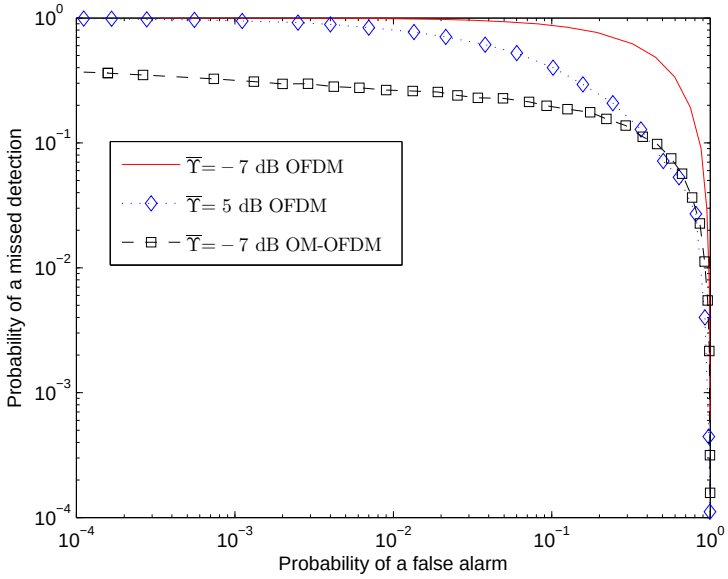

Figure 7.6: ROC comparison over a Rayleigh fading channel.

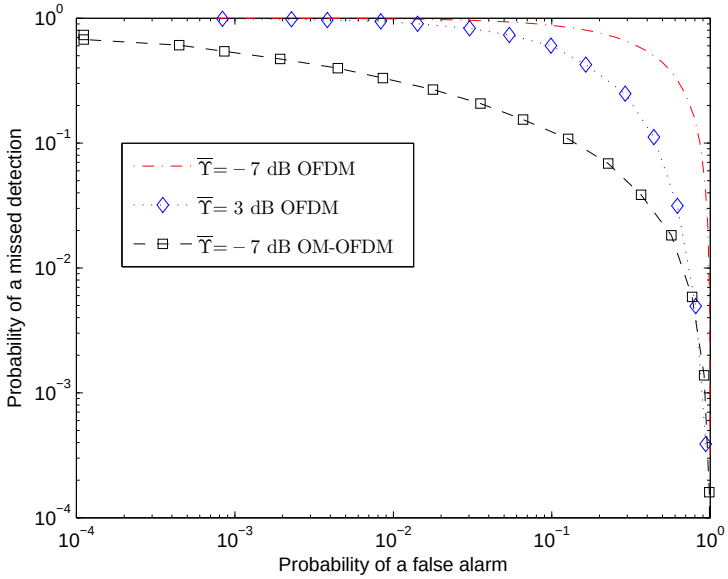

Figure 7.7: ROC comparison over a 3-tap typical urban area.

($\overline{\Upsilon}$=−7 dB and $\overline{\Upsilon}$=5 dB) transmissions are 0.9 and 0.53 (at a $P_{fa} = 10^{-1}$), respectively. All three comparisons, depicted in Fig. 7.5, Fig. 7.6 and Fig. 7.7 have been summarised in Table 7.2 and Table 7.3. From Table 7.2, the P_{md} of an OM-OFDM transmission is between $0.096 - 0.18$ and the P_{md} of an OFDM transmission is between $0.84 - 0.9$ (at a $P_{fa} = 10^{-1}$ and average SNR of -7dB) for a Rician, Rayleigh and frequency selective fading channel

Table 7.2: Summarised P_{md} results for a $\overline{\Upsilon}$=−7 dB OFDM and $\overline{\Upsilon}$=−7 dB OM-OFDM transmission at a $P_{fa} = 10^{-1}$

Channel	P_{md}	
	OFDM	OM-OFDM
Rician	0.86	0.096
Rayleigh	0.84	0.18
FSF	0.9	0.1

Table 7.3: Summarised P_{md} results for an OFDM and OM-OFDM transmission at a $P_{fa} = 10^{-1}$

Channel	P_{md}				
	$\overline{\Upsilon}$ (dB)	OFDM	$\overline{\Upsilon}_o$ (dB)	OM-OFDM	$\overline{\Upsilon} - \overline{\Upsilon}_o$ (dB)
Rician	5	0.4	−7	0.096	12
Rayleigh	5	0.4	−7	0.18	12
FSF	3	0.533	−7	0.1	10

conditions. This indicates that an OM-OFDM transmission offers significantly better detection characteristics than an OFDM transmission. Similarly in Table 7.3, the P_{md} of an OM-OFDM transmission is shown to be between $0.096 - 0.18$ and the P_{md} of an OFDM transmission is between $0.4 - 0.53$ (at a $P_{fa} = 10^{-1}$) for varied channel conditions. In addition, in Table 7.3, the OM-OFDM method is shown to operate at a 10 dB - 12 dB lower SNR value than an OFDM transmission, while still offering better detection characteristics than an OFDM transmission under various channel conditions. The significant performance improvement offered by OM-OFDM is possible (as discussed Section 7.3) because of the presence of a dominant frequency component in an OM-OFDM transmission.

7.6 CONCLUSIONS

The OM-OFDM method has been proposed for cognitive radio applications. An examination of an OM-OFDM bandwidth occupancy highlights its attractive detection properties. Furthermore, a simplified theoretical closed-form relationship between the probability

of a missed detection and the probability of a false alarm, for an unknown deterministic signal, is derived and validated. Previous expressions have been derived which relate the probability of a missed detection to the probability of a false alarm. However, they have not been presented in such a closed-form expression which can be used for any unknown deterministic signal (for instance OFDM and OM-OFDM).

Thereafter, by using energy detection, the offset modulation method is shown to operate at a 10 dB - 12 dB lower SNR value than an OFDM transmission, while still offering better detection characteristics than an OFDM transmission under Rician, Rayleigh and frequency selective fading conditions. The ROC curves indicate that the P_{md} of an OM-OFDM transmission is between $0.096 - 0.18$ and the P_{md} of an OFDM transmission is between $0.84 - 0.9$ (at a $P_{fa} = 10^{-1}$ and average SNR of -7dB) for Rician, Rayleigh and frequency selective fading channel conditions. These aspects make it a promising candidate for cognitive radio.

CHAPTER 8

CONCLUSION

8.1 SUMMARY

The author can summarise the work presented in this thesis as follows

8.1.1 Introduction to OFDM, PAPR and a PAPR literature review

In Chapter 2 the OFDM concept was introduced. The origin of the high PAPR problem associated with an OFDM transmission was discussed. This high PAPR reduces the battery life of a mobile device, which is not desirable. Various methods have been suggested to reduce the PAPR of an OFDM transmission, these are clipping, decision-aided reconstruction clipping, coding, partial transmission sequence, selective mapping, companding transforms, active constellation extension, tone reservation and CE-OFDM, amongst others. The drawbacks associated with all these methods were discussed.

8.1.2 Introduction of OM-OFDM and a decision metric

In Chapter 3, a novel method called offset modulation was proposed to control the PAPR of an OFDM transmission. The proposed OM-OFDM method was shown not to result in a number of the drawbacks experienced by current methods in the field. The theoretical bandwidth occupancy of the offset modulation signal was derived. Using these bandwidth occupancy results, a closed-form theoretical BER expression for an offset modulation

transmission was derived. This mathematically derived BER expression has been shown to agree with the simulated results, thus validating the derivation.

A newly applied decision metric was also introduced, which can be utilised to compare various methods in the PAPR field. This decision metric can also be utilised to investigate whether the proposed OM-OFDM transmission has an optimum solution and whether a net gain exists for such a solution.

8.1.3 Differences between OM-OFDM and CE-OFDM

The proposed OM-OFDM method appears to be similar to a well-known CE-OFDM transmission. In Chapter 4 the significant modulation, structural and performance differences between the OM-OFDM and CE-OFDM methods were demonstrated. In addition, the OM-OFDM method was able to control the PAPR of a transmission accurately for a targeted BER. This is currently not possible with CE-OFDM.

By utilising a power performance decision metric, the OM-OFDM method was shown to offer a net power performance gain of 34 dB and 3.44 dB (at a BER of 10^{-4}) when compared to CE-OFDM and traditional OFDM transmissions for frequency selective fading channel conditions, respectively.

8.1.4 Comparative performance of OM-OFDM

In Chapter 5, the proposed OM-OFDM method was compared to an OFDM transmission as well as existing PAPR reduction methods. A BER comparison between OM-OFDM and OFDM at a PAPR value of 13 dB indicated that both methods offer similar BER characteristics for frequency selective fading channel conditions. Furthermore, when utilising the power performance decision metric, OM-OFDM was shown to offer a net power performance gain of between 4 dB - 1.2 dB (60.4%-23.6%) and 4.1 dB - 1.2 dB (60.8%-23.6%), at a BER of 10^{-4}, for AN10858 and FPD2000AS RF power amplifiers respectively, when compared to clipped OFDM, OFDM, TR and ACE transmissions in a frequency selective fading channel.

Thereafter, by using a CCDF, the OM-OFDM method was shown to offer a PAPR reduction of between 3.2 dB - 2.3 dB (at a CCDF of 10^{-1}) when compared to OFDM, TR, ACE and clipped OFDM transmissions. The proposed offset method was shown to offer a performance improvement when compared to both simple (clipping) as well as more well-established (ACE and TR) PAPR reduction methods, without the need for an iterative (30-60 iterations) process.

8.1.5 Combination of OM-OFDM and ACE

In Chapter 6, the OM-OFDM method was combined with an existing active constellation extended PAPR reduction method. This introduced a novel method called offset modulation with active constellation extension, to control the PAPR of an OFDM signal. A closed-form bandwidth occupancy and theoretical BER expression for this OM-ACE transmission was presented and validated.

Thereafter, by using a power performance decision metric, the OM-ACE transmission was shown to offer a net power performance gain of between 5.7 dB - 2 dB (73.02%-37.71%), at a BER of 10^{-4}, when compared to clipped OFDM, OFDM and ACE transmissions, in a frequency selective fading channel. By using a CCDF, the OM-ACE method is shown to offer a PAPR reduction of between 2.6 dB - 1.6 dB (at a CCDF of 10^{-1}) when compared to OFDM, ACE and clipped OFDM transmissions.

8.1.6 A Cognitive radio application of OM-OFDM

The OM-OFDM method was also proposed for cognitive radio applications. Cognitive radio applications require transmissions that are easily detectable. In Chapter 7 an examination of an OM-OFDM bandwidth occupancy highlights its attractive detection properties. Furthermore, a generic theoretical closed-form relationship between the probability of a missed detection and the probability of a false alarm, for an unknown deterministic signal, was derived and validated. Previous expressions had been derived, which related the P_{md} to P_{fa}. However, they had not been presented in such a generic closed-form expression, which can

be used for any unknown deterministic signal (for instance OFDM and OM-OFDM). Thereafter, by using energy detection, the offset modulation method was shown to operate at a 10 dB - 12 dB lower SNR value than an OFDM transmission, while still offering better detection characteristics than an OFDM transmission under Rician, Rayleigh and frequency selective fading conditions. The receiver operating characteristic curves indicate that the P_{md} of an OM-OFDM transmission was between $0.096 - 0.18$ and the P_{md} of an OFDM transmission was between $0.84 - 0.9$ (at a $P_{fa} = 10^{-1}$ and average SNR of -7dB) for Rician, Rayleigh and frequency selective fading channel conditions.

8.2 CONCLUDING REMARKS

In addition to its attractive cognitive radio properties, OM-OFDM also offers good PAPR properties when compared to an OFDM transmission. These performance gains combined with the fact that OM-OFDM requires low implementation complexity and does not lead to a severe BER degradation as the number of carriers increases. Neither does it require any additional bandwidth expansion or the transmission of any side information to reconstruct the original message signal. All these aspects make OM-OFDM a good alternative approach to current methods already in the field.

8.3 FURTHER WORK

8.3.1 Investigate reducing the number of pilot symbols

As discussed in Chapter 3, the OM-OFDM method contains a prominent dominant frequency component. The receiver has knowledge of this dominant component by examining the PAPR of the received transmission. Under flat fading channel conditions, without using pilot symbols, this dominant component can be used to extract CSI, thus eliminating the need for pilot symbols.

This concept can be extended further by dividing an OM-OFDM transmission into smaller multi-user sub-blocks. If under frequency selective fading conditions, flat fading

occurs for each sub-block, the number of pilot symbols required would be reduced. This would in turn improve throughput.

8.3.2 Investigate further hybrid OM methods

In Chapter 6, the OM-OFDM method was combined with the ACE method to control the PAPR of an OFDM signal. Various other PAPR reduction methods, such as clipping, DAR clipping, companding transforms and tone reservation, amongst others, can be incorporated in an OM-OFDM transmission to produce other hybrid methods.

8.3.3 Investigate co-operative OM-OFDM sensing for cognitive radio applications

In Chapter 7, a simplified non-cooperative theoretical closed-form relationship, between the probability of a missed detection and the probability of a false alarm for an unknown deterministic signal (e.g. OM-OFDM) was derived. This relationship between P_{md} and P_{fa} can be further extended to investigate co-operative detection characteristics for an unknown deterministic signal.

8.3.4 Synchronisation

In this thesis perfect timing and carrier synchronisation is assumed at the receiver. However, in practice this is not a valid assumption, since these synchronisation aspects severely degrade the BER performance of a system. Thus an interesting research avenue would be to perform an analysis of different synchronisation schemes for an OM-OFDM transmission.

8.3.5 Implementation of an OM-OFDM transmission on a hardware platform

This thesis has presented a mathematical and simulated description of the proposed OM-OFDM method. The next step can be the implementation of the OM-OFDM method onto a hardware platform. For instance, the implementation of OM-OFDM onto a field-

programmable gate array (FPGA) board. Such a practical implementation of OM-OFDM would demonstrate the benefits of the method.

8.3.6 Investigate other standards

This thesis focused on the DVB-T2 standard. The various PAPR reduction methods developed can be applied to other standards. For instance if the methods developed in this thesis were applied to LTE, it might remove the current SC-FDMA uplink and replace it with an OFDM uplink instead. This will improve transmitter efficiencies, as well as improve the up-link capabilities of the device.

REFERENCES

[1] R. Prasad, *OFDM for Wireless Communications Systems*, 1st ed. Artech House, August 2004.

[2] A. R. S. Bahai and B. R. Saltzberg, *Multi-Carrier Digital Communications Theory and Applications of OFDM*, 2nd ed. Springer, October 2004.

[3] J. G. Proakis, *Digital Communication*, 4th ed. McGraw-Hill, 2002.

[4] H. Harada and R. Prasad, *Simulation and software radio for mobile communication*, 1st ed. Artech House, May 2002.

[5] M. Parker, *Digital Signal Processing*. Elsevier Inc, 2010.

[6] J. G. Proakis and D. G. Manolakis, *Digital Signal Processing, Principles, Algorithms and Applications*. Prentice Hall, May 1996.

[7] R. R. Mosier and R. G. Clabaugh, "Kineplex, a Bandwidth-Efficient Binary Transmission System," *AIEE Transactions*, vol. 76, pp. 723–728, January 1958.

[8] M. S. Zimmerman and A. L. Kirsch, "The AN/GSC-10 (KATHRYN) Variable Rate Data Modem for HF Radio," *IEEE Transactions on Communication Technology*, vol. 15, no. 2, pp. 197–204, 1967.

[9] G. Porter, "Error Distribution and Diversity Performance of a Frequency-Differential PSK HF Modem," *IEEE Transactions on Communication Technology*, vol. 16, no. 4, pp. 567–575, August 1968.

[10] B. R. Saltzberg, "Performance of an Efficient Parallel Data Transmission System," *IEEE Transactions on Communication Technology*, vol. 15, no. 6, pp. 805–811, December 1967.

[11] R. W. Chang and R. A. Gibby, "A Theoretical Study of Performance of an Orthogonal Multiplexing Data Transmission Scheme," *IEEE Transactions on Communication Technology*, vol. 16, no. 4, pp. 529–540, August 1968.

[12] R. W. Chang, "Orthogonal frequency division multiplexing," US Patent 3,488,445, January 6, 1970.

[13] S. B. Weinstein and P. M. Ebert, "Data Transmission by Frequency-Division Multiplexing Using the Discrete Fourier Transform," *IEEE Transactions on Communication Technology*, vol. 19, no. 5, pp. 628–634, October 1971.

[14] L. J. Cimini, Jr., "Analysis and Simulation of a Digital Mobile Channel Using Orthogonal Frequency Division Multiplexing," *IEEE Transactions on Communication*, vol. 33, no. 7, pp. 665–675, July 1985.

[15] J. S. Chow, J. C. Tu, and J. M. Cioffi, "A Discrete Multitone Transceiver System for HDSL Applications," *IEEE Journal on Selected Areas in Communication*, vol. 9, no. 6, pp. 895–908, August 1991.

[16] P. S. Chow, J. C. Tu, and J. M. Cioffi, "Performance Evaluation of a Multichannel Transceiver system for ADSL and VHDSL Services," *IEEE Journal on Selected Areas in Communication*, vol. 9, no. 6, pp. 909–918, August 1991.

[17] A. Ruiz, J. M. Cioffi, and S. Kasturia, "Discrete Multiple Tone Modulation with Coset Coding for the Spectrally Shaped Channel," *IEEE Transactions on Communications*, vol. 40, no. 6, pp. 1012–1029, June 1992.

[18] J. M. Cioffi and J. A. C. Bingham, "A Data-Driven Multitone Echo Canceller," *IEEE Transactions on Communications*, vol. 42, no. 10, pp. 2853–2869, October 1994.

[19] S. H. Han and J. H. Lee, "An overview of peak-to-average power ratio reduction techniques for multicarrier transmission," *IEEE Wireless Communications Magazine*, vol. 12, no. 2, pp. 56–65, April 2005.

[20] A. Goldsmith, *Wireless Communications*. Cambridge University Press, August 2005.

[21] S. Ahmadi, *Mobile WiMAX: A Systems Approach to Understanding IEEE 802.16m Radio Access*. Elsevier, November 2010.

[22] Y. S. Cho, J. Kim, W. Y. Yang, and C. G. Kang, *MIMO-OFDM Wireless Communications with Matlab*. John Wiley and Sons, November 2010.

[23] T. Jiang and Y. Wu, "An overview: Peak-to-average power ratio reduction techniques for OFDM signals," *IEEE Transactions on Broadcasting*, vol. 54, no. 2, pp. 257–268, June 2008.

[24] L. Xiadong and L. J. Cimini, Jr., "Effect of Clipping and Filtering on the Performance of OFDM," *IEEE Communication Letters*, vol. 2, no. 5, pp. 131–133, May 1998.

[25] H. Ochiai and H. Imai, "Performance Analysis of Deliberately Clipped OFDM Signals," *IEEE Transactions on Communications*, vol. 50, no. 1, pp. 89–101, January 2002.

[26] J. Armstrong, "Peak-to-average power reduction for OFDM by repeated clipping and frequency domain filtering," *IET Electronic Letters*, vol. 38, no. 8, pp. 246–247, February 2002.

[27] H. Ochiai and H. Imai", "Performance of the Deliberate Clipping with Adaptive Symbol Selection for Strictly Band-Limited OFDM Systems," *IEEE Journal on Selected Areas in Communication*, vol. 18, no. 11, pp. 2270–2277, November 2000.

[28] D. Kim and G. L. Stuber, "Clipping noise mitigation for OFDM by Decision-Aided Reconstruction," *IEEE Communications Letters*, vol. 3, no. 1, pp. 4–6, January 1999.

[29] H. Chen and A. M. Haimovich, "Iterative Estimation and Cancellation of Clipping Noise for OFDM Signals," *IEEE Communication Letters*, vol. 7, no. 2, pp. 305–307, July 2003.

[30] L. Wang and C. Tellambura, "A Simplified Clipping and Filtering Technique for PAR Reduction in OFDM Systems," *IEEE Signal Processing Letters*, vol. 12, no. 6, pp. 453–456, June 2005.

[31] H. Saeedi, M. Sharif, and F. Marvasti, "Clipping Noise Cancellation in OFDM Systems Using Oversampled Signal Reconstruction," *IEEE Communication Letters*, vol. 6, no. 2, pp. 73–75, February 2002.

[32] U. K. Kwon, D. Kim, and G. H. Im, "Amplitude Clipping and Iterative Reconstruction of MIMO-OFDM Signals with Optimum Equalization," *IEEE Transactions on Wireless Communication*, vol. 9, no. 1, pp. 268–277, January 2009.

[33] J. A. Davis and J. Jedwab, "Peak-to-mean power control in OFDM, Golay complementary sequences, and Reed-Muller codes," *IEEE Transactions on Information Theory*, vol. 45, no. 7, pp. 2397–2417, November 1999.

[34] A. E. Jones, T. A. Wilkinson, and S. K. Barton, "Block coding scheme for reduction of peak to mean envelope power ratio of multicarrier transmission schemes," *IET Electronics Letters*, vol. 30, no. 8, pp. 2098–2099, December 1994.

[35] K. G. Paterson, "Generalized Reed-Muller Codes and Power Control in OFDM Modulation," *IEEE Transactions on Information Theory*, vol. 46, no. 1, pp. 104–120, January 2000.

[36] K. G. Paterson and V. Tarokh, "On the Existence and Construction of Good Codes with Low Peak-to-Average Power Ratios," *IEEE Transactions on Information Theory*, vol. 46, no. 6, pp. 1974–1987, September 2000.

[37] D. Wulich and L. Goldfeld, "Reduction of Peak Factor in Orthogonal Multicarrier

Modulation by Amplitude Limiting and Coding," *IEEE Transactions on Communication*, vol. 47, no. 1, pp. 18–21, January 1999.

[38] T. Jiang and G. X. Zhu, "Complement Block Coding for Reduction in Peak-to-Average Power Ratio of OFDM Signals," *IEEE Communications Magazine*, vol. 43, no. 9, pp. S17–S22, September 2005.

[39] K. Yang and S. Chang, "Peak-to-Average Power Control in OFDM Using Standard Arrays of Linear Block Codes," *IEEE Communications Letters*, vol. 7, no. 4, pp. 174–176, April 2003.

[40] T. Ginige, N. Rajatheva, and K. M. Ahmed, "Dynamic Spreading Code Selection Method for PAPR Reduction in OFDM-CDMA Systems With 4-QAM Modulation," *IEEE Communications Letters*, vol. 5, no. 10, pp. 408–410, October 2001.

[41] C. V. Chong and V. Tarokh, "A Simple Encodable/Decodable OFDM QPSK Code With Low Peak to-Mean Envelope Power Ratio," *IEEE Transactions on Information Theory*, vol. 47, no. 7, pp. 3025–3029, November 2001.

[42] P. Fan and X. G. Xia, "Block coded modulation for the reduction of the peak to average power ratio in OFDM systems," *IEEE Transactions on Consumer Electronics*, vol. 45, no. 4, pp. 1025–1029, November 1999.

[43] S. H. Muller and J. B. Huber, "OFDM with reduced peak-to-average power ratio by optimum combination of partial transmit sequences," *Electronic Letters*, vol. 33, no. 5, pp. 368–369, February 1997.

[44] L. J. Cimini, Jr. and N. R. Sollenberger, "Peak-to-Average Power Ratio Reduction of an OFDM Signal Using Partial Transmit Sequences," *IEEE Communication Letters*, vol. 4, no. 3, pp. 86–88, March 2000.

[45] S. H. Han and J. H. Lee, "PAPR reduction of OFDM signals using a reduced complexity PTS technique," *IEEE Signal Processing Letters*, vol. 11, no. 11, pp. 887–890,

November 2004.

[46] A. D. S. Jayalath and C. Tellambura, "Adaptive PTS approach for reduction of peak-to-average power ratio of OFDM signal," *IET Electronics Letters*, vol. 36, no. 14, pp. 1226–1228, July 2000.

[47] C. Tellambura, "Improved Phase Factor Computation for the PAR Reduction of an OFDM Signal Using PTS," *IEEE Communications Letters*, vol. 5, no. 4, pp. 135–137, April 2001.

[48] L. Yang, R. S. Chen, Y. M. Siu, and K. K. Soo, "PAPR reduction of an OFDM signal by use of PTS with low computational complexity," *IEEE Transactions on Broadcasting*, vol. 52, no. 1, pp. 83–86, March 2006.

[49] A. Alavi, C. Tellambura, and I. Fair, "PAPR Reduction of OFDM Signals Using Partial Transmit Sequence: An Optimal Approach Using Sphere Decoding," *IEEE Communication Letters*, vol. 9, no. 11, pp. 982–984, November 2005.

[50] Y. Xiao, X. Lei, Q. Wen, and S. Li, "A Class of Low Complexity PTS Techniques for PAPR Reduction in OFDM Systems," *IEEE Signal Processing Letters*, vol. 14, no. 10, pp. 680–683, October 2007.

[51] H. Chen and H. Liang, "PAPR Reduction of OFDM Signals Using Partial Transmit Sequences and Reed-Muller Codes," *IEEE Communication Letters*, vol. 11, no. 6, pp. 528–530, June 2007.

[52] R. W. Bauml, R. F. H. Fischer, and J. B. Huber, "Reducing the peak-to-average power ratio of multicarrier modulation by selected mapping," *IET Electronics Letters*, vol. 32, no. 22, pp. 2056–2057, October 1996.

[53] M. Breiling, S. H. Muller-Weinfurtner, and J. B. Huber, "SLM peak-power reduction without explicit side information," *IEEE Communications Letters*, vol. 5, no. 6, pp. 239–241, June 2001.

[54] D. W. Lim, J. S. No, C. W. Lim, and H. Chung, "A New SLM OFDM Scheme With Low Complexity for PAPR Reduction," *IEEE Signal Processing Letters*, vol. 12, no. 2, pp. 93–96, February 2005.

[55] C. L. Wang and Y. Ouyang, "Low-complexity selected mapping schemes for peak-to-average power ratio reduction in OFDM systems," *IEEE Transactions on Signal Processing*, vol. 53, no. 12, pp. 4652–4660, December 2005.

[56] S. H. Han and J. H. Lee, "Modified Selected Mapping Technique for PAPR Reduction of Coded OFDM Signal," *IEEE Transactions on Broadcasting*, vol. 50, no. 3, pp. 335–341, September 2004.

[57] S. J. Heo, H. S. Noh, J. S. No, and D. J. Shin, "A Modified SLM scheme With Low Complexity for PAPR Reduction of OFDM Systems," *IEEE Transactions on Broadcasting*, vol. 53, no. 4, pp. 804–808, December 2007.

[58] R. J. Baxley and G. T. Zhou, "Comparing Selected Mapping and Partial Transmit Sequence for PAR Reduction," *IEEE Transactions on Broadcasting*, vol. 53, no. 4, pp. 797–803, December 2007.

[59] X. Wang, T. T. Tjhung, and C. S. Ng, "Reduction of peak-to-average power ratio of OFDM system using a companding technique," *IEEE Transactions on Broadcasting*, vol. 45, no. 3, pp. 303–307, September 1999.

[60] T. Jiang, Y. Yang, and Y. Song, "Exponential Companding Technique for PAPR Reduction in OFDM Systems," *IEEE Transactions on Broadcasting*, vol. 51, no. 2, pp. 244–248, June 2005.

[61] T. Jiang and G. Zhu, "Nonlinear companding transform for reducing peak-to-average power ratio of OFDM signals," *IEEE Transactions on Broadcasting*, vol. 50, no. 3, pp. 239–241, September 2004.

[62] X. Huang, J. Lu, J. Zheng, K. B. Letaief, and J. Gu, "Companding transform for

reduction in peak-to-average power ratio of OFDM signals," *IEEE Transactions on Wireless Communications*, vol. 3, no. 6, pp. 2030–2039, November 2004.

[63] Y. P. Tsividis, V. Gopinathan, and L. Toth, "Companding in signal processing," *IET Electronics Letters*, vol. 26, no. 17, pp. 1331–1332, April 1990.

[64] X. Huang, J. Lu, J. Zheng, J. Chuang, and J. Gu, "Reduction of peak-to-average power ratio of OFDM signals with companding transform," *IET Electronics Letters*, vol. 37, no. 8, pp. 506–507, April 2001.

[65] T. Jiang, W. Yao, P. Guo, Y. Song, and D. Qu, "Two Novel Nonlinear Companding Schemes With Iterative Receiver to Reduce PAPR in Multi-Carrier Modulation Systems," *IEEE Transactions on Broadcasting*, vol. 52, no. 2, pp. 268–273, June 2006.

[66] T. Jiang, W. D. Xiang, P. C. Richardson, D. M. Qu, and G. X. Zhu, "On the nonlinear companding transform for reduction in PAPR of MCM signals," *IEEE Transactions on Wireless communications*, vol. 6, no. 6, pp. 2017–2021, June 2007.

[67] T. G. Pratt, N. Jones, L. Smee, and M. Torrey, "OFDM Link Performance With Companding for PAPR Reduction in the Presence of Non-linear Amplification," *IEEE Transactions on Broadcasting*, vol. 52, no. 2, pp. 261–267, June 2006.

[68] B. S. Krongold and D. L. Jones, "PAR Reduction in OFDM via Active Constellation Extension," *IEEE Transactions on Broadcasting*, vol. 49, no. 3, pp. 258–268, September 2003.

[69] D. L. Jones, "Peak power reduction in OFDM and DMT via active channel modification," in *Proceedings of the 33rd IEEE Asilomar Conference on Signals, Systems and Computers*, vol. 2, Monterey, CA, USA, 24–27 October 1999, pp. 1076–1079.

[70] Z. Yang, H. Fang, and C. Pan, "ACE With Frame Interleaving Scheme to Reduce Peak-to-Average Power Ratio in OFDM Systems," *IEEE Transactions on Broadcasting*, vol. 51, no. 4, pp. 571–575, December 2005.

[71] B. S. Krongold and D. L. Jones, "PAR Reduction in OFDM via Active Constellation Extension," in *Proceedings of the IEEE International Conference on Acoustic, Speech and Signal Processing*, Hong Kong, China, 6–10 April 2003, pp. 525–528.

[72] A. Saul, "Generalized Active Constellation Extension for Peak Reduction in OFDM Systems," in *Proceedings of the IEEE International Conference on Communications*, vol. 3, Seoul, Korea, 16–20 May 2005, pp. 1974–1979.

[73] A. Gatherer and M. Polley, "Controlling Clipping Probability in DMT Transmission," in *Proceedings of the 32nd IEEE Asilomar Conference on Signals, Systems and Computers*, Pacific Grove, CA, USA, 1–4 November 1998, pp. 578–584.

[74] K. Bae, J. G. Andrews, and E. J. Powers, "Adaptive Active Constellation Extension Algorithm for Peak-to-Average Ratio Reduction in OFDM," *IEEE Communication Letters*, vol. 14, no. 1, pp. 39–41, January 2010.

[75] B. S. Krongold and D. L. Jones, "An active-set approach for OFDM PAR reduction via tone reservation," *IEEE Transactions on Signal Processing*, vol. 52, no. 2, pp. 495–508, February 2004.

[76] L. Wang and C. Tellambura, "Analysis of Clipping Noise and Tone-Reservation Algorithms for Peak Reduction in OFDM Systems," *IEEE Transactions on Vehicular Technology*, vol. 57, no. 3, pp. 1675–1694, May 2008.

[77] B. S. Krongold and D. L. Jones, "A new tone reservation method for complex-baseband PAR reduction in OFDM systems," in *Proceedings of the IEEE Acoustics, Speech, and Signal Processing (ICASSP) Conference*, vol. 3, Orlando, Florida, USA, 13–17 May 2002, pp. 2321–2324.

[78] D. W. Lim, H. S. Noh, H. B. Jeon, J. S. No, and D. J. Shin, "Multi-Stage TR Scheme for PAPR Reduction in OFDM Signals," *IEEE Transactions on Broadcasting*, vol. 55, no. 2, pp. 300–304, June 2009.

[79] D. W. Lim, H. S. Noh, J. S. No, and D. J. Shin, "Near Optimal PRT Set Selection Algorithm for Tone Reservation in OFDM Systems," *IEEE Transactions on Broadcasting*, vol. 54, no. 3, pp. 454–460, September 2008.

[80] J. C. Chen and C. P. Li, "Tone Reservation Using Near-Optimal Peak Reduction Tone Set Selection Algorithm for PAPR Reduction in OFDM Systems," *IEEE Signal Processing Letters*, vol. 17, no. 11, pp. 933–936, November 2010.

[81] S. Janaaththanan, C. Kasparis, and B. G. Evans, " A Gradient Based Algorithm for PAPR Reduction of OFDM using Tone Reservation Technique," in *Proceedings of the IEEE Vehicular Technology Conference*, Marina Bay, Singapore, 11–14 May 2008, pp. 2977–2980.

[82] S. C. Thompson, J. G. Proakis, and J. R. Zeidler, "Constant envelope binary OFDM phase modulation," in *Proceedings of the IEEE Military Communications Conference*, vol. 1, Boston, USA, 13–16 October 2003, pp. 621–626.

[83] S. C. Thompson, A. U. Ahmed, J. G. Proakis, and J. R. Zeidler, "Constant envelope OFDM phase modulation: Spectral containment, signal space properties and performance," in *Proceedings of the IEEE Military Communications Conference*, vol. 2, Monterey, USA, 31 October–3 November 2004, pp. 1129–1135.

[84] S. C. Thompson, J. G. Proakis, and J. R. Zeidler, "Noncoherent reception of constant envelope OFDM in flat fading channels," in *Proceedings of the IEEE 16th International Symposium on Personal, Indoor and Mobile Radio Communications*, vol. 1, Berlin, Germany, 11–14 September 2005, pp. 517–521.

[85] Y. Tsai, G. Zhang, and J. L. Pan, "Orthogonal frequency division multiplexing with phase modulation and constant envelope design," in *Proceedings of the IEEE Military Communications Conference*, vol. 4, Atlantic City, USA, 17–20 October 2005, pp. 2658–2664.

[86] M. Kiviranta, A. Mammela, D. Cabric, D. A. Sobel, and R. W. Brodersen, "Con-

stant envelope multicarrier modulation: Performance evaluation in awgn and fading channels," in *Proceedings of the IEEE Military Communications Conference*, vol. 2, Atlantic City, USA, 17–20 October 2005, pp. 807–813.

[87] S. C. Thompson, "Constant Envelope Phase Modulation," PhD Thesis, University of California, San Diego, 2005.

[88] S. C. Thompson, J. G. Proakis, J. R. Zeidler, and M. Geile, "Constant envelope OFDM in multipath rayleigh fading channels," in *Proceedings of the IEEE Military Communications Conference*, Washington, USA, 23–25 October 2006, pp. 1–7.

[89] A. U. Ahmed, S. C. Thompson, and J. R. Zeidler, "Constant envelope OFDM with channel coding," in *Proceedings of the IEEE Military Communications Conference*, Washington, USA, 23–25 October 2006, pp. 1–7.

[90] S. C. Thompson, A. U. Ahmed, J. G. Proakis, J. R. Zeidler, and M. J. Geile, "Constant Envelope OFDM," *IEEE Transactions on Communications*, vol. 56, no. 8, pp. 1300–1312, August 2008.

[91] M. Abramowitz and I. A. Stegun, *Handbook of mathematical functions with formulas, graphs and mathematical tables*. Dover Publications, 1965.

[92] K. Dhuness and B. T. Maharaj, "An Offset Modulation scheme to control the PAPR of an OFDM transmission," in *Proceedings of the IEEE 72nd Vehicular Technology Conference*, Ottawa, Canada, 6–9 September 2010, pp. 1–5.

[93] K. Dhuness, P. Botha, and B. T. Maharaj, "A Decision Metric approach to PAPR performance analysis of an OM-OFDM Transmission," in *Southern Africa Telecommunication Networks and Application Conference*, Stellenbosch, South Africa, 5–8 September 2010, pp. 1–6.

[94] R. E. Zeimer and W. H. Tranter, *Principles of communications : systems, modulation, and noise*, 3rd ed. Washington D.C, 1990.

[95] ETSI EN 302 755, “Digital Video Broadcasting (DVB); Frame structure channel coding and modulation for a second generation digital terrestrial television broadcasting system (DVB-T2),” European Telecommunication Standard Doc. 302, September 2009.

[96] M. Patzold, *Mobile Fading Channels*. John Wiley and Son, 2002.

[97] J. G. Proakis and M. Salehi, *Communication systems engineering*, 2nd ed. Prentice-Hall, 2002.

[98] N. Semiconductors. (2010, March) AN10858.pdf. [Online]. Available: http://www.nxp.com/documents/application_note/

[99] C. Liang, J. Jong, W. E. Stark, and J. R. East, “Nonlinear Amplifier Effects in Communication Systems,” *IEEE Transactions on Microwave Theory and Techniques*, vol. 47, no. 8, pp. 257–268, August 1999.

[100] K. Dhuness and B. T. Maharaj, “Comparative performance of OM-OFDM in broadband systems,” *IET Electronics Letters*, vol. 48, no. 2, pp. 127–129, January 2012.

[101] R. M. Devices. (2009, November) FPD2000ASDS.pdf. [Online]. Available: http://www.rfmd.com/CS/Documents/

[102] Spectrum Efficiency Working Group, “Federal Communications Commission Spectrum Policy Task Force,” Federal Communications Commission, Tech. Rep. TR 02-155, November 2002.

[103] M. A. McHenry, “NSF Spectrum Occupancy Measurements Project Summary,” Shared Spectrum Company, January 2005, http://www.sharedspectrum.com. Last accessed on 02 February 2009.

[104] K. Dhuness and B. T. Maharaj, “A cognitive radio application of OM-OFDM,” in *Proceedings of the IEEE Africon*, Livingston, Zambia, 13–15 September 2011, pp. 1–5.

[105] J. Mitola and G. Q. Maguire, "Cognitive radio: making software radios more personal," *IEEE Personal Communications*, vol. 6, no. 4, pp. 13–18, August 1999.

[106] J. Mitola, "Cognitive Radio An Integrated Agent Architecture for Software Defined Radio," Doctor of Technology, Royal Institute of Technology (KTH), Stockholm, Sweden, May 2000.

[107] S. Haykin, "Cognitive radio: Brain-empowered wireless communications," *IEEE Journal on Selected Areas in Communications*, vol. 23, no. 2, pp. 201–220, February 2005.

[108] C. Cordeiro, B. Daneshrad, J. Evans, N. Mandayam, P. Marshall, and L. Cimini, "Guest Editorial - Adaptive, spectrum agile and cognitive wireless networks," *IEEE Journal on Selected Areas in Communications*, vol. 25, no. 3, pp. 513–516, April 2007.

[109] Y. C. Liang, Y. Zeng, E. C. Y. Peh, and A. T. Hoang, "Sensing-throughput tradeoff for cognitive radio networks ," *IEEE Transactions on Wireless Communications*, vol. 7, no. 4, pp. 1326–1337, April 2008.

[110] D. Cabric, S. M. Mishra, and R. W. Brodersen, "Implementation Issues in Spectrum Sensing for Cognitive Radios," in *Proceedings of the Thirty-Eighth Asilomar Conference on Signals, Systems and Computers*, vol. 1, California, USA, 7–10 November 2004, pp. 772–776.

[111] H. Urkowitz, "Energy Detection of Unknown Deterministic Signals," in *Proceedings of the IEEE*, April 1967, pp. 523–531.

[112] F. F. Digham, M. S. Alouini, and M. K. Simon, "On the energy detection of unknown signals over fading channels," in *Proceedings of the IEEE International Conference on Communications*, vol. 5, Anchorage, Alaska, USA, 11–15 May 2003, pp. 3575–3579.

[113] A. H. Nuttall, "Some intergrals involving the Q-function," Naval Underwater Systems

Center (NUSC), Tech. Rep. TR 4297, April 1972.

[114] K. B. Letaief and W. Zhang, "Cooperative Communications for Cognitive Radio Networks," *Proceedings of IEEE*, vol. 97, no. 5, pp. 878–893, 2009.

APPENDIX A

MODULATOR AND DEMODULATOR STRUCTURE

A.1 INTRODUCTION

In this appendix a discussion of an OM-OFDM modulator and OM-OFDM demodulator structure will be presented. Throughout this appendix various figures (Fig. A.1 and Fig. A.2), which represent the OM-OFDM modulator and OM-OFDM demodulator structure and the subsequent positions there-in will be discussed.

A.2 MODULATOR STRUCTURE

As previously discussed, consider the discrete complex output of an N-point IFFT OFDM signal, given by

$$m_n = \frac{1}{\sqrt{N}} \sum_{k=0}^{N-1} X_k e^{j\frac{2\pi nk}{N}}, \qquad n = 0, 1, ..., N-1 \tag{A.1}$$

$$= \frac{1}{\sqrt{N}} \sum_{k=0}^{N-1} (a_k + jb_k) \cdot \left(\cos\left(\frac{2\pi nk}{N}\right) + j \sin\left(\frac{2\pi nk}{N}\right) \right). \tag{A.2}$$

In Eq (A.1), X_k represents the complex signal, which may also be written as $a_k + jb_k$. This signal may be modulated using the method which follows.

$$\Phi_{1n} = \frac{\Re(m_n)}{\varsigma} = \frac{1}{\varsigma\sqrt{N}} \sum_{k=0}^{N-1} a_k \cos\left(\frac{2\pi nk}{N}\right) - b_k \sin\left(\frac{2\pi nk}{N}\right) \quad \text{and} \tag{A.3}$$

$$\Phi_{2n} = \frac{\Im(m_n)}{\varsigma} = \frac{1}{\varsigma\sqrt{N}} \sum_{k=0}^{N-1} b_k \cos\left(\frac{2\pi nk}{N}\right) + a_k \sin\left(\frac{2\pi nk}{N}\right). \tag{A.4}$$

Here $\Re$ and $\Im$, refer to the real and imaginary parts of the OFDM message signal, ς refers to a constant division term, whereas Φ_{1n} and Φ_{2n} represent the equivalent discrete real and imaginary OFDM phase mapping. The purpose of an OM-OFDM modulator is to transform the incoming complex OFDM message signal into the signal shown below

$$\cos(2\pi f_c t + \Phi_1(t) + \Psi_{os}) - \cos(2\pi f_c t + \Phi_2(t)) \tag{A.5}$$

where Ψ_{os} is an offset term, $\Phi_1(t)$ and $\Phi_2(t)$ represent the equivalent real and imaginary OFDM phase mapping. Applying the following identity [91]

$$\cos(z_1) - \cos(z_2) = 2\sin\left(\frac{z_2 - z_1}{2}\right) \cdot \sin\left(\frac{z_1 + z_2}{2}\right) \tag{A.6}$$

to Eq (A.5) results in

$$2\sin\left(\frac{\Phi_2(t) - \Phi_1(t) - \Psi_{os}}{2}\right) \cdot \sin\left(2\pi f_c t + \frac{\Phi_1(t) + \Psi_{os} + \Phi_2(t)}{2}\right). \tag{A.7}$$

In Fig. A.1, at (1) and (2), the incoming complex message signal is separated into its real

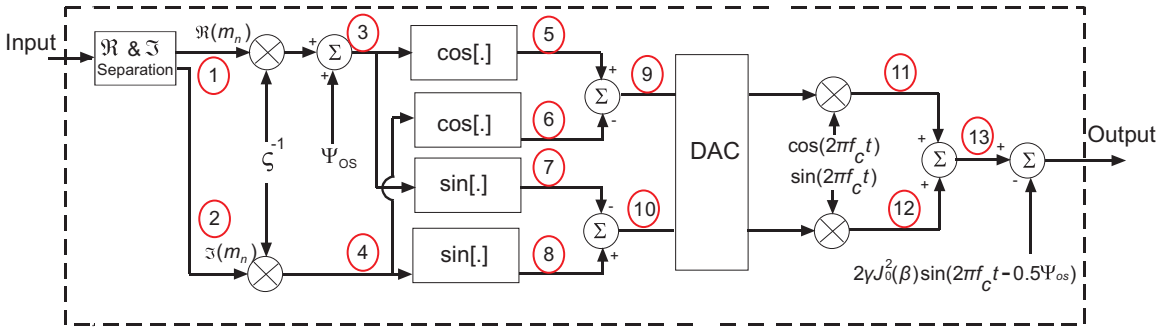

Figure A.1: OM modulator structure

(Eq (A.3)) and imaginary (Eq (A.4)) components. Thereafter, at (3), the signal can be expressed as $\Phi_{1n}+\Psi_{os}$ $\left(\text{where } \Phi_{1n}=\frac{\Re(m_n)}{\varsigma}\right)$. Similarly, the signal at (4) can be written as Φ_{2n} $\left(\text{where } \Phi_2=\frac{\Im(m_n)}{\varsigma}\right)$. At (5), the signal can be expressed as $\cos(\Phi_{1n}+\Psi_{os})$. Similarly, at (6), the signal can be written as $\cos(\Phi_{2n})$. In addition, at (7) the signal can be represented as $\sin(\Phi_{1n}+\Psi_{os})$ and the signal at (8) can be written as $\sin(\Phi_{2n})$. At (9) the signal can be expressed as

$$\begin{aligned}&\cos(\Phi_{1n}+\Psi_{os})-\cos(\Phi_{2n})\\ =\;&-2\sin\left(\frac{\Phi_{1n}+\Psi_{os}+\Phi_{2n}}{2}\right)\sin\left(\frac{-\Phi_{2n}+\Phi_{1n}+\Psi_{os}}{2}\right).\end{aligned}\tag{A.8}$$

At (10), the expression can be written as

$$\begin{aligned}&\sin(\Phi_{2n})-\sin(\Phi_{1n}+\Psi_{os})\\ =\;&-2\sin\left(\frac{-\Phi_{2n}+\Phi_{1n}+\Psi_{os}}{2}\right)\cos\left(\frac{\Phi_{1n}+\Psi_{os}+\Phi_{2n}}{2}\right).\end{aligned}\tag{A.9}$$

The subsequent signals are passed through a digital-to-analog converter (DAC). Thereafter at (11), the expression can be shown to be

$$-2\sin\left(\frac{\Phi_1(t)+\Psi_{os}+\Phi_2(t)}{2}\right)\sin\left(\frac{-\Phi_2(t)+\Phi_1(t)+\Psi_{os}}{2}\right)\cdot\cos(2\pi f_c t).\tag{A.10}$$

The expression at (12) can be represented by

$$-2\sin\left(\frac{-\Phi_2(t)+\Phi_1+\Psi_{os}}{2}\right)\cos\left(\frac{\Phi_1(t)+\Psi_{os}+\Phi_2(t)}{2}\right)\cdot\sin(2\pi f_c t).\tag{A.11}$$

Thereafter the signals from (11) and (12) are added to produce

$$\begin{aligned}&-2\sin\left(\frac{\Phi_1(t)+\Psi_{os}+\Phi_2(t)}{2}\right)\sin\left(\frac{-\Phi_2(t)+\Phi_1(t)+\Psi_{os}}{2}\right)\cdot\cos(2\pi f_c t)\\ &-2\sin\left(\frac{-\Phi_2(t)+\Phi_1(t)+\Psi_{os}}{2}\right)\cos\left(\frac{\Phi_1(t)+\Psi_{os}+\Phi_2(t)}{2}\right)\cdot\sin(2\pi f_c t).\end{aligned}\tag{A.12}$$

Thereafter it can be shown that Eq (A.12) simplifies to

$$\cos(2\pi f_c t + \Phi_1(t) + \Psi_{os}) - \cos(2\pi f_c t + \Phi_2(t)), \tag{A.13}$$

which is exactly (Eq (A.5)) the signal that was required for transmission.

A.3 DEMODULATOR STRUCTURE

In Fig. A.2, the subsequent positions in the OM-demodulator structure are presented. At (1)

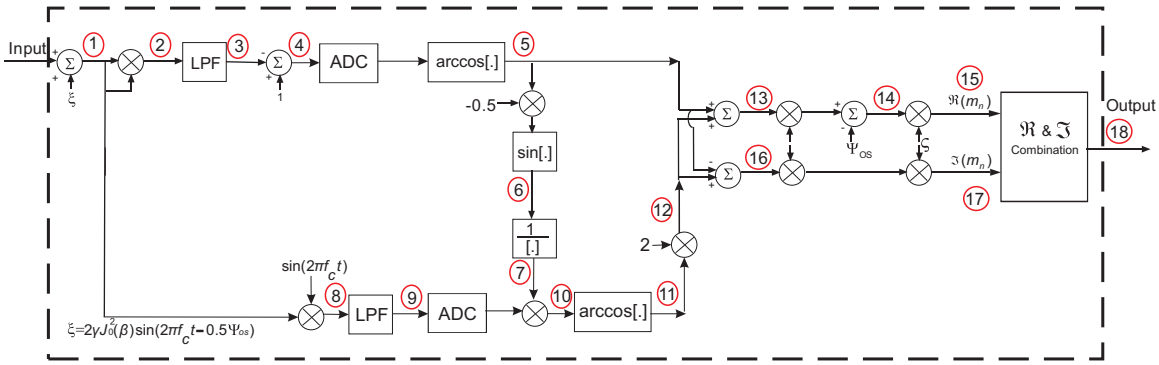

Figure A.2: OM demodulator structure

in Fig. A.2 a received OM-OFDM noise-free signal is given by

$$\cos(2\pi f_c t + \Phi_1(t) + \Psi_{os}) - \cos(2\pi f_c t + \Phi_2(t)). \tag{A.14}$$

Alternatively, Eq (A.14) may also be written as

$$2\sin\left(\frac{\Phi_2(t) - \Phi_1(t) - \Psi_{os}}{2}\right) \cdot \sin\left(2\pi f_c t + \frac{\Phi_1(t) + \Psi_{os} + \Phi_2(t)}{2}\right). \tag{A.15}$$

At (2), the signal can be expressed as

$$\begin{aligned} & \left(2\sin\left(\frac{\Phi_2(t) - \Phi_1(t) - \Psi_{os}}{2}\right) \cdot \sin\left(2\pi f_c t + \frac{\Phi_1(t) + \Psi_{os} + \Phi_2(t)}{2}\right)\right) \cdot \\ & \left(2\sin\left(\frac{\Phi_2(t) - \Phi_1(t) - \Psi_{os}}{2}\right) \cdot \sin\left(2\pi f_c t + \frac{\Phi_1(t) + \Psi_{os} + \Phi_2(t)}{2}\right)\right) \\ = \quad & \left(2\sin\left(\frac{\Phi_2(t) - \Phi_1(t) - \Psi_{os}}{2}\right) \cdot \sin\left(2\pi f_c t + \frac{\Phi_1(t) + \Psi_{os} + \Phi_2(t)}{2}\right)\right)^2 \end{aligned}$$

$$= 1-\cos(4\pi f_c t+\Phi_1+\Psi_{os}+\Phi_2)-\cos(-\Phi_2+\Phi_1+\Psi_{os}) + \frac{1}{2}\cos(2\Phi_2+4\pi f_c t)+\frac{1}{2}\cos(4\pi f_c t+2\Phi_1+2\Psi_{os}). \quad \text{(A.16)}$$

The low pass filter (LPF), before (3), removes the high-frequency components ($4\pi f_c t$); this results in

$$1-\cos(-\Phi_2(t)+\Phi_1(t)+\Psi_{os}). \quad \text{(A.17)}$$

A 4^{th} order low pass Butterworth filter proved to be sufficient to remove these high-frequency component signals. In addition, the delay introduced by the Butterworth filter needed to be compensated for. At (4), the signal can be expressed as

$$\cos(-\Phi_2(t)+\Phi_1(t)+\Psi_{os}). \quad \text{(A.18)}$$

The signal at (4) undergoes an analog-to-digital (ADC) conversion. The signal at (5), can be written as

$$-\Phi_{2n}+\Phi_{1n}+\Psi_{os} \quad \text{(A.19)}$$

where Φ_{1n} and Φ_{2n} represent the equivalent discrete real and imaginary OFDM phase mapping. Thereafter at (6), the signal can be expressed as

$$\sin\left(\frac{\Phi_{2n}-\Phi_{1n}-\Psi_{os}}{2}\right). \quad \text{(A.20)}$$

At (7), the signal can be shown to be

$$\frac{1}{\sin\left(\frac{\Phi_{2n}-\Phi_{1n}-\Psi_{os}}{2}\right)}. \quad \text{(A.21)}$$

The signal at (8), can be expressed as

$$(\cos(2\pi f_c t+\Phi_1(t)+\Psi_{os})-\cos(2\pi f_c t+\Phi_2(t)))\cdot\sin(2\pi f_c t) \quad \text{(A.22)}$$

$$= \frac{1}{2}\sin\left(4\pi f_c t + \Phi_1(t) + \Psi_{os}\right) - \frac{1}{2}\sin\left(\Phi_1(t) + \Psi_{os}\right) - \frac{1}{2}\sin\left(4\pi f_c t + \Phi_2(t)\right) + \frac{1}{2}\sin\left(\Phi_2(t)\right). \tag{A.23}$$

As previously mentioned the LPF removes the high frequency ($4\pi f_c t$) components of the signal. In addition, the delay introduced by the Butterworth filter needed to be compensated for. The signal at (9) is written as

$$-\frac{1}{2}\sin\left(\Phi_1(t) + \Psi_{os}\right) + \frac{1}{2}\sin\left(\Phi_2(t)\right). \tag{A.24}$$

Applying the following identity [91]

$$\sin(z_1) - \sin(z_2) = 2\cos\left(\frac{z_1 + z_2}{2}\right) \cdot \sin\left(\frac{z_1 - z_2}{2}\right), \tag{A.25}$$

to Eq (A.24), this results in

$$\cos\left(\frac{\Phi_1(t) + \Phi_2(t) + \Psi_{os}}{2}\right) \cdot \sin\left(\frac{\Phi_2(t) - \Phi_1(t) - \Psi_{os}}{2}\right). \tag{A.26}$$

The signal at (9) is passed through an ADC. As previously mentioned the signal at (7) is

$$\frac{1}{\sin\left(\frac{\Phi_{2n} - \Phi_{1n} - \Psi_{os}}{2}\right)}. \tag{A.27}$$

At (10) the signal is written as

$$\frac{\cos\left(\frac{\Phi_{1n} + \Phi_{2n} + \Psi_{os}}{2}\right) \cdot \sin\left(\frac{\Phi_{2n} - \Phi_{1n} - \Psi_{os}}{2}\right)}{\sin\left(\frac{\Phi_{2n} - \Phi_{1n} - \Psi_{os}}{2}\right)} = \cos\left(\frac{\Phi_{1n} + \Phi_{2n} + \Psi_{os}}{2}\right). \tag{A.28}$$

At (11), the signal can be expressed as

$$\frac{\Phi_{1n} + \Psi_{os} + \Phi_{2n}}{2}. \tag{A.29}$$

At (12), the signal can be written as

$$\Phi_{1n} + \Psi_{os} + \Phi_{2n}. \tag{A.30}$$

At (5) and (12), there are two equations (Eq (A.19) and Eq (A.30)), with two unknowns Φ_1 and Φ_2 (Ψ_{os} is known). To obtain (13), Eq (A.19) and Eq (A.30) ((5) and (12)) are added, this results in

$$(-\Phi_{2n} + \Phi_{1n} + \Psi_{os}) + (\Phi_{1n} + \Psi_{os} + \Phi_{2n}) = 2\Phi_{1n} + 2\Psi_{os}. \tag{A.31}$$

At (14), the signal can be written as Φ_{1n} and at (15), the real part of the message signal is extracted. In order to extract the imaginary components of the message signal, Eq (A.30) ((12)) is subtracted from Eq (A.19) ((5)), this results in (16), which can be shown to be $2\Phi_{2n}$. Thereafter, at (17), the imaginary part of the message signal is extracted. Both the real and imaginary components from (15) and (17) are combined to form the complex received message signal seen at (18).